

Research

Models for Fuel Rod Behaviour at High Burnup

Lars O. Jernkvist
Ali R. Massih

December 2004

SKI Perspective

Background

During recent years a considerable amount of work has been performed on studying the behaviour of nuclear fuel at high burnup and to model it in computer codes. SKI has previously performed an evaluation of FRAPCON (SKI Report 02.29). The evaluation confirms the applicability of FRAPCON to high burnup fuel rods, but also reveals weaknesses in the models for pellet thermal conductivity, clad oxidation, creep, plasticity and irradiation-induced growth.

Results and continued work

In this project the capability of the FRAPCON computer code to simulate fuel rod performance at high burnup is studied. Theoretical assessments of important models for fuel rod performance at high burnup are made. Different models are compared and evaluated against measured data. New models are also formulated for use within the FRAPCON code.

This project has contributed to the research goal of providing a basis for SKI:s supervision by means of illustrating the problems of modelling nuclear fuel behaviour. More precisely it has developed competence concerning the licensing of fuel at high burnup, which is an important safety issue. The results are useful as such, but also are the basis for modifications to FRAPCON in a following project.

Project information

Responsible for the project at SKI has been Jan In de Betou.

SKI-referens: 14.06-030848

Projektnummer: 200406006

Research

Models for Fuel Rod Behaviour at High Burnup

Lars O. Jernkvist
Ali R. Massih

Quantum Technologies AB
Uppsala Science Park
SE-751 83 Uppsala
Sweden

December 2004

This report concerns a study which has been conducted for the Swedish Nuclear Power Inspectorate (SKI). The conclusions and viewpoints presented in the report are those of the author/authors and do not necessarily coincide with those of the SKI.

List of contents

Summary.....	III
Sammanfattning.....	IV
1 Introduction	1
2 Models for uranium dioxide fuel behaviour	3
2.1 Formation of high-burnup microstructure	3
2.1.1 Background.....	3
2.1.2 Threshold for material restructuring.....	4
2.1.3 Porosity in restructured material.....	9
2.1.4 Athermal fission gas release from restructured material	13
2.2 Thermal fission gas release	15
2.2.1 Background.....	15
2.2.2 Gas release model: governing equations	18
2.2.3 Grain growth description	21
2.2.4 Calculation of gas release under grain growth	28
2.2.5 Results of sample computations	29
2.2.6 Analysis and discussion.....	34
2.3 Thermal conductivity.....	37
3 Models for zirconium alloy clad tube behaviour.....	41
3.1 Clad corrosion behaviour	41
3.1.1 Clad oxide growth	41
3.1.2 Clad hydrogen pickup.....	47
3.2 Clad mechanical properties	49
3.2.1 Yield stress	49
3.2.2 Rod axial growth	51
4 Summary and conclusions	55
5 References	57

List of appendices

Appendix A:	
Assessment case for high-burnup fuel restructuring	67
Appendix B:	
Fission gas production rate	69
Appendix C:	
Characteristic times of gas diffusion and grain growth.....	70
Appendix D:	
Fuel thermal conductivity correlation from HBRP	73
Appendix E:	
Fuel thermal conductivity correlation in FRAPCON-3.2.....	74

Summary

This report deals with release of fission product gases and irradiation-induced restructuring in uranium dioxide nuclear fuel. Waterside corrosion of zirconium alloy clad tubes to light water reactor fuel rods is also discussed. Computational models, suitable for implementation in the FRAPCON-3.2 computer code, are proposed for these potentially life-limiting phenomena.

Hence, an integrated model for the calculation of thermal fission gas release by intragranular diffusion, gas trapping in grain boundaries, irradiation-induced re-solution, grain boundary saturation, and grain boundary sweeping in UO_2 fuel, under time varying temperature loads, is formulated. After a brief review of the status of thermal fission gas release modelling, we delineate the governing equations for the aforementioned processes. Grain growth kinetic modelling is briefly reviewed and pertinent data on grain growth of high burnup fuel obtained during power ramps in the Third Risø Fission Gas Release Project are evaluated. Sample computations are performed, which clearly show the connection between fission gas release and grain growth as a function of time at different isotherms.

Models are also proposed for the restructuring of uranium dioxide fuel at high burnup, the so-called rim formation, and its effect on fuel porosity build-up, fuel thermal conductivity and fission gas release. These models are assessed by use of recent experimental data from the High Burnup Rim Project, as well as from post irradiation examinations of high-burnup fuel, irradiated in power reactors.

Moreover, models for clad oxide growth and hydrogen pickup in PWRs, applicable to Zircaloy-4, ZIRLOTM or M5TM cladding, are formulated, based on recent in-reactor corrosion data for high-burnup fuel rods¹. Our evaluation of these data indicates that the oxidation rate of ZIRLO-type materials is about 20% lower than for standard Zircaloy-4 cladding under typical PWR conditions. Likewise, the oxidation rate of M5 seems to be about 40% lower than for Zircaloy-4. Finally, the applicability of FRAPCON-3.2 to fuel rods with ZIRLO and M5 cladding is also assessed by comparing the models for clad yield stress and axial growth to experimental data for these materials.

¹ ZIRLO and M5 are trademarks of the Westinghouse Electric Company and Framatome ANP, respectively.

Sammanfattning

Denna rapport behandlar fissionsgasfrigörelse och bestrålningsinducerade mikrostrukturförändringar i kärnbränsle av urandioxid. Dessutom behandlas korrosion av zirconiumbaserade kapslingsrör till lättvattenreaktorbränsle. Beräkningsmodeller, lämpade för implementering i datorprogrammet FRAPCON-3.2, föreslås för dessa potentiellt livslängdsbegränsande fenomen.

Således formuleras en integrerad modell för beräkning av termisk fissionsgasfrigörelse från urandioxidbränsle genom intragranulär diffusion, gasinfångning i korngränser, bestrålningsdriven återlösning av gas, mättnad av korngränser, samt korngränssvepning under tidsberoende temperaturförhållanden. Vi formulerar de styrande ekvationerna för dessa processer, efter en kortfattad översikt av gängse modeller för termisk fissionsgasfrigörelse. En kortfattad översikt ges även av modeller för korntillväxt, liksom en utvärdering av relevanta data för korntillväxt i högutbränt bränsle under effektramper från Third Risø Fission Gas Release Project. Beräkningar utförs, som för olika temperaturer tydligt illustrerar det tidsberoende sambandet mellan fissionsgasfrigörelse och korntillväxt.

Modeller föreslås även för den förändring av urandioxidens mikrostruktur, den så kallade rimbildning, som sker vid hög utbränning, samt dess effekt på porositetsuppbyggnad, bränslets värmeledningsförmåga och fissionsgasfrigörelse. Dessa modeller utvärderas med hjälp av nyligen publicerade experimentella data från High Burnup Rim Project. Dessutom används resultat från efterbestrålningsundersökningar av högutbränt bränsle från kraftgenererande reaktorer för utvärdering av dessa modeller.

Slutligen formuleras modeller för oxidtillväxt och väteupptag hos kapslingsrör avsedda för tryckvattenreaktorer. Dessa modeller, vilka avser kapslingsmaterialen Zircaloy-4, ZIRLO™ och M5™, baseras på korrosionsdata för högutbrända bränslestavar från kraftgenererande reaktorer. Vår utvärdering av dessa data antyder att ZIRLO-material har ungefär 20 % lägre oxidationshastighet än standard Zircaloy-4 vid typiska tryckvattenreaktorförhållanden. Oxidationshastigheten hos M5 är under samma förhållanden ungefär 40 % lägre än för Zircaloy-4. Slutligen utvärderas möjligheterna att använda FRAPCON-3.2 för modellering av bränslestavar med kapsling av ZIRLO eller M5 även genom att jämföra programmets modeller för kapslingens flytspänning och axiella längdtillväxt mot mätdata för dessa material.

1 Introduction

When light water reactor (LWR) nuclear fuel is operated with long residence times in the core to achieve a high released energy density (burnup), several phenomena come into play that are potentially life-limiting for the fuel rods. Among these phenomena is the release of gaseous fission products from the fuel pellets. The noble gases xenon and krypton are generated during fission of uranium and plutonium isotopes. A fraction of these gaseous fission products is released into the free volume of the fuel rod, thereby increasing the internal fuel rod gas pressure. In addition, the gas released into the pellet-cladding gap degrades the thermal conductance of the gas in the gap, causing higher fuel temperature and further enhancement of fission gas release. Fission gas release is generally considered to be a potentially life-limiting (burnup-limiting) factor because of its consequences to fuel rod pressure build-up and clad tube integrity.

Several physical processes contribute to fission gas release (FGR) in UO_2 nuclear fuel, and they are usually divided into athermal and thermal release mechanisms (Olander, 1976). Athermal release takes place by recoil and knockout of fission gas atoms by energetic fission fragments. Since these mechanisms generally result in release of less than 1% of the fission gas produced within the fuel pellets, athermal release alone has to date not been considered a potential problem for excessive fuel rod pressure build-up. However, there is concern that the restructuring of UO_2 at high burnup, the so-called rim zone formation, could enhance athermal FGR in high-burnup fuel.

Thermal release mechanisms have potential for much larger release fractions than the athermal mechanisms. The thermal release is highly temperature dependent and is driven by thermal processes in irradiated fuel. These processes include gas diffusion to grain boundaries, grain growth, grain boundary saturation and release. In-reactor experiments, performed by ramping nuclear fuel rods to different power levels, indicate that, at above a certain linear heat generation rate (LHGR), fission gas release is significantly enhanced. The increase in fuel temperature due to the rise in LHGR enhances volume diffusion of fission product gases to the grain boundaries of UO_2 fuel. It may also cause grain growth, which sweeps the gases to the grain boundaries. Upon saturation of grain boundaries with gases, rapid gas release to the free volume of the fuel rod will occur.

Another potentially life-limiting phenomenon in LWR fuel rods is the waterside corrosion of the clad tubes. The corrosion leads to thinning of the clad tube wall, and also to absorption of hydrogen in the metal. Both effects lead to loss of clad strength and ductility with increasing fuel rod exposure. The corrosion-induced clad embrittlement is known to limit the survivability of high-burnup fuel rods, especially if the rods are subjected to accidents or off-normal operational conditions.

Fuel fission gas release and clad waterside corrosion are thus two important phenomena with relevance to fuel rod integrity at high burnup, and in particular, to the fuel rod integrity under transients and power excursions. The FRAPCON-3.2 computer code (Berna et al. 1997), which is used by the Swedish Nuclear Power Inspectorate to analyse the thermo-mechanical performance of LWR fuel rods, comprise a set of models for these phenomena. Some of these models have limited applicability to high burnup fuel. For instance, the code does not comprise models that explicitly treat the formation of a high-burnup fuel microstructure and its consequences to the fuel behaviour. In the work presented here, such models are formulated and assessed for use within FRAPCON-3.2, together with several other models for application to high-burnup fuel rods.

The report is organized as follows:

Section 2 of the report deals with the behaviour of UO₂ fuel pellets at high burnup. More precisely, the mechanisms behind irradiation-induced fuel restructuring, athermal and thermal fission gas release, fuel pellet grain growth and fuel thermal conductivity degradation at high burnup are discussed, and models for these phenomena are proposed. Section 3 deals with the cladding tubes, and in particular with the waterside corrosion of PWR clad materials. The current models for PWR clad corrosion in FRAPCON-3.2 are revised, and their applicability is extended to Zr-Nb type clad materials (ZIRLO, M5) by use of recent in-reactor corrosion data for high burnup fuel rods, reported in literature. Moreover, the applicability of FRAPCON-3.2 to fuel rods with ZIRLO and M5 cladding is also assessed by comparing the models for clad yield stress and axial growth to measured data for these materials.

2 Models for uranium dioxide fuel behaviour

2.1 Formation of high-burnup microstructure

2.1.1 Background

A restructuring of the UO_2 fuel material takes place at the pellet peripheral rim in high-burnup fuel. This restructuring is characterized by grain subdivision, increase in porosity and depletion of fission gas from the UO_2 matrix, (Matzke, 1995) and (Spino et al. 1996). The resulting microstructure is usually referred to as the 'rim zone structure', which is somewhat misleading, since the microstructure is related to enhanced local burnup and fission rate in combination with low temperature at the pellet rim, rather than to the radial position in itself. Consequently, we will use the term 'high-burnup structure', as proposed by Lassmann et al. (1995), to denote the restructured part of the fuel material.

There is ample experimental evidence that the high-burnup structure starts to form at a local burnup of $60\text{-}70 \text{ MWd}(\text{kgU})^{-1}$ by subdivision of grains at the fuel pellet outer surface and at pores and bubbles close to the surface. At conditions typical of LWR fuel, the pellet radial average burnup is about $45 \text{ MWd}(\text{kgU})^{-1}$ when this restructuring starts at the pellet rim. The fully restructured material has a typical grain size of 200-300 nm, which is much smaller than that of the original material ($\approx 10 \mu\text{m}$). In early investigations, it was not clear whether this grain subdivision resulted from the local build-up of plutonium, or if it was a result of accumulated irradiation damage. From later studies on fuels with different initial enrichments, it is clear that the rim zone formation is due primarily to accumulation of irradiation damage, and not to the generation of plutonium (Kameyama et al. 1994) and (Kinoshita et al. 2000).

The restructured grains are depleted of fission gas, with the fuel matrix containing only about one fifth of the fission gas present within the large original grains, (Mogensen et al. 1999) and (Walker, 1999). Numerous measurements by electron probe microanalysis (EPMA) have shown that the restructured grains contain 0.20-0.25 wt% Xe. EPMA is a local technique, by which the amount of Xe, atomically dissolved in the fuel matrix and comprised in sub-nanometre sized intragranular bubbles, is measured within very small volumes of the material. With the X-ray fluorescence (XRF) and secondary ion mass spectrometry (SIMS) techniques, it is possible to measure the average gas content in larger volumes, which comprise gas also on grain boundaries and in pores. By combining EPMA with XRF or SIMS, it has been shown that only a minor part of the fission gas that is depleted from the grain matrix is released to the rod free volume during the grain restructuring (Mogensen et al. 1999) and (Noirot et al. 2004). The major part of the gas is trapped in newly formed, micron-sized pores, which make the rim zone microstructure appear as cauliflower in micrographs.

The presence of a porous microstructure at the pellet rim may affect the behaviour of high-burnup fuel in several ways (Turnbull, 2002).

Firstly, the high-burnup structure has potential to enhance athermal fission gas release. Secondly, as further discussed in section 2.3, there is concern for degraded thermal conductivity of the porous restructured material. Thirdly, the restructuring of the fuel material may change the deformation behaviour of the pellet, with consequences to the pellet-clad mechanical interaction (PCMI). The potential for gas-induced swelling and fragmentation of the porous high-burnup structure at elevated temperatures should be considered in analyses of accidents and off-normal fuel operation.

The current version of the FRAPCON code (version 3.2) does not comprise models that explicitly treat the formation of a high-burnup microstructure and its consequences to the fuel rod behaviour. Such models have therefore been formulated and assessed for use within FRAPCON-3.2. The models are presented in the following subsections.

2.1.2 Threshold for material restructuring

In order to model the high-burnup fuel microstructure, we first need to define the threshold conditions at which the material restructuring occurs. As mentioned in the preceding section, experimental investigations have revealed that the high-burnup structure starts to form at the pellet outer surface, when a local burnup of 60-70 $\text{MWd}(\text{kgU})^{-1}$ is reached. These numbers are approximate. Distinct thresholds cannot be defined, since the fuel restructuring is a gradual process, and restructured grains may co-exist with original, untransformed grains up to a local burnup of 120 $\text{MWd}(\text{kgU})^{-1}$ (Walker, 1999). The burnup threshold for restructuring is also influenced by the original grain size of the material. Large-grain UO_2 materials have markedly higher resistance to restructuring than small-grained materials (Une et al. 2000) and (Tsukuda et al. 2003).

Several hypotheses have been proposed to explain the observed restructuring of UO_2 at a certain burnup threshold. The restructuring has been attributed to the diminution of potential recrystallization sites in the material due to interaction with vacancy-impurity pairs (Rest & Hofman, 1994) or with fission gas bubbles (Rest, 2004). Other investigators have proposed that the restructuring is caused by build-up of stored energy in the material due to irradiation damage (Thomas et al. 1992), stresses produced as a result of over-pressurized fission gas bubbles (Matzke, 1992), or instability phenomena (Kinoshita, 1997). These hypotheses lead to conflicting conclusions about the influence of temperature and fission rate on the burnup threshold for fuel restructuring.

As an example, Rest and Hofman (1994) proposed an atomistic model for fuel restructuring, in which the stored energy in the material is assumed to be concentrated on a network of dislocation-induced nuclei that diminish with dose, due to interaction with radiation-produced defects. Grain subdivision is assumed to occur when the energy per nucleus gets high enough that the creation of grain-boundary surfaces is offset by the creation of strain free volumes, with a resultant net decrease in free energy of the material. Departing from these assumptions, Rest and Hofman (1994) formulated a theoretical threshold burnup for restructuring of UO_2 , as a function of temperature and fission rate. For simplicity, they postulated that both temperature and fission rate were constant during the entire fuel lifetime. Still, their expression for the burnup threshold is rather complex, and the tenacious reader is referred to the original works for a detailed description of the subject (Rest & Hofman, 1994 and 1995).

The predicted burnup threshold for grain subdivision from their model is shown with respect to fuel temperature and fission rate in figure 2.1. Clearly, the calculated burnup threshold increases markedly at temperatures above 900 K. This trend is not supported by recent experimental data from the international High Burnup Rim Project (HBRP), where UO_2 fuel has been irradiated in the Halden test reactor up to $96 \text{ MWd}(\text{kgU})^{-1}$ under isothermal conditions in order to determine the influence of temperature on the burnup threshold for fuel restructuring. These experiments have shown that the fuel restructuring process is practically unaffected by temperature in the range of 800 to 1300 K, and in particular, that the burnup threshold seems independent of temperature within this range (Kinoshita et al. 2004). Since the atomistic model by Rest and Hofman (1994) is in conflict with these results, the model must be rejected. To this end, we note that Rest has recently revised the model (Rest, 2004). We will return to the revised model in the sequel.

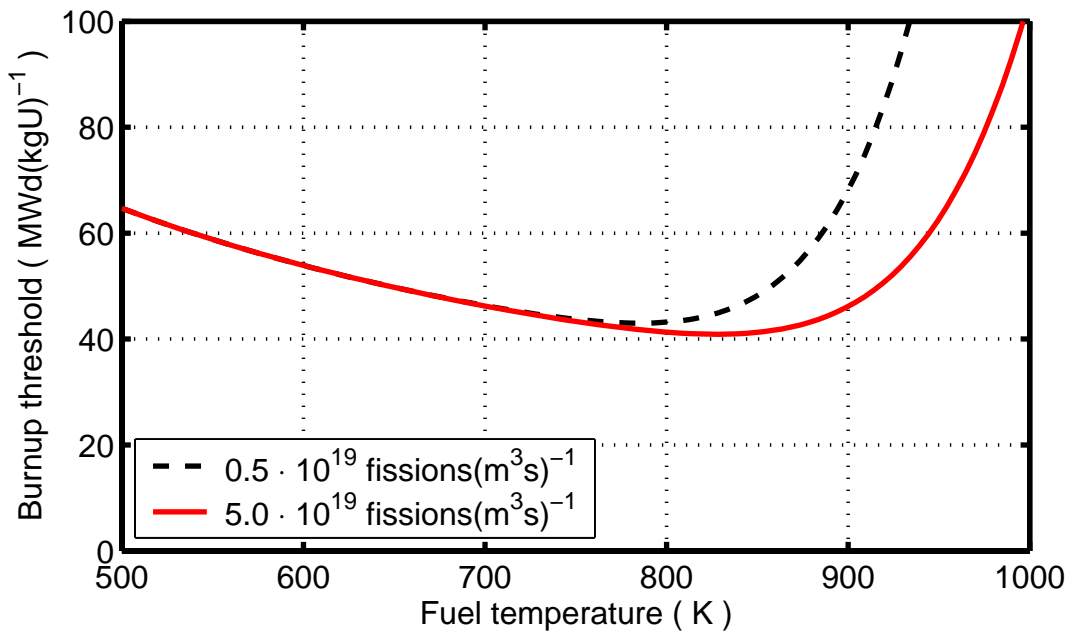


Figure 2.1: Burnup threshold for UO_2 restructuring, calculated with the temperature dependent model by Rest and Hofman (1994). Typical fission rates in LWR fuel under normal operation are bounded by the two values indicated in the figure.

An empirical temperature-independent threshold for fuel restructuring, equal to $70 \text{ MWd}(\text{kgU})^{-1}$ in terms of local fuel burnup, was applied by Lassmann et al. (1995) for modelling the inward propagation of the high-burnup structure towards the pellet centre under steady-state fuel operation. The model was successful in predicting the width of the rim zone as a function of pellet average burnup, but as they themselves pointed out, the approach could only be used up to an average pellet burnup of $70 \text{ MWd}(\text{kgU})^{-1}$. When the pellet average burnup exceeded the local burnup threshold, their model predicted restructuring of the entire pellet cross-section, which is in conflict with experimental observations. To circumvent this problem, they proposed that their fixed burnup threshold should be complemented with a threshold temperature, above which fuel restructuring cannot occur. The HBRP experiments have later revealed that this threshold temperature is $1100 \pm 100 \text{ }^\circ\text{C}$ (Kinoshita et al. 2004).

It should be pointed out that the HBRP experiments were carried out under isothermal irradiation conditions, and it is not clear if the results are directly applicable to conditions in commercial LWRs, where the fuel temperature decreases gradually with time. However, in the sequel, we will assess the applicability of the following condition for fuel restructuring

$$E \geq 70 \text{ MWd(kgU)}^{-1} \quad \text{if } T < 1373 \text{ K.} \quad (2.1)$$

Here, E and T are fuel local burnup and temperature, respectively. For fuel temperatures above 1373 K, fuel restructuring is assumed not to occur. Equation (2.1) is basically the model proposed by Lassmann et al. (1995), extended with the temperature threshold found in the HBRP experiments (Kinoshita et al. 2004). It should be remarked that the notion of distinct thresholds for both burnup and temperature in the restructuring of UO_2 is too simplistic, and that equation (2.1) is merely an empirical relation.

A temperature independent burnup threshold for restructuring of UO_2 was recently proposed by Rest (2004), based on an atomistic model. In short, the model considers the evolution of a cellular dislocation structure, which provides potential nuclei for recrystallization of the material. With increasing burnup, the number of potential recrystallization nuclei is gradually reduced by interaction with nanometre-sized fission gas bubbles. Fuel restructuring is assumed to occur when the density of viable recrystallization nuclei equals the equilibrium number of nuclei, which is calculated based on thermodynamics. The reader is referred to Rest (2004) for a description of the theory behind this model. The resulting condition for recrystallization of UO_2 is²

$$E \geq \frac{3.34 \cdot 10^4}{\varphi^{2/15}}, \quad (2.2)$$

where E is the fuel local burnup in MWd(kgU)^{-1} and φ is the local fission rate in $\text{fissions(m}^3\text{s)}^{-1}$. Hence, according to the model by Rest (2004), the burnup threshold for fuel restructuring is independent of temperature, but weakly dependent on fission rate. It should be remarked that Rest presented equation (2.2) as a threshold for *initiation* of recrystallization, which he distinguished from the subsequent progression and eventual consumption of the original grain structure.

We have implemented equations (2.1) and (2.2) in the FRAPCON-3.2 computer code, in order to assess these two conditions for fuel restructuring. The assessment was made by comparing the calculated evolution of the fuel high-burnup structure with experimental data by Manzel and Walker (2000, 2002), who determined the width of the fuel rim zone as a function of pellet average burnup by optical microscopy of commercial PWR fuel rods. The calculations with FRAPCON-3.2 were done by simulating the operational history of these rods. The fuel rod design data and rod irradiation history that were used in calculations are summarized in appendix A. In the calculations, the conditions for fuel restructuring in equations (2.1) and (2.2) were checked for each radial position (annulus) of the discretized fuel pellet.

² The original condition by Rest is given in terms of accumulated fission density. It is here converted to burnup by use of an assumed energy per fission of 200 MeV.

By repeating this procedure for consecutive time steps through the irradiation history, the inward growth of the restructured zone was calculated as a function of increasing exposure. The results are compared with experimental data by Manzel and Walker (2000) in figure 2.2. The step-like nature of the calculated curves in figure 2.2 reflects the radial discretization of the fuel pellet in FRAPCON-3.2: the pellet is here divided into 25 annuli. Obviously, the model by Lassmann et al. (1995) in equation (2.1) drastically overestimates the width of the rim zone for pellet average burnups exceeding 50 $\text{MWd}(\text{kgU})^{-1}$. Since calculated fuel temperatures are low for the case considered here, the threshold temperature of 1373 K in equation (2.1) does not limit the inward propagation of the rim zone, and at an average pellet burnup of 82 $\text{MWd}(\text{kgU})^{-1}$, the restructured zone is predicted to extend over the entire pellet cross-section. We note that the measured rim width at this burnup is 400-500 μm .

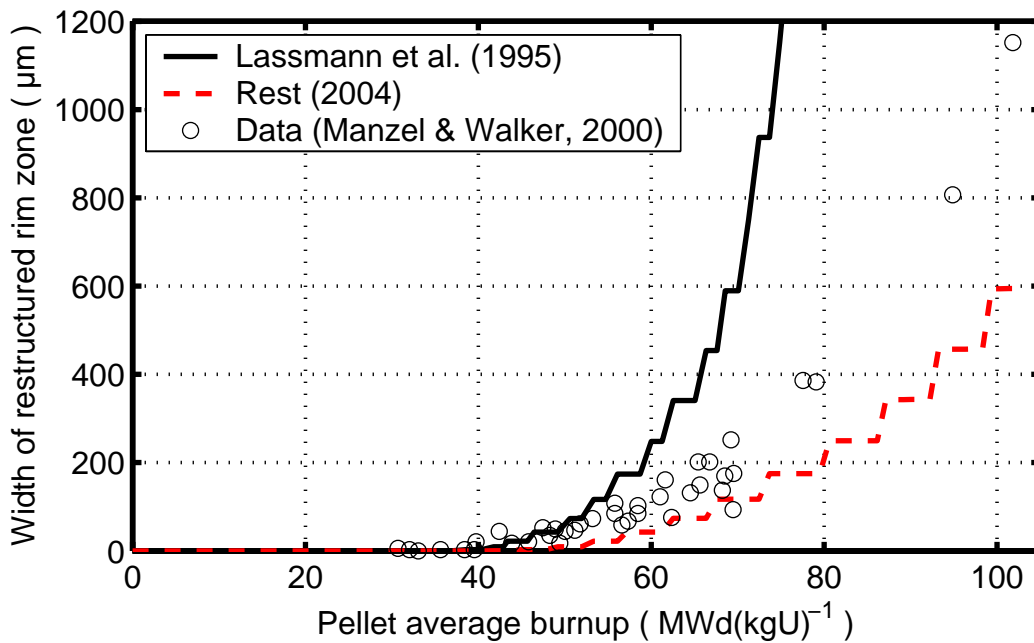


Figure 2.2: Calculated width of restructured zone (rim zone), in comparison with optical microscopy data for UO_2 fuel pellets from commercial PWR fuel rods.

On the other hand, the burnup threshold for fuel restructuring proposed by Rest (2004) underestimates the width of the rim zone over the entire burnup range spanned by the data. However, the trend with respect to burnup is in fair agreement with the optical microscopy data by Manzel and Walker (2000). Moreover, the calculated fuel restructuring is effectively confined to the pellet periphery through the fission rate dependence of the burnup threshold in equation (2.2). Hence, the theoretically based model by Rest seems to capture the trend in data, although it underestimates the width of the rim zone. Consequently, we scale the burnup threshold on the right-hand-side of equation (2.2), to obtain a best fit to the experimental data in figure 2.2. In addition, we introduce an empirical correction factor for the influence of original grain size on fuel restructuring, based on the work of Une et al. (2000).

The resulting condition for UO_2 restructuring is

$$E \geq \frac{2.94 \cdot 10^4}{\phi^{2/15}} \left(\frac{S_o}{10^{-5}} \right)^{0.1}, \quad (2.3)$$

where S_o is the grain size [m] of the fuel before restructuring. Other parameters in equation (2.3) are defined earlier in this section. Equation (2.3) is the condition for fuel restructuring, which we have implemented in FRAPCON-3.2. As shown in figure 2.3, the calculated rim width agrees quite well with measurements over the entire burnup range spanned by the data of Manzel and Walker.

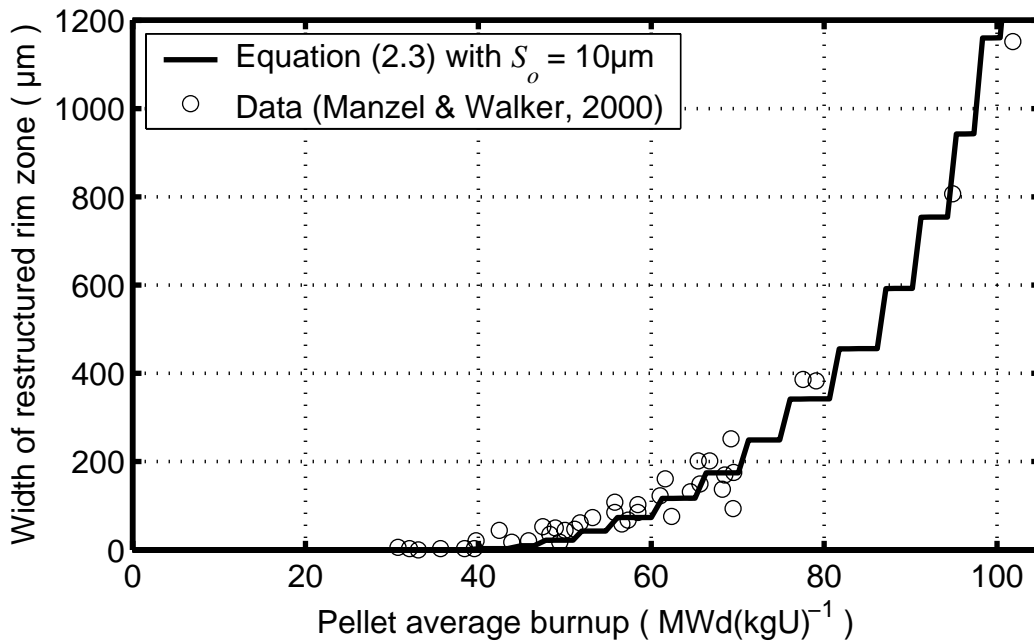


Figure 2.3: Calculated width of restructured zone from equation (2.3), in comparison with optical microscopy data for UO_2 fuel pellets from commercial PWR fuel rods.

In figure 2.4, the predicted influence of fuel grain size on the fuel restructuring process is compared with experimental data by Tsukuda et al. (2003), who measured the width of the restructured rim zone in fuel pellets from high-burnup PWR fuel rods by ceramography. The fuel rods were fabricated with UO_2 fuel pellets with an as-fabricated average grain size of either 9, 12 or 30 μm . The variation in grain size was reached by modifying the manufacturing process, and not by changing the chemical composition of the fuel by additives (Tsukuda et al. 2003). As clearly revealed by the data in figure 2.4, the fuel restructuring is affected by the grain size. The inward growth of the restructured zone was calculated by use of FRAPCON-3.2 and equation (2.3), assuming a fuel as-fabricated grain size of 10 and 30 μm . The model seems to underestimate the width of the restructured zone for pellet average burnups in the range of 40 to 50 $\text{MWd}(\text{kgU})^{-1}$. However, the agreement with experimental data is fair, considering that the calculations were done with approximate input data, due to lack of information about the true irradiation conditions for these fuel rods.

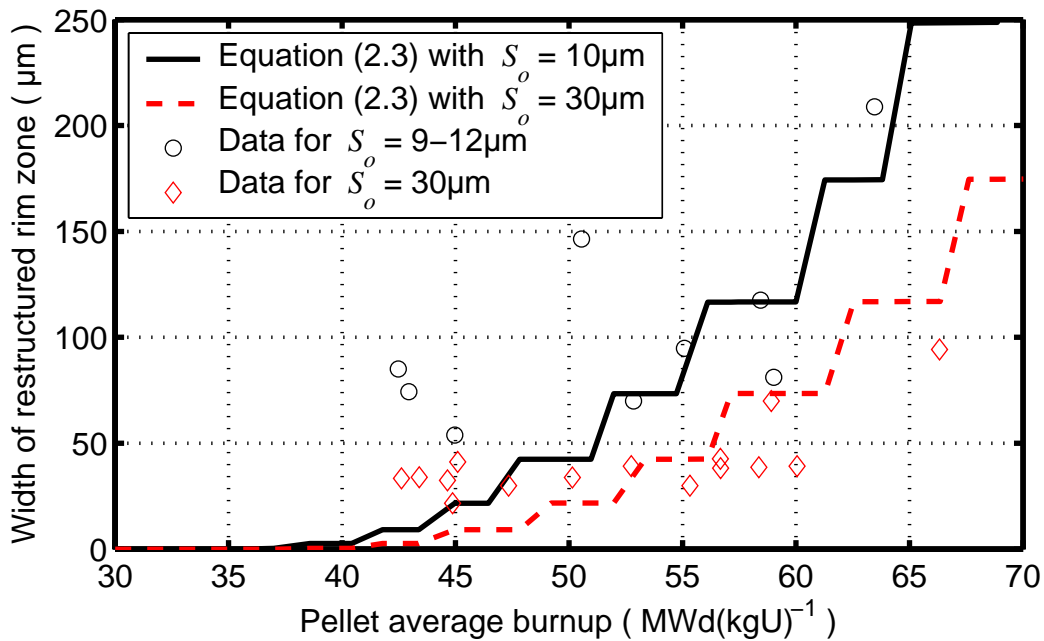


Figure 2.4: Calculated width of restructured zone from equation (2.3), in comparison with optical microscopy data for UO_2 fuel pellets with two different as-fabricated grain sizes (Tsukuda et al. 2003).

2.1.3 Porosity in restructured material

Prior to fuel restructuring, gaseous fission products at the pellet periphery are accumulated predominantly in nanometre-sized intragranular bubbles, although some gas is also found in solid solution and in fuel as-fabricated porosity (Noirot et al. 2004). When the original grains are recrystallized, the intergranular bubbles are swept out of the fuel matrix, and the new grains are free of small-size bubbles. A minor part of the gas may possibly escape to the rod free volume during the recrystallization process, but most of the gas is trapped in bubbles at the newly formed grain boundaries, where they coalesce into micron-sized pores (Kinoshita et al. 2004). Spino et al. (1996) reported that the micron-sized pores form early in the restructuring process, and that the pores are surrounded by a shell with recrystallized material that grows thicker as the restructuring proceeds. They also reported that the mean pore size remains constant at approximately $1.3 \mu\text{m}$, whereas the pore number density increases as the restructuring process continuous. In fully restructured material, the porosity may reach 20 vol% and higher, but it is considerably lower in fuel that experiences mechanical restraint from pellet-clad mechanical interaction. Hence, rim zone porosity above 15 vol% is rarely observed in fuel subjected to PCMI (Une et al. 2000, 2001). Models for build-up of porosity in the restructured material have been presented by Baron et al. (1996) and by Lee et al. (2001). The latter model is fairly simple, and with minor modifications, it lends itself for implementation in FRAPCON-3.2. The fundamental assumptions behind this model are based on the experimental observations mentioned above:

- As the material is restructured, the accumulated fission gas content is trapped within a population of equal-sized spherical pores with radius R_p .

- After restructuring, the gas remains trapped in the pores, whose radii do not change with time. A minor part of the fission gas that diffuse from the interior of grains to the grain boundaries in the restructured material is directly vented to the rod free volume, but most of the gas is without delay collected in newly formed pores, whose radii are also R_p , see section 2.1.4. Hence, within the high-burnup structure, all gas except for gas atoms in solution within the fuel grains is comprised in equal-sized pores. Moreover, the number density of pores in the high-burnup structure increases with exposure, but the pore size is assumed not to change.
- The fission gases within the pores obey the equation of state for an ideal gas.

From the last assumption, we find

$$P_p V_p = n_p k_B T_p, \quad (2.4)$$

where P_p [Pa] and T_p [K] are the pressure and temperature of gas contained in a pore of volume V_p [m³]. The number of gas atoms within the pore is n_p , and k_B is Boltzmann's constant. The gas pressure in the pore is calculated from

$$P_p = P_{ext} + \frac{2\gamma}{R_p} + \frac{\mu b}{R_p}, \quad (2.5)$$

where P_{ext} is the external hydrostatic pressure (mean compressive stress) in the solid material surrounding the pore, and γ , μ and b are the surface tension, shear modulus and Burger's vector of UO₂, respectively. In our implementation of the model in FRAPCON-3.2, P_{ext} is set equal to the pellet-clad contact pressure. Constant values are used for the remaining quantities in equation (2.5), as defined in table 2.1.

The first two terms on the right-hand-side of equation (2.5) correspond to the equilibrium pressure in the pore. The last term is an excess pressure, which is connected with distortion of the crystal lattice (Nogita & Une, 1995). With the material properties given in table 2.1, this overpressure is 45 MPa.

Uranium dioxide material property	Value
Surface tension, γ	[Nm ⁻¹] 1.0
Shear modulus, μ	[GPa] 75
Burger's vector, b	[nm] 0.39
Rim zone pore radius, R_p	[μ m] 0.65

Table 2.1: Properties assumed for the material within the high-burnup structure.

Since we assume that the fission gas inventory outside the grains of the high-burnup structure is contained within the micron-sized pores, the bulk concentration of gas outside the grains, C_{og} [atoms m⁻³], follows from

$$C_{og} = F_p \frac{n_p}{V_p}, \quad (2.6)$$

where F_p is the porosity volume fraction (dimensionless) of the restructured material.

By combining equations (2.4) to (2.6), we find

$$F_p = \frac{C_{og} k_B T}{P_{ext} + (2\gamma + \mu b)/R_p}. \quad (2.7)$$

Hence, equation (2.7) can be used to calculate the local porosity in the high-burnup structure as a function of fuel local fission gas content, temperature and hydrostatic pressure. The fission gas content outside the grains, C_{og} , is in our implementation of the model in FRAPCON-3.2 calculated from the generated amount of gas, minus the gas contained within the restructured grains and gas released by athermal processes and by possible thermal mechanisms; see sections 2.1.4 and 2.2.

The radial variation of porosity in a high-burnup fuel pellet, as calculated through equation (2.7), is in figure 2.5 compared with experimental data by Manzel and Walker (2000). These data were obtained from optical micrographs of a fuel pellet cross section from a commercial PWR fuel rod that reached a peak pellet average burnup of $102 \text{ MWd}(\text{kgU})^{-1}$. The calculated curve in figure 2.5 results from analyses of this rod with FRAPCON-3.2, as described in appendix A.

The as-fabricated porosity of the fuel was 4 vol%, and the step-like raise in calculated porosity from this value at a relative pellet radius of 0.7 marks the boundary to the restructured outer part of the pellet. In the experimental data, the corresponding boundary is found at $r/r_o \approx 0.65$, and there seems to be a gradual transition to the restructured part of the pellet. Moreover, the calculated porosity close to the pellet surface is underestimated. It should be pointed out that both the calculated and measured porosity has a local minimum at $r/r_o \approx 0.9$. For the calculated curve, it is clear that this minimum follows from the product of gas content and temperature in the numerator to equation (2.7): since the gas content increases and the temperature decreases monotonously with pellet radius, the calculated product attains a local minimum at $r/r_o \approx 0.84$. The local minimum for the experimental data is slightly closer to the pellet surface, but the trend in data agrees quite well with the model.

The impact of mechanical restraint on the build-up of porosity within the high-burnup structure is illustrated in figure 2.6. The experimental data are taken from the compilation presented by Une et al. (2000, 2001). By comparing the measured rim zone porosity from eight different experimental investigations, they concluded that mechanical restraint from pellet-clad mechanical interaction has a strong limiting effect on porosity build-up. Fuel samples irradiated under prototypical conditions, i.e. under restraining forces from PCMI, attain a lower degree of porosity than samples irradiated without other mechanical restraints than the weight of the fuel stack. This is clearly revealed by the data in figure 2.6, although there is a considerable spread in measured porosity. The spread is mainly due to the fact that the fuel initial porosity ranged from 2 to 5 vol% in the eight considered studies. Moreover, the porosity in the high-burnup structure was measured by different methods for quantitative image analyses, and the samples were irradiated at various fission rates and temperatures.

The calculated curves in figure 2.6 correspond to analyses of rod 12C3 with FRAPCON-3.2, as described in appendix A.

The porosity was calculated through equation (2.7) by setting the hydrostatic pressure equal to either the pellet-clad contact pressure ('PCMI') or to zero ('No PCMI'). The calculated end-of-life contact pressure was about 40 MPa in this particular case.

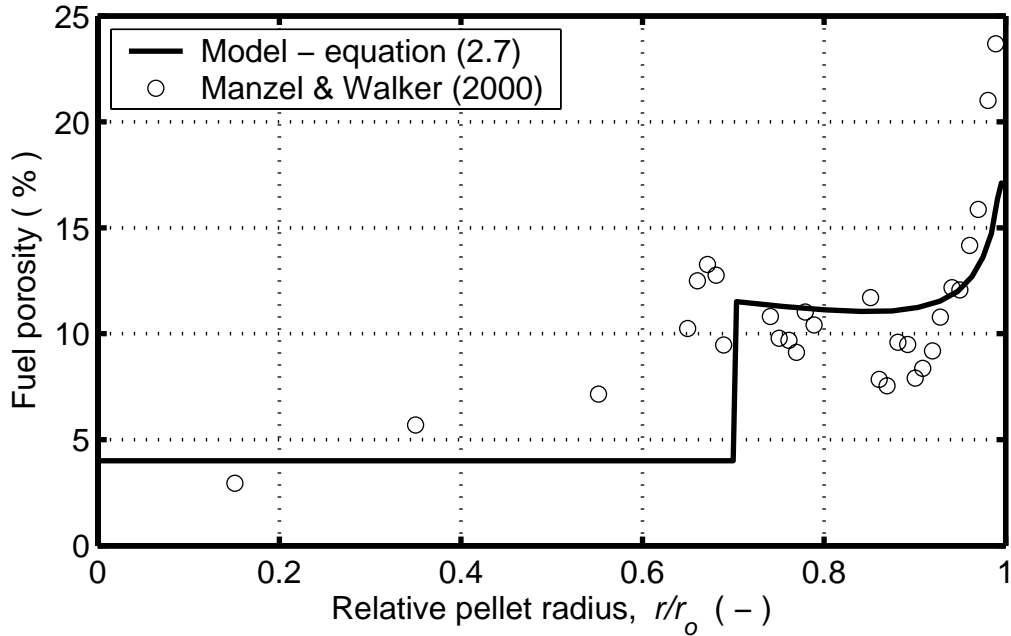


Figure 2.5: Calculated distribution of pellet micron-sized porosity, in comparison with optical microscopy data for UO_2 fuel pellets from commercial PWR fuel. The as-fabricated fuel porosity was 4%. The porosity of the high-burnup structure ($r/r_o > 0.7$) is calculated through equation (2.7), which has been implemented in FRAPCON-3.2.

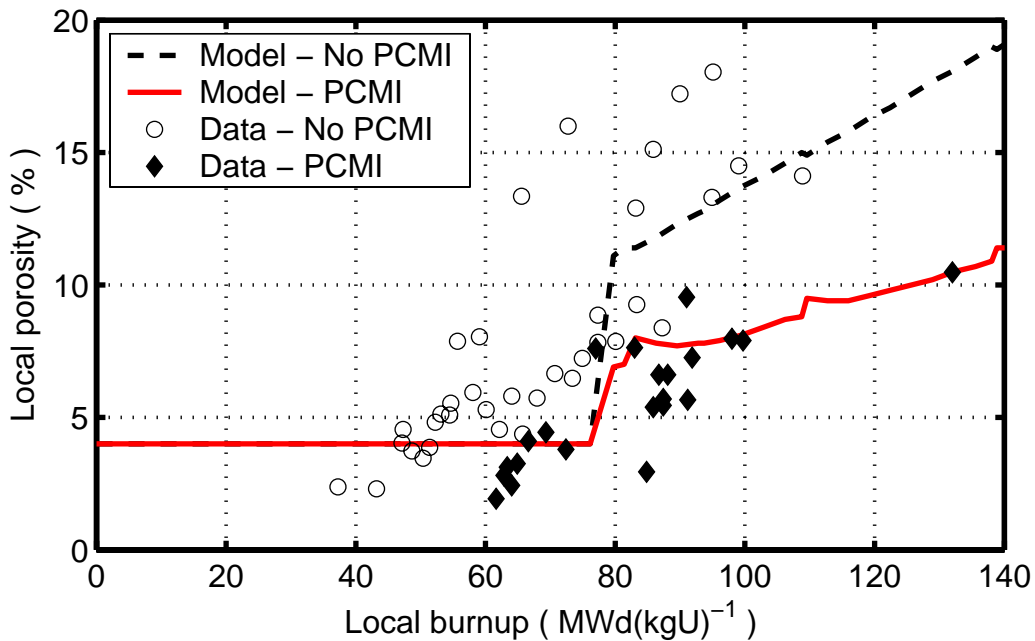


Figure 2.6: Calculated build-up of porosity in the pellet high-burnup structure, in comparison with experimental data from the works of Une et al. (2000, 2001).

Obviously, the model is in fair agreement with data for the case of PCMI, but it underestimates the porosity build-up in fuel samples irradiated without mechanical restraint.

In conclusion, it seems that the outlined approach can be used for calculating the porosity in restructured UO_2 under conditions that are typical of commercial LWR fuel rods at high burnup, i.e. when the fuel pellet is restrained by pellet-clad mechanical interaction. The calculated porosity across the rim zone will be used as input to the correlation for fuel thermal conductivity, as described in section 2.3. Moreover, the rim zone porosity is an essential input parameter for analyses of the fuel rod behaviour under reactivity-initiated accidents.

The model presented here is intended for analyses of the porosity build-up under normal, steady-state fuel operation, and it is not applicable to overpower transients. Under such transients, the overpressurized pores are expected to expand by creep in the surrounding solid material, an effect that is not considered here. It should be pointed out that equation (2.7) implies that the porosity of the high-burnup structure grows linearly with the fission gas content of the material. Hence, the build-up of porosity is not assumed to saturate as burnup increases, unless some kind of excessive fission gas release takes place from the high-burnup structure. However, for typical LWR fuel rods, a gradual attenuation of the porosity build-up is expected, since for normal operating conditions, increasing burnup implies lower fuel temperatures and higher pellet-clad contact pressures.

2.1.4 Athermal fission gas release from restructured material

Fission gas release process in UO_2 fuel can be considered to consist of two mechanisms: an athermal release and thermal release. The athermal release accounts for the contribution of release caused by *direct recoil* of fission fragments within a layer equal to the range penetrated by the fission fragments in the fuel ($\approx 10 \mu\text{m}$), and by a *knockout* mechanism, which is an elastic collision between fission fragments and fission product gas atoms in the fuel (Olander, 1976). Hence, we may write the athermal release rate as a sum of two contributions: $\mathfrak{R}_{\text{ather}} = \mathfrak{R}_{\text{rec}} + \mathfrak{R}_{\text{kn}}$, where $\mathfrak{R}_{\text{rec}}$ and \mathfrak{R}_{kn} are the recoil and knockout release rates, respectively. Both quantities are proportional to the fission rate and the range of fission fragments. Moreover, they depend on the fuel specific surface, i.e. the surface to volume ratio of the solid (S/V). In knockout, release is proportional to the total surface area of the fuel, which includes the surfaces of internal cracks in the fuel pellet, whilst recoil is proportional to the geometric surface area. This is due to the fact that a recoiling fission fragment, with kinetic energy of about 80 MeV, is capable of re-entering any region of the fuel (Lewis, 1987).

In light water reactor fuel, athermal gas release is nearly a linear function of the fuel burnup, up to a burnup of around $40 \text{ MWd}(\text{kgU})^{-1}$. In engineering practice, the athermal gas release fraction, i.e. the ratio of released to produced gas, is calculated according to $F_{\text{ath}} = CE$ where E is the fuel burnup [$\text{MWd}(\text{kgU})^{-1}$] and C is a constant of proportionality. For example, Lorenz (1979) found that $C=8.5 \times 10^{-5}$, based on evaluation of athermal fission product gas release data obtained from rods irradiated up to an average burnup of around $40 \text{ MWd}(\text{kgU})^{-1}$.

As mentioned in section 2.1, the high-burnup microstructure in the pellet rim zone has potential to enhance the athermal fission gas release. One of the first major experimental programs directed towards fission gas release in high-burnup light water reactor fuel was the international High Burnup Effects Program (HBEP), in which the fission gas release in altogether 82 well-characterized fuel rods with various designs and with rod average burnups in the range of 22 to 69 MWd(kgU)⁻¹ were studied (Barner et al. 1993). An upper-bound correlation, fitted to experimental data, showed that an increase in fractional fission gas release by at most 4% could be expected at a pellet average burnup of 80 MWd(kgU)⁻¹.

Some investigators have proposed that this fission gas release occurs as a direct and immediate consequence of the fuel restructuring (Sontheimer & Landskron, 2000). However, studies of restructured fuel material with XRF and SIMS have revealed that no appreciable fission gas release occurs as a direct consequence of restructuring, see e.g. the works of (Mogensen et al. 1999) and (Noirot et al. 2004). The same conclusion has also been drawn from the High Burnup Rim Project, where the fission gas content of restructured UO₂ fuel samples was determined by high-temperature annealing of the material (Kinoshita et al. 2004).

Other investigators have argued that the enhanced athermal gas release is an indirect effect of the restructuring. For instance, Bernard et al. (2002) have pointed out that the usual athermal mechanisms for fission gas release, recoil and knockout, are enhanced by an increase in the specific surface (S/V) of the porous restructured material. This theory seems plausible, but according to several experimental observations, the rim zone porosity is not interconnected, and should therefore not significantly increase the fuel specific surface (Spino et al. 1996) and (Une et al. 1997). An alternative hypothesis to the increased fission gas release rate from the restructured material is due to Lassmann et al. (2000), who recognized that irradiation enhanced athermal diffusion from the interior of the small restructured grains to the grain boundaries is sufficiently fast to explain the observed matrix depletion of gas, and that the same mechanism could possibly contribute to enhanced fission gas release from the pellet rim zone.

Hence, there is currently no general consensus on how the enhanced fission gas release from the high-burnup structure occurs. Further experimental data are needed to unambiguously identify the physical processes behind the fission gas release from the restructured material, before mechanistic models for the release process can be formulated. In the current version of FRAPCON, fission gas release from the high-burnup structure is considered by assuming an additional contribution to the athermal release, when the pellet average burnup exceeds 45 MWd(kgU)⁻¹. The model is a purely empirical upper-bound correlation, which is based on experimental data from the HBEP (Barner et al. 1993). An obvious weakness with this simple approach, in which the release is correlated to the pellet *average* burnup, is that the true radial distributions of burnup and fission product gases at the pellet rim are not considered.

For this reason, we have introduced a new model for rim zone athermal fission gas release in FRAPCON-3.2. In contrast to the standard model in FRAPCON, the new model is locally applied, which means that the model is applied to radial nodes (annuli) located within the restructured part of the fuel pellet.

The model thus relies on the calculated evolution of the restructured rim zone, as described in section 2.1.2. Moreover, the model makes use of the governing equations for diffusional gas transport to the grain boundaries, defined in section 2.2.2. The key assumptions behind the new athermal fission gas release model are as follows:

- In the restructured part of the fuel pellet, the original grain size is reduced to 0.3 μm . This implies a significant reduction of the diffusion length for intragranular gas atoms, which means that gas arrives to the grain boundaries at a significantly higher rate in the restructured material than in the original material. From the characteristic time for gas diffusion, defined in section 2.2.6, we find that the rate is increased by a factor $(S_o/S_n)^2$, where S_o and S_n are the sizes of the original and restructured grains, respectively. Consequently, diffusion of gas to the grain boundaries may be significant in the rim zone, even though the temperature and diffusivity are low.
- A certain fraction of the fission gas that arrives to the grain boundaries by diffusion from the interior of restructured grains is directly vented and released to the rod free volume. The remaining gas is supposed to be trapped in micron-sized pores, as described in section 2.1.3. From evaluations of fission gas release data from low-power LWR fuel rods at high burnup, the aforementioned release fraction is set to 0.30.

The advantage of this model, in comparison with the current empirical correlation for rim zone athermal fission gas release in FRAPCON-3.2, is that the model is well integrated and consistent with the proposed models for fuel restructuring and thermal fission gas release. Hence, the fission gas release from the high-burnup microstructure is calculated with consideration of the true width of the rim zone and the local conditions (yield and diffusivity of fission gas) within the restructured material.

2.2 Thermal fission gas release

2.2.1 Background

Gases xenon and krypton, produced during fission of uranium and plutonium isotopes, have low solubility in UO_2 ; hence, after a relatively short irradiation period a large number of fission gas filled bubbles are generated within the fuel grain. Fission gas bubbles in grains remain small, less than 30 nm (Matzke, 1980), whereas lenticular bubbles up to a few microns can be observed at grain boundaries (Turnbull & Tucker, 1974). It is generally accepted that the process of irradiation-induced re-solution is responsible for the destruction of intragranular bubbles (Turnbull, 1980), ensuing a large population of small bubbles and ample fraction of produced gas atoms in enforced solution. The gas atoms in the solution migrate to the grain boundaries unless the bubbles trap them. The re-solution process should also act on the intergranular gas bubbles; however at the grain boundary the abundance of vacancies allow bubbles to grow to larger sizes. When these bubbles interlink, they form a tunnel network (Tucker & Turnbull, 1975), through which a fraction of gaseous fission products is released into the free volume of fuel rod increasing the internal fuel rod pressure. The bubble interlinkage is a cyclic process, since the tunnel network can close again under the effect of surface tension when the outgoing flow of gas atoms offset their supply.

In the past decades there have been many efforts to develop physically based theoretical frameworks for calculations of fission product gas release in nuclear fuel. From our vantage point, these comprise seminal works of Booth and Kennedy (Booth, 1957) on intragranular diffusional release and Speight (1969), which included the effect of gas precipitation, re-resolution and grain boundary saturation and release. The problem of time varying parameters (diffusion coefficient and gas production rate) was analysed among others by Matthews and Wood (1980), and later by Forsberg and Massih (1985a) analytically. Moreover, Forsberg and Massih (1985b, 1986) extended the time-varying conditions to include the effect of re-resolution and the intergranular gas release. Lassmann and Benk (2000) and Lassmann (2000) have recently evaluated the accuracy of these methods. Moreover, Hermansson and Massih (2002) have analysed the generality and accuracy of the original Forsberg-Massih model rigorously. The current model for thermal fission gas release in FRAPCON-3.2 is claimed to follow the work by Forsberg and Massih (1985b), but in reality, the implemented algorithm differs from their work (Lanning et al. 1997a). This was observed by Jernkvist and Massih (2002), who introduced a corrected algorithm for the fission gas release model into the SKI version of FRAPCON-3.2.

At temperatures where ample grain growth occurs, other processes than atomic diffusion may contribute to the accumulation of gases on grain boundaries. Grain boundary movement can sweep up fission gas atoms more rapidly than they could have arrived at the boundary by diffusion (Hargreaves & Collins 1976). The Forsberg-Massih model was reformulated and extended to account for diffusional release under grain growth (Forsberg et al. 1994). The results of this formalism,³ based on analytical calculations, were compared with accurate numerical analysis of the proposed governing equations (Hede 1994). A more detailed theoretical description of this model is presented in (Forsberg & Massih, 2001). A general theoretical method for calculation of the release of volatile fission gas products has been provided by Paraschiv et al. (1999). This method models the phenomena of grain growth, grain boundary bubble growth and re-resolution based on their earlier studies on the release of stable fission product gases from nuclear fuel.

The moving boundary equation (Forsberg & Massih 2001) does not account for the detailed behaviour of the grain boundary gas atoms during irradiation. The interconnection of gas bubbles is assumed to occur when the grain boundary gas concentration of gas atoms reaches a saturation concentration, N_{sat} , determined by the equation of state for the gas (Forsberg & Massih 2001, White & Tucker 1983).

Kogai (1997) presented a pragmatic model to describe the behaviour of grain boundary gas atoms. He partitioned the grain boundary into two zones, namely the grain boundary surface, where fission gas atoms are in solid solution, and the intergranular bubbles, where they exist in pockets of gas. Fission gas atoms arriving to the grain boundary are placed on the grain boundary surface and the intergranular bubbles, depending on the ratio of the bubble coverage to the total area of grain boundary. The gas atoms on the grain boundary surface diffuse to the intergranular bubbles in the presence of a temperature gradient.

³Time evolution of gas concentration in the grain and grain growth (using the same grain growth model) were evaluated.

Intergranular bubbles are taken to be spherical; they grow and shrink depending on the difference between the bubble pressure and the external hydrostatic stress. The density of intergranular bubbles are supposed to be constant before the interlinkage, and then it is decreased with the growth of bubbles after the geometrical interlinkage point. Kogai (1997) verified his model against fission gas release data obtained from highly irradiated fuel, where temperatures were also measured.

Van Uffelen (2000, 2002) extended Kogai's model and put forward a more detailed description of precipitation of fission products at grain boundaries. Van Uffelen's model accounts for changes of fuel chemistry during irradiation and can distinguish between the behaviour of different migrating species. The model comprises the effect of irradiation-induced resolution associated with the intragranular and intergranular gas bubbles. As discussed by Van Uffelen (2000), precipitation of fission products can occur at different types of "traps", e.g. at grain boundaries, line defects, gas filled bubbles, pores and metallic precipitates (Walker et al. 1988). Also, fission products such as caesium and iodine can get immobilized by means of chemical interaction with the UO_2 fuel and other fission products, e.g. CsI. Hence, the precipitation of fission products depends on fuel temperature and burnup, the particular species, fuel stoichiometry, as well as on the number density and size of the trapping centres. Van Uffelen has analysed the effect of the trapping properties on the precipitation rate in grain boundaries according to various studies (Van Uffelen, 2000). The rate of grain boundary precipitation is quantified in terms of a quantity called the capture rate coefficient (Van Uffelen, 2000). As a result he has found that the cell model with a source term provides a suitable relation for the capture rate coefficient, since it accommodates all the important parameters affecting this quantity.⁴

Another issue of interest in this regard is the importance of grain boundary gas diffusion to the gas release process. It is generally believed that thermal fission gas release occurs via interlinkage of grain boundary gas bubbles. Olander and Van Uffelen (2001) have investigated the role of grain boundary diffusion in fission gas release. Their model calculations indicate that in the presence of a population of intergranular gas bubbles with the areal density and fractional coverage observed in irradiated fuel, a xenon atom will be trapped after a migration distance in the grain boundary equal to the size of the grain (around 8 micron). Based on this result, they conclude that grain boundary transport is not a release mechanism for fission gas in irradiated fuel.

Fission gas bubbles in UO_2 grain remain small (≤ 30 nm) throughout the irradiation period (Matzke, 1980), since the effective irradiation-induced re-resolution limits their growth. The bubbles are virtually immobile at least up to temperatures of 2100 K. Also, it is argued that bubbles of radii less than 50 nm are pinned by line defects (dislocations) and they in turn immobilize bubbles in the 10 nm range (Olander, 1976). Accordingly, in light water reactors under normal conditions and even during moderate power transients, gas atom diffusion is the prevailing fission gas release process (Combette et al. 1999).

⁴ The cell model assumes the presence of a regular array of traps in the matrix consisting of fission gas bubbles. A unit cell defines a capture surface, which surrounds each gas bubble. The entire grain surface is divided into N identical cells (circles), each cell containing one trap at its centre. The diffusion equation governing the spatial-temporal distribution of gas concentration is solved with appropriate boundary condition in each cell.

In this section, we outline a general method for calculation of thermal fission product gas release by gas atom diffusion, irradiation-induced re-solution, grain boundary saturation, and grain boundary sweeping in UO₂ fuel under time varying temperature loads. We suppose that UO₂ grains are spherical of equal size. Then the diffusion equation for gas atoms in the grain, which allows for the time variations of gas diffusion coefficient, gas production rate, and grain size (moving boundary), is formulated for an equivalent spherical grain. The equation is subjected to a boundary condition, which accounts for grain boundary gas accumulation, re-solution (to the grain), and grain boundary saturation prior to release. A kinetic equation for grain growth is coupled to the above boundary value problem. Moreover, the correlations used for the calculation of UO₂ grain growth during irradiation are reappraised in light of experimental data, and revised correlations that treat the data more appropriately have been proposed. The governing equations for gas diffusion problem and some sample calculations were briefly presented in an earlier overview paper (Forsberg et al. 1994) and a more detail calculation was presented in (Forsberg & Massih 2001). Here, an outline of the main equations is presented. The obtained equations are used to calculate fission gas release and grain growth as a function of irradiation time for different isotherms.

2.2.2 Gas release model: governing equations

The fission gas release equations considered here originate from the seminal works of Speight (1969). Speight considered the diffusion of fission gas atoms in a spherical grain of UO₂, which contains a fixed number of saturated traps, see figure 2.7. The gas concentration in the trap can be labelled by M to distinguish it from the matrix or dissolved gas K . Absorption of the matrix gas into the traps takes place at a rate g ; and re-solution, from the traps back into the matrix, occurs at a rate ν_g . Thus, the governing equations are expressed as

$$\left. \begin{aligned} \frac{\partial K(r,t)}{\partial t} &= D\nabla^2 K(r,t) - gK(r,t) + \nu_g M(t) + \beta \\ \frac{dM(t)}{dt} &= gK(r,t) - \nu_g M(t) \end{aligned} \right\}. \quad (2.8)$$

where D is the gas diffusion coefficient in the UO₂ lattice and β is the gas production rate. The total gas concentration is

$$C(r,t) = K(r,t) + M(t). \quad (2.9)$$

Speight assumed that the gas bubbles are saturated and hence a steady-state prevails, giving

$$\frac{dM}{dt} = 0; \Rightarrow \frac{g}{\nu_g} = \frac{M}{K}. \quad (2.10)$$

This means that the ratio of the capture rate to the re-solution rate equals the ratio of the gas concentrations in the bubbles to that in the matrix.

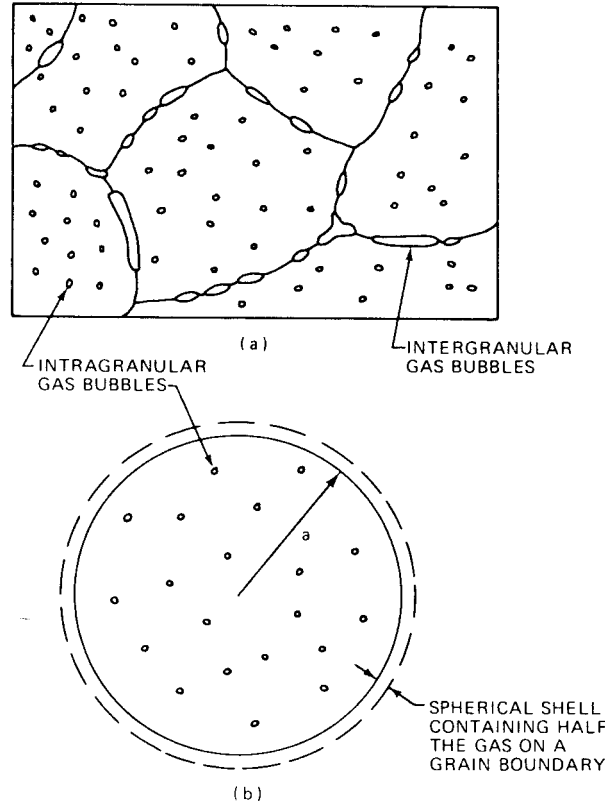


Figure 2.7: Schematic visualization of gas bubbles in UO_2 grains and on grain boundaries (a) Realistic configuration, (b) Idealized spherical grain employed in Speight's model (1969); from Olander (1976).

Combining equations (2.8)-(2.10), we obtain

$$\frac{\partial C(r,t)}{\partial t} = D_{eff} \nabla^2 C(r,t) + \beta \quad (2.11)$$

with $D_{eff} \equiv \frac{v_g D}{v_g + g}$.

The capture rate depends on the concentration of gas bubbles in the grain, C_b , which following Ham (1958), it can be estimated according to

$$g = 4\pi DC_b \bar{R}_b, \quad (2.12)$$

where \bar{R}_b is the mean bubble radius. The re-solution rate may be defined as the probability per second that a gas atom within a bubble undergoes re-solution. It is proportional to the fission rate φ and the fission fragment range l (Turnbull 1980). It is expressed as

$$v_g = 2\pi\varphi l (\bar{R}_b + \delta)^2, \quad (2.13)$$

where δ is the damage radius of a fission fragment, estimated to be around 1 nm (Turnbull 1980).

Equation (2.11) is reformulated to account for the problem of fission product gas release under time varying temperature (Forsberg et. al., 1994). The differential equation for concentration of gas atoms at position r in a spherical grain of radius R at time t , $C(r, t)$ is given by

$$\frac{\partial C(r, t)}{\partial t} = D(t) \nabla_r^2 C(r, t) + \beta(t) \quad \text{for } 0 < r < R(t), \quad (2.14)$$

where we have dropped the subscript *eff* from the effective diffusivity D_{eff} for convenience. The boundary conditions imposed on $C(r, t)$ are

$$\frac{\partial C(0, t)}{\partial r} = 0 \quad (2.15)$$

$$\text{and } C(R(t), t) = \frac{B(t) N(t)}{D(t)}. \quad (2.16)$$

The initial condition is $C(r, 0) = 1$. Here $B(t) = v_b \lambda/2$, v_b is the grain boundary re-resolution rate and $\lambda/2$ the re-resolution depth from the grain face. All the considered variables are time dependent. The boundary condition (2.16) was first used by Turnbull (1974), in a time invariant form, in order to account for the presence of intergranular bubbles situated at the surface $r = R$. It signifies that the sink at grain boundary is imperfect and the irradiation-induced re-resolution is a controlling mechanism for grain boundary saturation.

The total amount of gas $G(t)$ per unit volume in a grain of radius R and on its boundary is written as

$$G(t) = \frac{3D(t)C(R, t)}{2R(t)B(t)} + \frac{3 \int_0^R r^2 C(r, t) dr}{R^3(t)}. \quad (2.17)$$

Here, the first term on the right hand side of equation (2.17) expresses the amount of gas residing on the grain boundary in equilibrium with the gas inside the grain, whilst the second term represents the amount of gas inside the grain whose distribution is governed by the diffusion equation.

We assume that the ratio $B(t)/\beta(t)$ is time independent, since both v_b and β are proportional to the fission rate. If no gas is released, we have

$$G(t) = \int_0^t \beta(s) ds. \quad (2.18)$$

When concentration of gas at the grain boundary reaches a certain saturation value, $C_s(t)$, given by

$$C_s(t) = \frac{B(t) N_{sat}}{D(t)}, \quad (2.19)$$

then gas release will occur, where N_{sat} is the area density of gas atoms at grain faces at saturation.

The amount of release F is calculated according to

$$F(t) = \int_0^t \beta(s) ds - G(t) . \quad (2.20)$$

The analytical solutions for equations (2.14)-(2.17) have been detailed elsewhere (Forsberg & Massih 2000 & 2005); therefore they are not repeated here.

2.2.3 Grain growth description

2.2.3.1 Modelling overview

Grain growth of polycrystalline materials such as UO_2 is a thermally activated process. Here, we consider only the so-called *equiaxed normal* grain growth, which is characterized by the following two main attributes (Atkinson 1988):

- *Uniformity*- Relatively speaking, there is a narrow range of grain sizes and shapes.
- *Self-similarity* – A simple change in scale is enough to render the distribution of sizes at two different time points coincide. Meaning that the form of the distribution is time invariant.

Normal grain growth is dissimilar to abnormal grain growth (also called secondary recrystallization) in which a few large grains extend and consume a matrix of smaller ones, eventually interrupting the normal grain growth.

Burke and Turnbull (1952) developed one of the first physically motivated grain growth models. They deduced a parabolic relation for the temporal evolution of grain size. They accounted for the migration of a boundary by transport of matter under a pressure due to surface curvature. It was argued that the boundary tends to migrate toward its centre of curvature, since this reduces the area of boundary and hence its associated energy. By assuming the mean radius of curvature of the boundary is proportional to the average grain size $S = 2R$, they showed that

$$\frac{dS}{dt} = \frac{k}{S} , \quad (2.21)$$

where k is the rate of the boundary motion, which is temperature dependent. Integration of this equation leads to parabolic grain growth description

$$S^2 - S_0^2 = kt , \quad (2.22)$$

where $S = S(t)$ is the mean grain size at time t and S_0 is the initial mean grain size. In UO_2 fuel and many other ceramic materials, however, the exponent of S is found to be larger than 2. For example, Ainscough et al. (1973) found that the exponent n in $S = kt^n$ is always less than 0.36 and hence equation (2.22) does not provide a quantitative description of UO_2 grain growth.

It has been known that both pores and inclusions (e.g. fission products) can hamper the grain boundary motion (Burke & Turnbull, 1952).

Burke and Turnbull have proposed an equation, which accounts for the retarding forces that arise from the interactions of grain boundaries with inclusions and pores. It can be expressed in the form

$$\frac{dS}{dt} = k \left(\frac{1}{S} - \frac{1}{S_m} \right), \quad (2.23)$$

where S_m is the limiting grain size at which grain growth ceases. Ainscough et al. (1973) utilized this equation to describe grain growth kinetics of UO_2 fuel and determined the temperature dependence of the parameters k and S_m , which have Arrhenius form, see table 2.2. Moreover, they scaled S_m with fuel burnup in the manner: $S_m \Rightarrow S_m / (1 + 0.2E)$, where E is the local burnup $[\text{MWd}(\text{kgU})^{-1}]$, in order to account for the accumulation of fission products in grain boundaries during irradiation.

The next level of grain growth analysis is the so-called effective field or the mean field approach (Atkinson 1988), which treats the change in size of an isolated grain embedded in a field of other grains. It represents the effective influence of the entire array of grains. This approach was initially proposed by Feltham (1957) and further developed by Hillert (1965). It may be explained as follows: During normal grain growth, there is an increase in the mean grain size and a decrease in the number of grains in the system. This process can be observed as the change of grain size distribution $f(S,t)$ with time, figure 2.8. This change is a result of (i) a diffusion-like process, where grains larger than the mean size get larger due to the concentration gradient (df/dS) and (ii) a velocity ($v = dS/dt$), caused by a driving force that tends to reduce the boundary curvature.

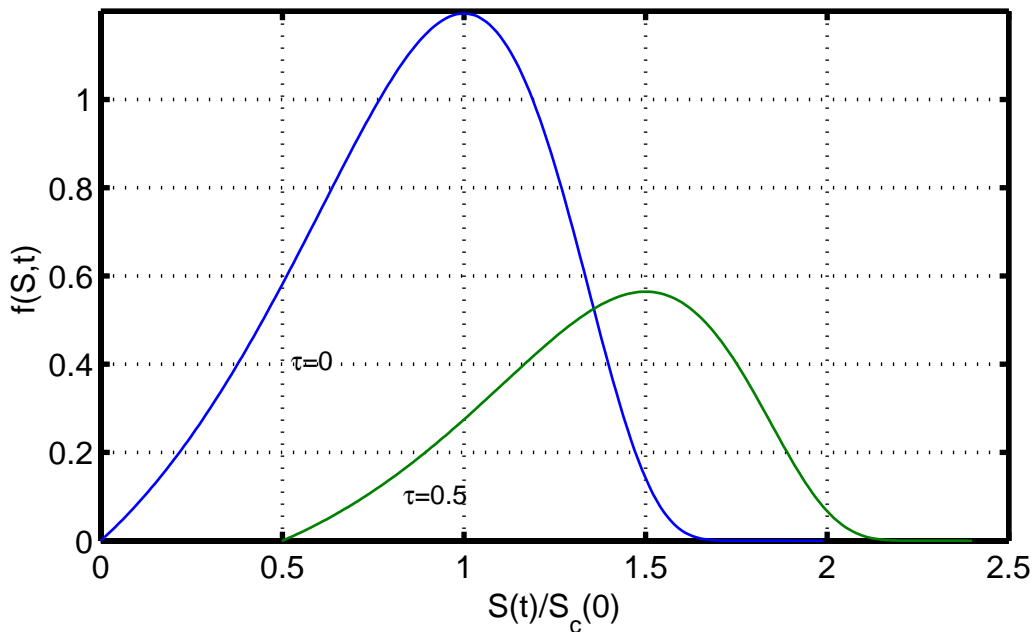


Figure 2.8: Evolution of grain size distribution à la Hillert (1965). Here, τ is the normalized time, i.e. the actual time divided by the time constant. Note that we have normalized the grain size with the initial critical size.

Feltham (1957) and Hillert (1965), as in (Burke & Turnbull, 1952), assumed implicitly that the driving force dominates the normal grain growth and that the driving force is related to the elimination of grain boundary area. There are two possible ways to determine a mean growth rate: (a) Using a particular expression for the drift velocity and then calculate the grain size distribution; (b) using an experimentally determined expressions for v and f . Hillert (1965) selected the first approach, while Feltham (1957) the second.

Hillert utilized concepts from the Lifshitz–Slyozov theory (Lifshitz and Slyozov 1961) to derive the kinetic equation of growth and a grain size distribution function $f(S,t)$. Hillert’s kinetic equation for the evolution of grain is similar in form as in equation (2.23):

$$\frac{dS}{dt} = \alpha\mu\gamma\left(\frac{1}{S_c} - \frac{1}{S}\right), \quad (2.24)$$

where α is a geometric factor, μ the mobility of the boundary, γ the surface energy of the boundary, and S_c the critical grain size which varies with time; for $S > S_c$ the grain will grow, whereas for $S < S_c$ the grain will shrink.

Hillert’s model (Hillert, 1965), which was originally formulated for metals, was adopted to oxide nuclear fuel by El-Saied and Olander (1993) and Paraschiv et al. (1997), where the latter authors also evaluated the original theory of Lifshitz and Slyozov (1961). Paraschiv et al.’s evaluation indicates that the original Lifshitz and Slyozov model provides a more suitable description of grain growth than Hillert’s model. Above all, they find that the fission gas release predictions based on Lifshitz–Slyozov’s theory for normal grain growth are more realistic than predictions based on Hillert’s, mainly because of the smaller grain sizes predicted at the end of irradiation by the former theory.

The mean field approaches alluded here are only a first approximation to the modelling of normal grain growth, which is a complex kinetic phenomenon. It should be treated through the kinetic equations of a distribution function with consideration given to the interactions between the grains. The topic of grain growth modelling is a subject of an active research; a recent overview can be found in (Phillips, 2001).

2.2.3.2 Present grain growth model for fuel behaviour

For the analysis of fuel behaviour under power ramps, we have chosen a single grain modelling approach of Burke and Turnbull (1953) following the work of Ainscough et al. (1973). However, the UO₂ grain growth data of fuel subjected to power ramps obtained within the Third Risø Project (Bagger et al. 1994) indicate that the Ainscough et al.’s model is unsuitable to the power transient case in which a few hours of grain growth follows many days of burnup accumulation. This can be due to the fact that the correlations employed by Ainscough et al. (1973) for $k(T)$ and $S_m(T)$ were intended to calculate the grain size when the burnup increases as the grain growth proceeds. There has been a recent attempt (Khoruzhii et al. 1999) to extend the Ainscough et al. (1973) model by adding a power density dependence term $1/S_{irr}(T)$, while dropping the burnup dependence of $S_m(T)$ in the right hand side of equation (2.23).

We have attempted to revise the Ainscough et al. (1973) correlations by closely examining the Risø data (Bagger et al. 1994) obtained by power ramp tests. More specifically, we have modified both $k(T)$ and $S_m(T)$ expressions in order to capture the data reported by Bagger et al. (1994).

But let us first express the Burke-Turnbull equation (2.23) in a normalized form by introducing the following dimensionless parameters for grain size and time:

$$u = \frac{S}{S_m}; \quad v = \frac{t}{S_m^2/k}. \quad (2.25)$$

Here S_m^2/k denotes a *time constant* for the grain boundary motion.⁵ Hence equation (2.23) is re-expressed in normalized form

$$\frac{du}{dv} = \frac{1-u}{u}. \quad (2.26)$$

This equation can be integrated to give:

$$v = \ln\left(\frac{u_0 - 1}{u - 1}\right) + u_0 - u, \quad (2.27)$$

where $u_0 = S_0/S_m < 1$ is the initial (as-fabricated) normalized grain size. Equation (2.26) is a non-linear equation that can be solved numerically to calculate u vs. v , then using relations (2.25) one can find the actual time evolution of grain size. Figure 2.9 shows “master curves”, illustrating grain growth using equation (2.27) for several values of the initial grain size.

Bagger et al. (1994) report empirical data based on measurements of grain size limit vs. temperature in UO₂ fuel that was subjected to a power ramp with a ramp terminal level (RTL) of 45 kWm⁻¹ for a hold time of 62 h. In addition, they provide data on grain size vs. temperature for two fuel specimens, namely CB6-19 which experienced an RTL of 45 kWm⁻¹ and CB6-29 sample with RTL of 39.8 kWm⁻¹. The data for the two samples fall into the same curve, except that the latter data for 45 kWm⁻¹ extend to higher temperatures. This means that the increase in power density only widens the temperature field, but the form of grain size vs. temperature relation remains invariant. Furthermore, the Risø data indicate that the threshold temperature for grain growth is about 1550 K.

We have fitted an Arrhenius type relation for $S_m(T)$ to the data of Bagger et al. (1994) with consideration given to the initial grain size S_0 of the examined fuel, which was about 6 μm. We formulate a correlation in the form

$$S_m(T) = \begin{cases} S_0 & \text{for } T < T_g \\ A \exp(-Q/T) & T \geq T_g \end{cases}, \quad (2.28)$$

where we have chosen $T_g = 1550$ K; other constants are given in table 2.2.

⁵ Note that the variable k is the diffusivity and is a product of the mobility of the boundary and the surface energy of the boundary.

Figure 2.10 depicts measured data (symbols) vs. the outputs of the correlations for $S_m(T)$. It is seen that the AOW (Ainscough, Oldfield, Ware) correlation overestimates the measured data substantially and the adjusted curve fit is a retrodiction according to equation (2.28), which can be regarded as an upper bound of the data.

Parameters in equation (2.23), Ainscough et al. (1973)	Unit
$k = 5.24 \times 10^7 \exp(-32114.51/T)$	$\mu\text{m}^2\text{h}^{-1}$
$S_m = 2.23 \times 10^3 \exp(-7260/T)$	μm
Parameters in equation (2.23), present analysis	
$k = 1.048 \times 10^7 \exp(-32114.51/T)$	$\mu\text{m}^2\text{h}^{-1}$
$S_m = 615.59 S_0 \exp(-9955/T)$	μm

Table 2.2: Temperature dependence of parameters deduced by Ainscough et al. (1973) for grain growth of un-irradiated UO_2 fuel and the corresponding values obtained by our analysis of Risø data; T is the absolute temperature and S_0 the initial grain size.

In figure 2.11, we have plotted the results of our calculations, grain size vs. temperature, made with the AOW model vs. the present model. The present model is adjusted to bound the Bagger et al. (1994) data, while the AOW model substantially overestimates grain growth. The time evolution of grain growth is calculated by solving the ordinary differential equation (2.26) numerically. The results for a constant temperature of 2000 K are depicted in figure 2.12, where the prediction of the AOW model is compared with the present model.

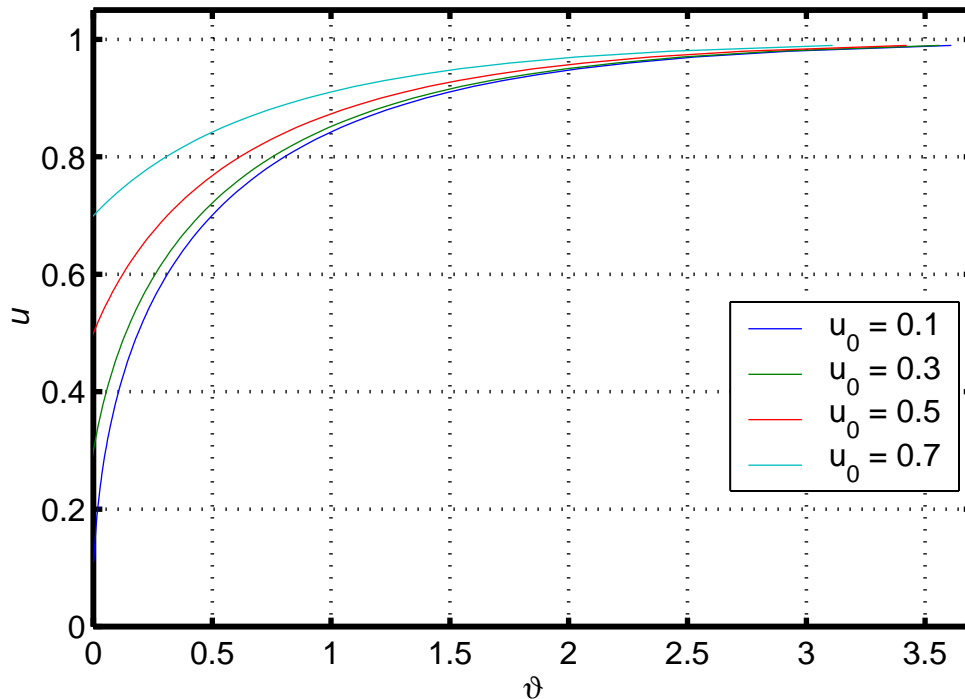


Figure 2.9: Master curves illustrating the evolution of grain size u as a function of time v for different values of the initial grain size. The quantities u and v are normalized with the grain size limit and the time constant; cf. the subsequent figures.

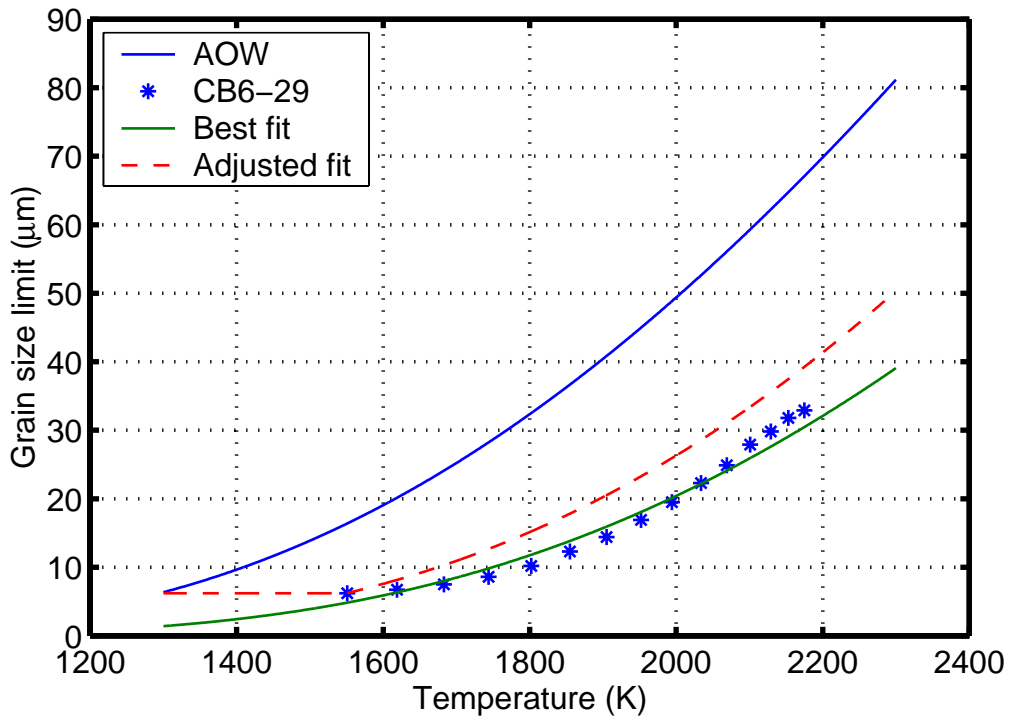


Figure 2.10: Grain size limit as a function of temperature for irradiated UO₂ fuel calculated by various empirical correlations and measurements of Bagger et al. (1994) made on specimen CB6-29. AOW refers to the Ainscough et al. (1973) correlation.

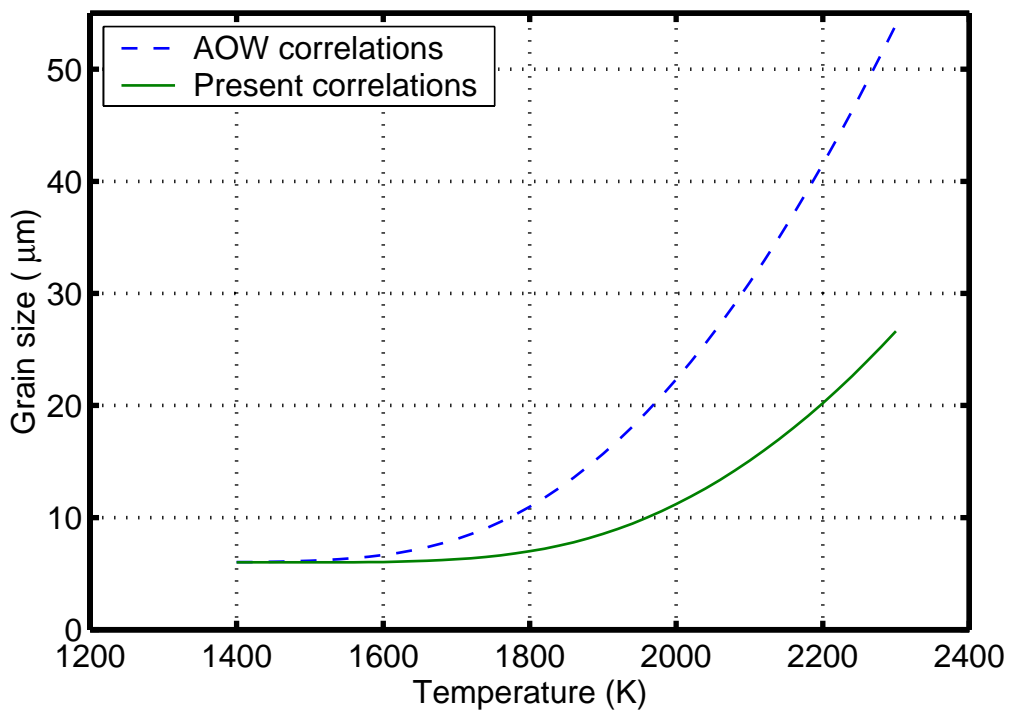


Figure 2.11: Grain size as a function of temperature for irradiated UO₂ fuel calculated by using the AOW correlations (Ainscough et al. 1973) vs. the present correlations, for a hold time of 62 h, cf. Bagger et al. (1994).

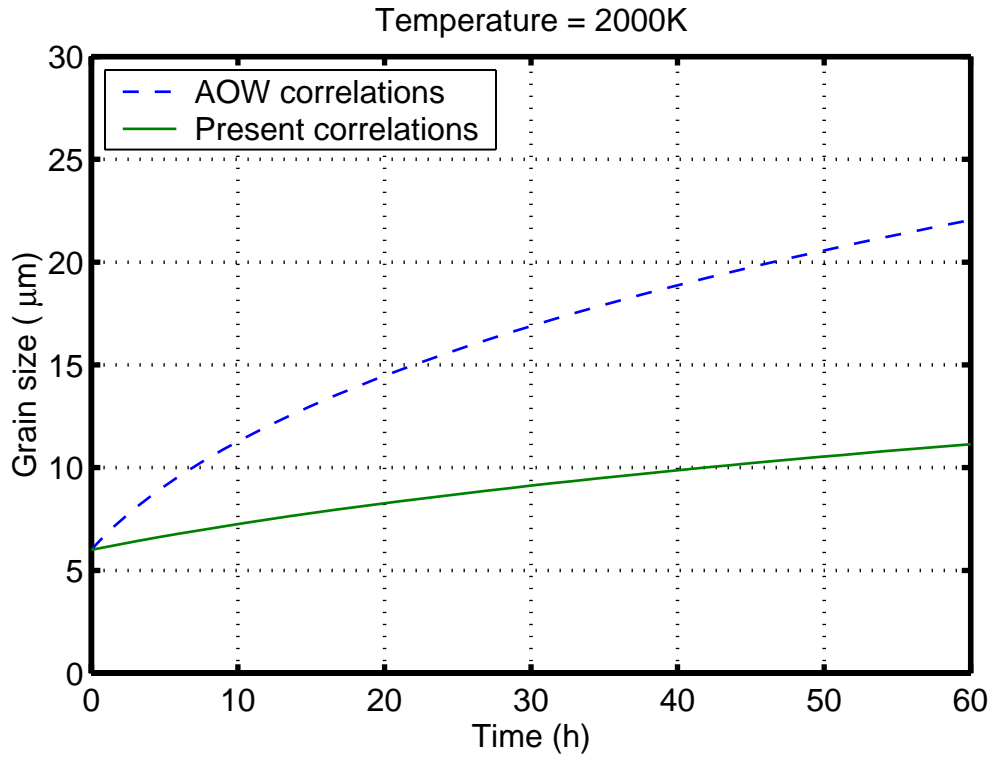


Figure 2.12: Time evolution of grain size for irradiated UO_2 fuel calculated by the AOW correlations (Ainscough et al. 1973) vs. the present correlations, at $T=2000K$.

We should mention that our present evaluation does not consider the effect of burnup, which accumulates fission products in fuel during irradiation, on grain growth explicitly; instead we have treated fission gas bubble and metallic precipitates generated under the power ramps. The fuel investigated by Bagger et al. (1994) for this purpose had a pin burnup of about $40 \text{ MWd}(\text{kgU})^{-1}$. It may be more adequate to scale the limiting grain size with fission product density at the grain boundary. In fact, Ito et al. (1985) and Nakajima and Saito (1985) suggest $S_m \Rightarrow S_m / (1 + f(\rho_{gb}))$, where $f(\rho_{gb})$ is a function of gas bubble ratio at grain boundary. The bubble ratio ρ_{gb} is defined as the ratio of the gas atom concentration at grain boundary to its saturation capacity. More specifically Ito et al. (1985) suggest that $f = \eta N / N_{sat}$, where η is an empirical constant obtained from grain size measurements. This type of analysis has not been pursued in the present work.

2.2.4 Calculation of gas release under grain growth

The surface density of gas atoms at grain faces, $N(t)$, is determined by using equations (2.16) -(2.18), i.e.

$$N(t) = \frac{2}{3} R(t) \int_0^t \beta(s) ds - \frac{2 \int_0^{R(t)} r^2 C(r,t) dr}{R^2(t)}, \quad (2.29)$$

where the first term on the right hand side denotes the gas production density and the second term the gas residing in the grain. Note that the grain radius, $R(t) = S(t)/2$, is a function of time. We assume that once the grain boundary is saturated with gas, i.e. when $N(t)$ reaches the saturation value N_{sat} , gas release will occur. Then grain boundary (intergranular bubbles) has to be filled with the incoming gas up to the saturation level again, before the next burst release would take place. The quantity N_{sat} can be calculated through an equation of state for gas atoms in the grain boundary, see below. The density of gas at the grain boundary at saturation is $C_{gb}^s \equiv C_s = 3N_{sat} / 2R$.

In computations, the time between subsequent release bursts can get very short, consequently necessitating many burst release computations. In order to avoid this situation the high frequency burst release process is replaced by a continuous release scheme (Forsberg & Massih 2001), where the gas concentration within the intergranular bubbles is taken to be the average of the concentrations before and after the release, or $C_{av} = [C_s + (1-f)C_s] / 2$, here f is the fraction of gas released at saturation, which in our computations is taken to be $f=0.7$. We note that this formulation says that gas release occurs by a continuous process above $0.65 C_s$. The amount of gas release during the time step is calculated by taking the gas content initially present in the intergranular bubbles, adding the gas generated during the time step, and subtracting the amount of gas present at the end of the time step. This technique reasonably approximates several burst gas release events that would require many short time steps and hence would demand long execution times in computer analyses.

The gas arriving at grain boundaries with a given rate will eventually saturate the boundaries through a network of interconnected bubbles. If the ideal gas equation of state is assumed, the density of the intergranular gas bubble at saturation is given by

$$N_{sat} = \frac{4r_f f(\theta) f_b}{3k_B T \sin^2 \theta} \left(\frac{2\gamma}{r_f} + P_{ext} \right), \quad (2.30)$$

where $f(\theta) = 1 - 1.5 \cos \theta + 0.5 \cos^3 \theta$ is a shape factor, θ the dihedral angle between the bubble surface and grain boundary, k_B the Boltzmann constant, T the absolute temperature, r_f the projected radius of the curvature of the capillary surface of the bubble, γ its surface tension, and P_{ext} the external gas pressure, (see figure 2.13). Using appropriate values for the constants (White & Tucker 1983), we find

$$N_{sat} = \frac{8.72 \times 10^{-9}}{T} \left(\frac{2\gamma}{r_f} + P_{ext} \right) \text{ [mole m}^{-2}\text{]}, \quad (2.31)$$

where in calculations, we use $2\gamma/r_f = 2.4 \times 10^6$ [Pa].

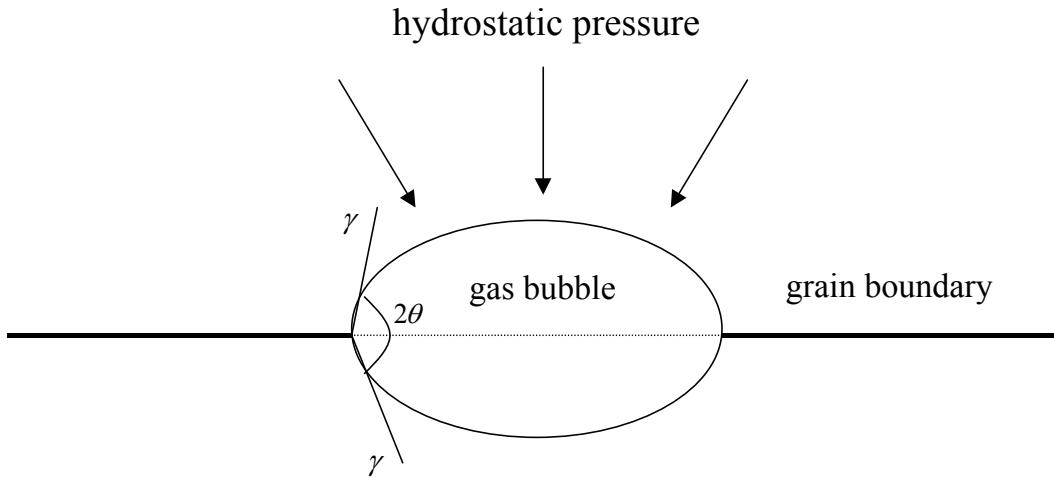


Figure 2.13: Sketch of a lenticular intergranular gas bubble subjected to a hydrostatic pressure. The angle $\theta = 50^\circ$ for UO_2 with a typical projected bubble radius of about 50 nm, see (White & Tucker 1983).

2.2.5 Results of sample computations

In this section, we present the results of sample computations performed by applying the foregoing models on thermal gas release and grain growth. More specifically, we calculate fission product gas release and the associating grain growth in UO_2 fuel under isothermal conditions. These computations provide insight to the connection between release and grain growth and also offer sample cases for verification of release calculations in fuel modelling computer codes. The material properties used for the calculations consist of relations for UO_2 fuel grain growth and the diffusion coefficient for fission gas in UO_2 during irradiation. The grain growth kinetic model applied here was presented in subsection 2.2.3.2. The relations utilized for the gas diffusion coefficient for UO_2 fuel are based on the work of Turnbull et al. (1982), White and Tucker (1983), Turnbull, White and Wise (1988), and Matzke (1980). The utilized correlations and constants are presented in table 2.3. Figure 2.14 shows the temperature dependence of the used diffusion coefficient.

The relations presented in this paper are programmed in a computer routine for calculation of fission gas release and grain growth as a function of irradiation time at different constant temperatures. The required input parameters for our computations are listed in table 2.4. Fission gas production in fuel is a function of the power density and the fission product yield; see appendix B for a pragmatic approach used here.

The results of the computations of the fission product gas release as a function of temperature and time at a constant power density of 707 Wm^{-3} (45 kWm^{-1}) are presented in figures 2.15 and 2.16. The associating results for the evolution of grain size are plotted in figures 2.17 and 2.18. It can be seen from figure 2.15 that after a certain irradiation time, fission gas release increases with temperature reaching a maximum value then it decreases as the temperature is increased.

Correlations/parameters/constants	Unit	Definition
$D_{eff} \equiv v_g D / (v_g + g)$	$m^2 s^{-1}$	Effective gas diffusion coefficient
$D = C_1 e^{-Q_1/T} + 4C_2 \sqrt{\varphi_m} e^{-Q_2/T} + 4C_3 \varphi_m$	$m^2 s^{-1}$	Gas diffusion coefficient in trap free media
$v_g = 3.03\pi l \varphi_m (\bar{R}_b + \delta)^2$	s^{-1}	Intragranular bubble gas re-solution rate
$\bar{R}_b = 1.453 \times 10^{-10} \exp(1.023 \times 10^{-3} T)$	m	Mean intragranular bubble radius
$g = 4\pi \bar{R}_b C_b^{tot} D$	s^{-1}	Fission gas captured rate by intragranular bubble
$C_b^{tot} = 1.52 \times 10^{27} / T - 3.3 \times 10^{23}$	m^{-3}	Total gas bubble density
$l = 6 \times 10^{-6}$	m	Fission fragment range
$\delta = 10^{-9}$	m	Bubble fission fragment distance
$\varphi_m = N_A \varphi$	$m^{-3} s^{-1}$	Fission density
$\varphi = 5.189 \times 10^{-14} q_v$	$mol.m^{-3} s^{-1}$	Fission density
q_v	Wm^{-3}	Power density
$N_A = 6.022 \times 10^{23}$	atom/mol.	Avagadro number
$C_1 = 7.6 \times 10^{-10}$	-	-
$C_2 = 1.41 \times 10^{-25}$	-	-
$C_3 = 2.0 \times 10^{-40}$	-	-
$Q_1 = 3.5247 \times 10^4$	K	-
$Q_2 = 1.38 \times 10^4$	K	-

Table 2.3: Relations and constants used for calculation of the fission gas diffusion coefficient in UO_2 fuel. Here, T is the absolute temperature, confer (White & Tucker 1983), (Turnbull et al. 1988).

Parameter	Unit	Definition
$d_{pellet} = 9.0$	mm	Fuel pellet diameter
$\rho_{TD} = 0.937$	-	Relative (to T.D.) pellet density
$R_0 = 3.0$	μm	Initial UO_2 grain radius
$P_{ext} = 0.0$	Pa	External gas pressure acting on intergranular gas bubbles
$v_b \lambda / \beta(t) = 5.7 \times 10^{-8}$	$ms^{-1} / (mol.m^{-3} s^{-1})$	Ratio of gas re-solution rate to gas production rate
$q_l = 45$	kWm^{-1}	Linear power density
$\Delta t = 10$	h	Time step used in computation

Table 2.4: Input parameter values used in fission gas release computations.

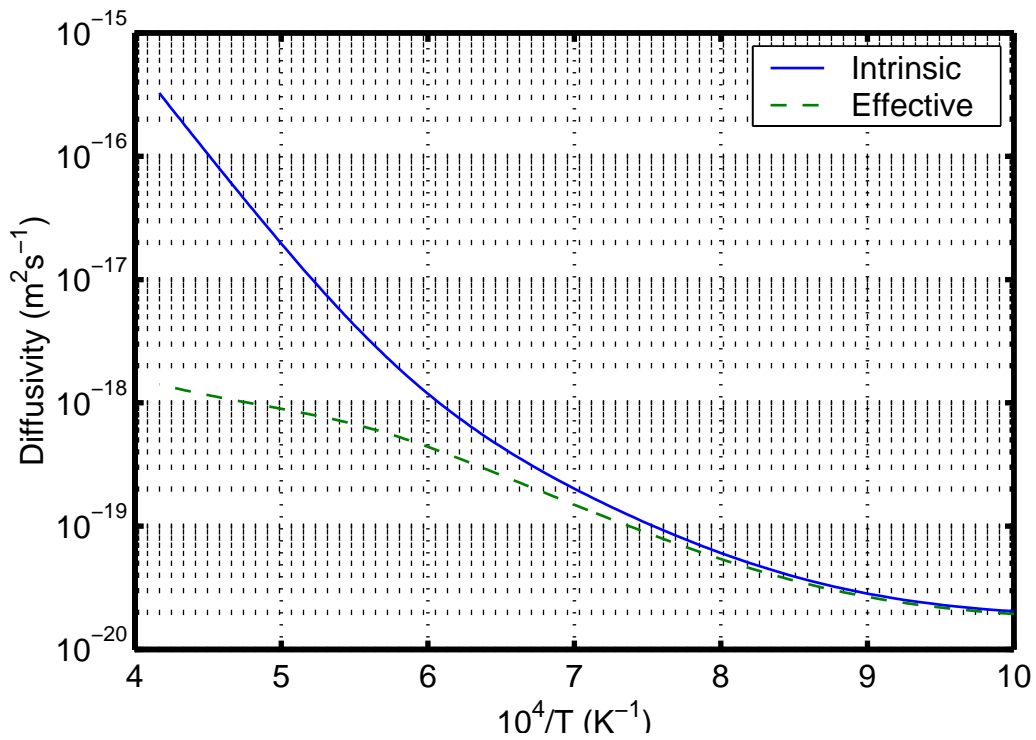


Figure 2.14: The diffusion coefficient of fission gas atoms in UO_2 as a function of temperature, in the range 1000 to 2400 K, for a power density of 707 MWm^{-3} .

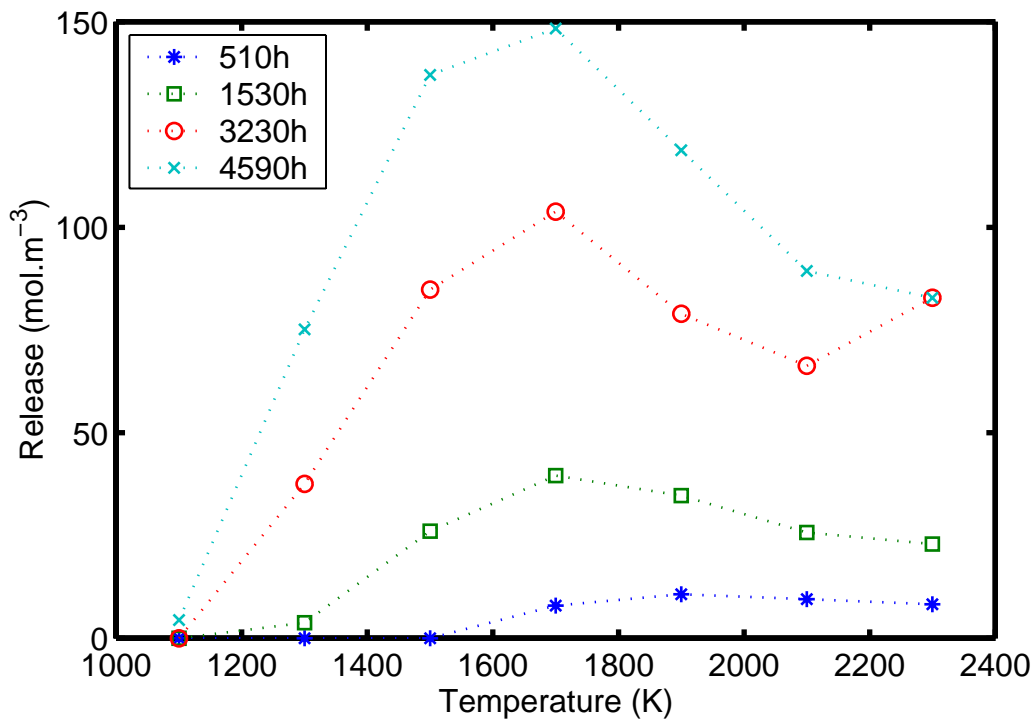


Figure 2.15: Temperature-time dependence of fission gas release under grain growth; gas release by grain boundary sweeping.

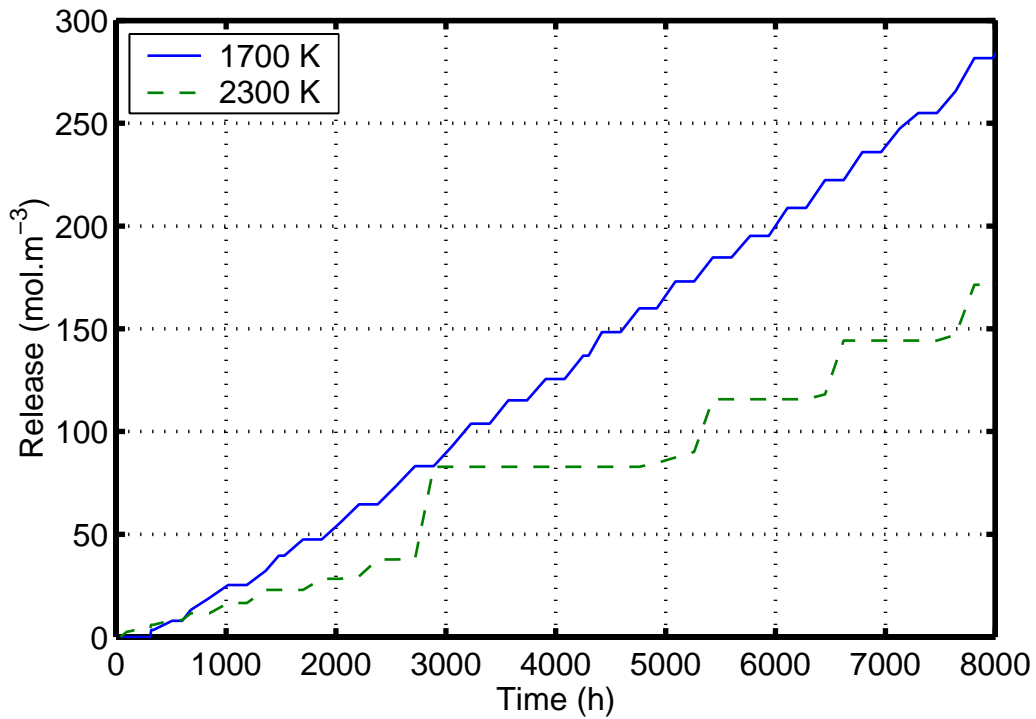


Figure 2.16a: Time evolution of fission gas release at two different temperatures under grain growth at a constant power density. It is seen that the release at the lower temperature gets larger after 600 h of irradiation due to excessive grain growth, see figure 2.16b.

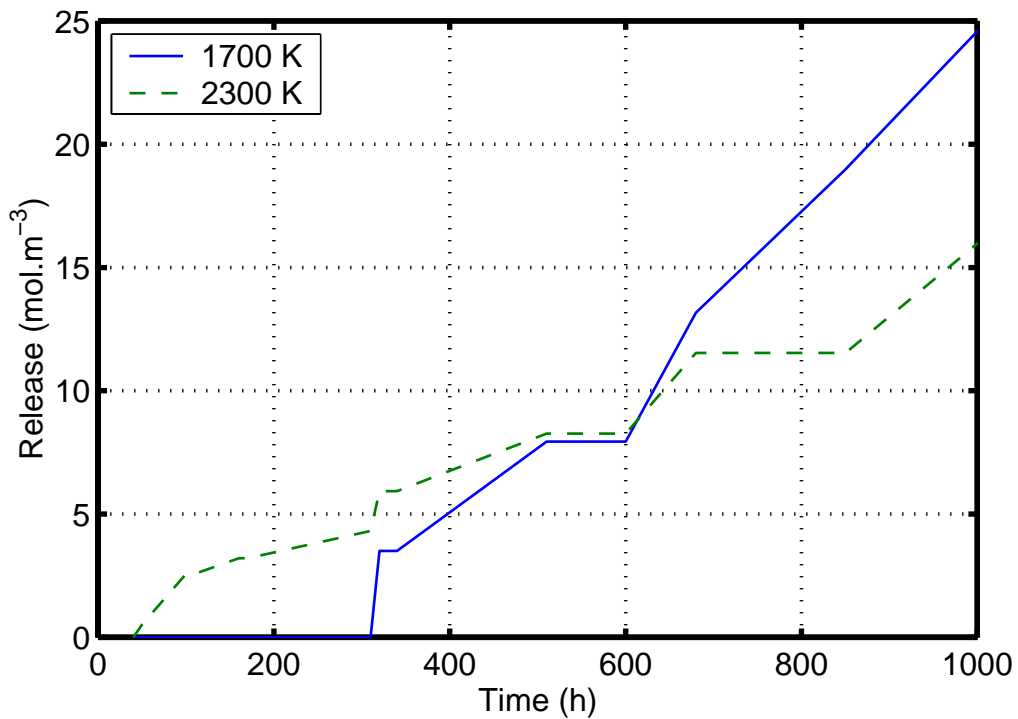


Figure 2.16b: Time evolution of fission gas release at two different temperatures under grain growth after 1000 h of irradiation at a constant power density; as in figure 2.16a.

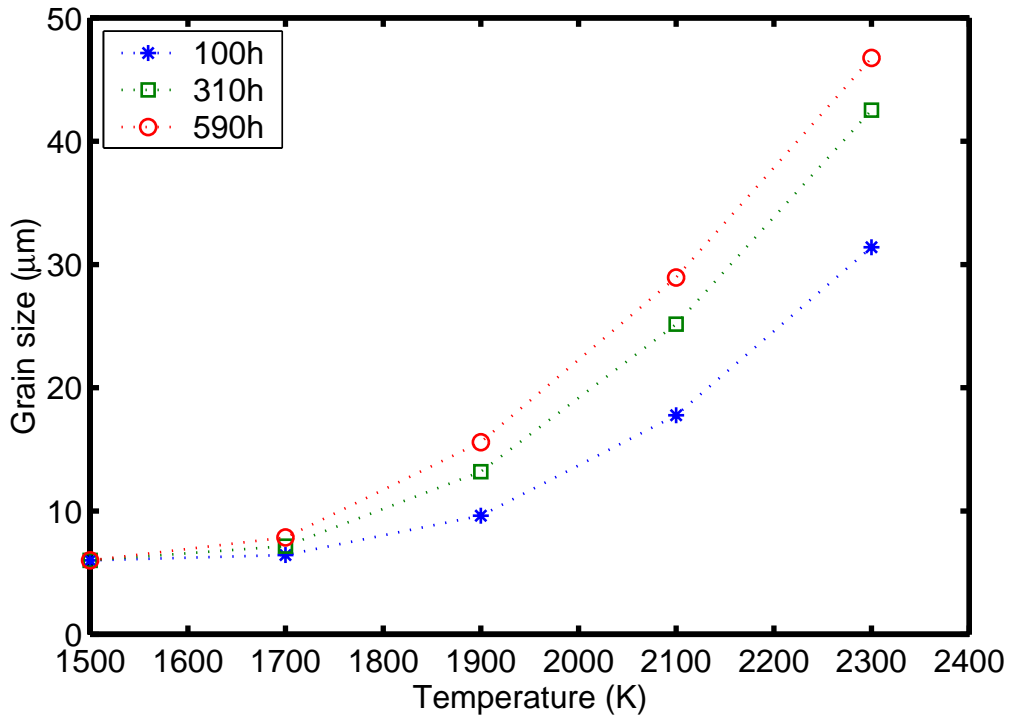


Figure 2.17: Temperature-time dependence of UO₂ grain growth.

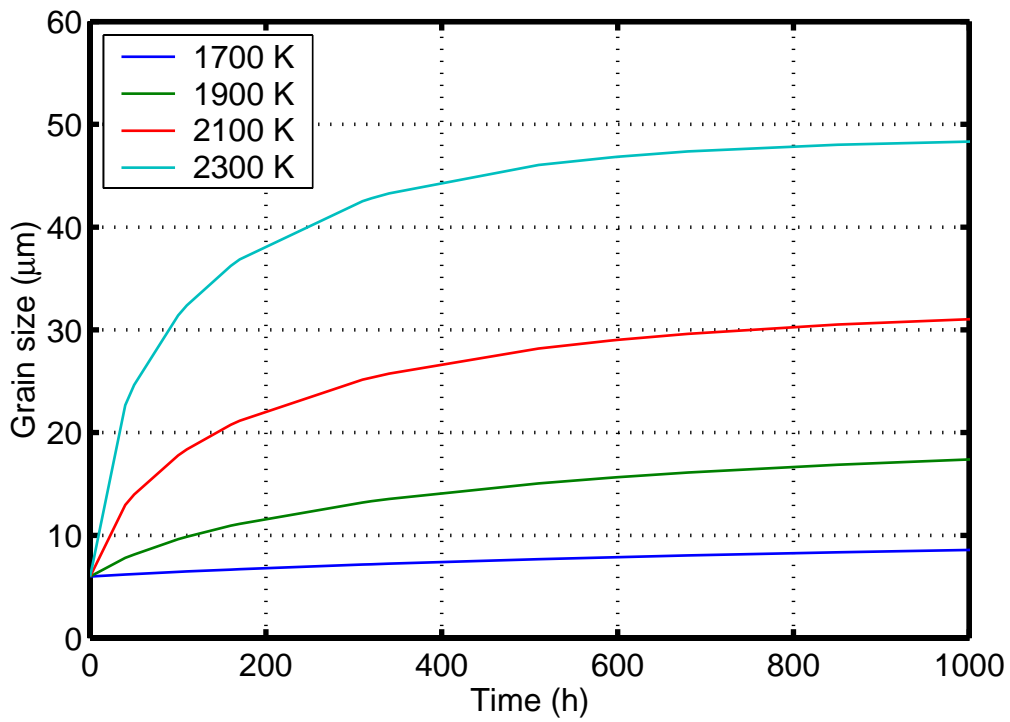


Figure 2.18: Time evolution of UO₂ grain size at different temperatures.

The reason for the decrease is the increase in grain size with temperature resulting in a longer diffusion path for gas atoms to reach the grain boundary, figures 2.17 and 2.18. However, higher temperatures leads also to faster diffusion to grain boundaries. Hence thermal release involves a highly non-linear behaviour depending on thermal activation, kinetics of gas diffusion, grain growth and grain boundary sweeping. The step-wise increase in gas release is a sign of grain boundary saturation and burst release at high fuel temperatures, figure 2.16a. As can be seen, release at 1700 K gets larger than at 2300 K after 500 h of irradiation due to the affect of enlarged grain at the higher temperature.

2.2.6 Analysis and discussion

The remarkable effect of the temperature dependence of fission gas release during grain growth (see figure 2.15) as predicted by the thermal fission gas release method presented in the foregoing sections is briefly discussed in this section. This effect may be elucidated if we compare the characteristic times for gas diffusion and grain growth, see appendix C. The *characteristic times* for gas diffusion τ_D and grain growth τ_G are defined by

$$\tau_D \equiv \frac{R^2}{2D}; \quad \tau_G \equiv \frac{R}{2(dR/dt)}. \quad (2.32)$$

Using the grain growth model presented in subsection 2.2.3.2 and the diffusion coefficient relations given in table 2.3, we have calculated τ_D and τ_G as a function of temperature for a variable grain size with an initial radius $R_0 = 3 \mu\text{m}$. That is, we have calculated grain size development for a fixed duration (62 h) according to the results presented in figure 2.11 and then used these results to obtain τ_D and τ_G as a function of temperature, see figure 2.19a. We note that for the considered case at temperatures below 1600 K the diffusion time gets shorter than the growth characteristic time. At 1550 K, $\tau_G = \infty$ because according to our model assumption there is no grain growth below this temperature. Note also that the diffusion time gets longer and longer at temperatures above 1800 K, due to the increasing grain size (grain growth). This means that gas diffusion to grain boundaries gets delayed. Moreover, at temperatures above 2100 K, τ_G levels off. Same calculations are repeated for a duration of 620 h, figure 2.19b. It is seen that τ_D goes through a minimum at about 1830 K, after which it starts to increase until it reaches $R = R_m$, whereupon growth ceases and $\tau_G = \infty$. This type of computations aids us to interpret whether fission gas release is diffusion controlled or grain growth driven. Parametric analysis of the characteristic times at a fixed grain size provides further insight on the interplay between grain growth and fission gas release, see appendix C.

We should remark, nevertheless, that the results presented here depend on the accuracy and the range of validity of the material models (diffusivity and grain growth) utilized. Only direct comparison with an accurate and detailed experiment can validate the prediction of a theory. We have consciously carried out our calculations beyond 2000 K, although we are aware that other mechanisms, which have not been taken into account in the present analysis, may contribute to fission product release beyond this temperature.

Thermal gas release concomitant with grain growth has been observed in boiling water reactor (BWR) 8×8 fuel both during normal operation (Grapengiesser et al. 1988) and in power ramp experiments, (Schrire & Lysell 1991). Schrire and Lysell (1991) studied UO₂ fuel microstructure and fission product distribution by power ramping a rod, pre-irradiated in a commercial BWR to a fuel burnup of 35 MWd/kgU, in Studsvik's R2 test reactor to a maximum linear power density of 43 kW/m and compared the results with a similar reference fuel rod which had experienced a maximum linear power density of 26 kW/m during its final cycle in the BWR. The power bump started with a 72 h irradiation at a peak LHGR of 25 kWm⁻¹ in order to build sufficient amount of short-lived fission products. Then ramping was performed at a rate of 0.69 kW(mh)⁻¹ to a ramp terminal level of 43 kWm⁻¹, and held at this power for 3 hours to redistribute and release fission product gases. Schrire and Lysell's (1991) scanning electron microscopy of fuel pellet revealed a strong coupling between fission product gas release and grain growth across pellet radius for the ramped rod. The average grain size at the centre of the pellet (with radius of 5 mm) had increased by a factor of two (from 5.5 to 11 μm) and the release fraction from less than 0.05 to 0.74 from the periphery to the centre to of the pellet, respectively. The experiment clearly shows the importance of physically based models to describe the phenomena of grain growth and fission product gas release in reactor fuel concurrently. Quantitative analyses of in-reactor experiments, such as that made by Schrire and Lysell (1991) requires implementation of the mathematical method presented here in a nuclear fuel modelling computer program and simulation of the experiment. Our aim in the present report has been to provide a consistent theoretical framework for analysis of such experiments and events.

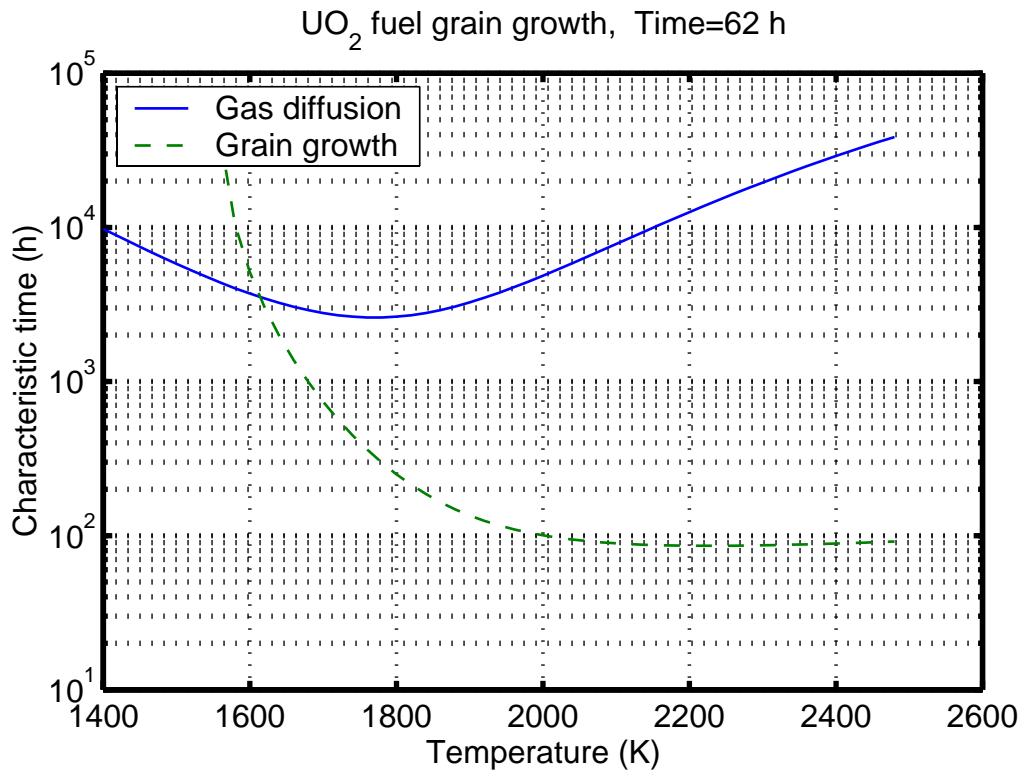


Figure 2.19a: Characteristic times for gas diffusion and grain growth in UO₂ fuel, upon 62 h of growth. The gas diffusivity used in the calculations is the effective diffusivity as presented in figure 2.14 and table 2.3.

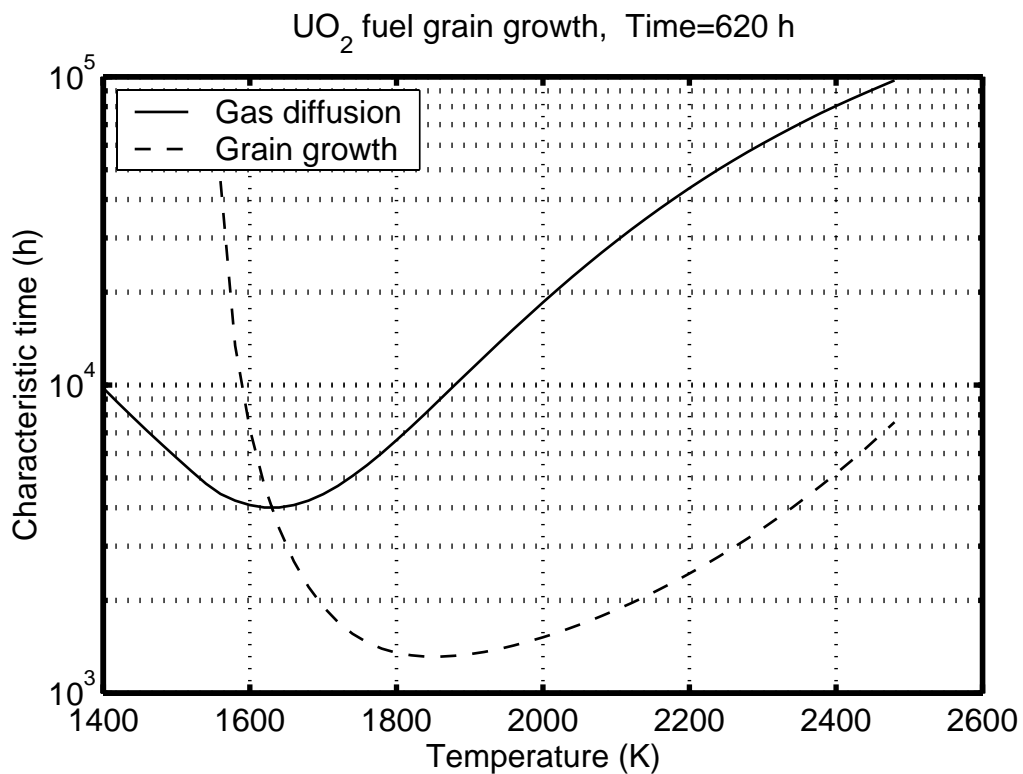


Figure 2.19b: Characteristic times for gas diffusion and grain growth in UO₂ fuel, as in figure 2.19a, upon 620 h of growth.

2.3 Thermal conductivity

Thermal conductivity of UO_2 is a key parameter for the thermal behaviour of nuclear fuel rods during reactor operation. In particular, the fuel pellet temperature, thermal expansion, thermal fission gas release, grain growth and gaseous swelling are strongly influenced by the thermal conductivity of the fuel material.

Prevalent models for thermal conductivity of UO_2 are usually in the form of empirical correlations, where fuel temperature, burnup and porosity are the governing parameters. The correlations are fitted either to out-of-reactor laser flash measurements of thermal diffusivity or to in-reactor measurements of fuel centreline temperatures. Most correlations give fairly consistent estimates of thermal conductivity for un-irradiated fuel, but differences are found in the predicted burnup-dependence of the thermal conductivity. A short review of the subject, with comparisons of widely used thermal conductivity models for UO_2 , was presented by Jernkvist and Massih (2002).

A more recent study is due to Ronchi et al. (2004), in which novel laser flash data on highly irradiated UO_2 fuel from the HBRP and a new thermal conductivity model were presented. The formulation of this thermal conductivity model is unfortunately not suited for implementation in a fuel performance computer code such as FRAPCON-3.2. However, based on the recent laser flash measurements mentioned above, Kinoshita et al. (2004) proposed a more tractable model for the thermal conductivity of high-burnup UO_2 . This model, which is better suited for implementation in FRAPCON, is given in appendix D.

It is worthwhile to compare the model proposed by Kinoshita et al. (2004) with the current correlation for UO_2 thermal conductivity in FRAPCON-3.2. The latter model is based on the work of Ohira and Itagaki (1997), who developed a conductivity correlation based on fuel thermal diffusivity measurements on irradiated fuel and also verified it against in-reactor fuel centreline temperature data. Lanning et al. (2000) evaluated this correlation, and introduced it in FRAPCON-3.2 with some modifications. Since this modified correlation is not documented elsewhere, it is given in appendix E for reference.

Figure 2.20 shows a comparison of the current model for thermal conductivity in FRAPCON-3.2 with the correlation proposed by Kinoshita et al. (2004). It should be remarked that the thermal conductivity is plotted for a fixed fuel porosity of 5 vol%, i.e. the porosity evolution that follows as a consequence of material restructuring at high burnup is not accounted for in the calculated thermal conductivities. Clearly, the two models yield similar predictions of thermal conductivity for un-irradiated fuel, and also for fuel with a burnup of about $80 \text{ MWd}(\text{kgU})^{-1}$. Large differences between the models are found at very high fuel burnup, but more surprisingly, also at a fairly moderate burnup of $50 \text{ MWd}(\text{kgU})^{-1}$. Figure 2.21 shows a comparison of the two models at $50 \text{ MWd}(\text{kgU})^{-1}$.

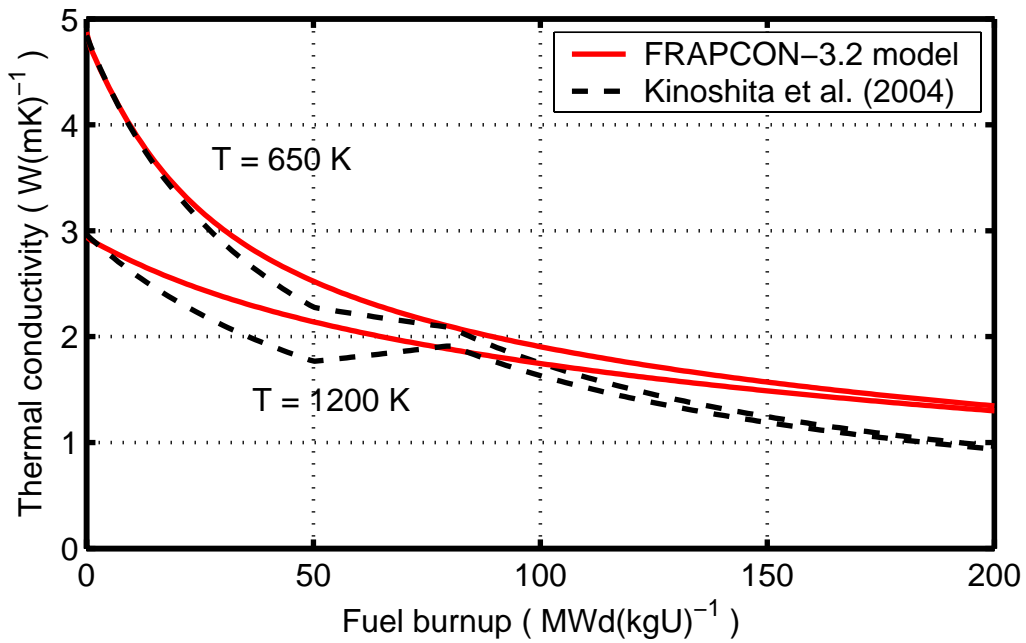


Figure 2.20: Comparison of the current model for thermal conductivity in FRAPCON-3.2 with the correlation proposed by Kinoshita et al. (2004). The conductivity is calculated for a fixed fuel porosity of 5 vol%.

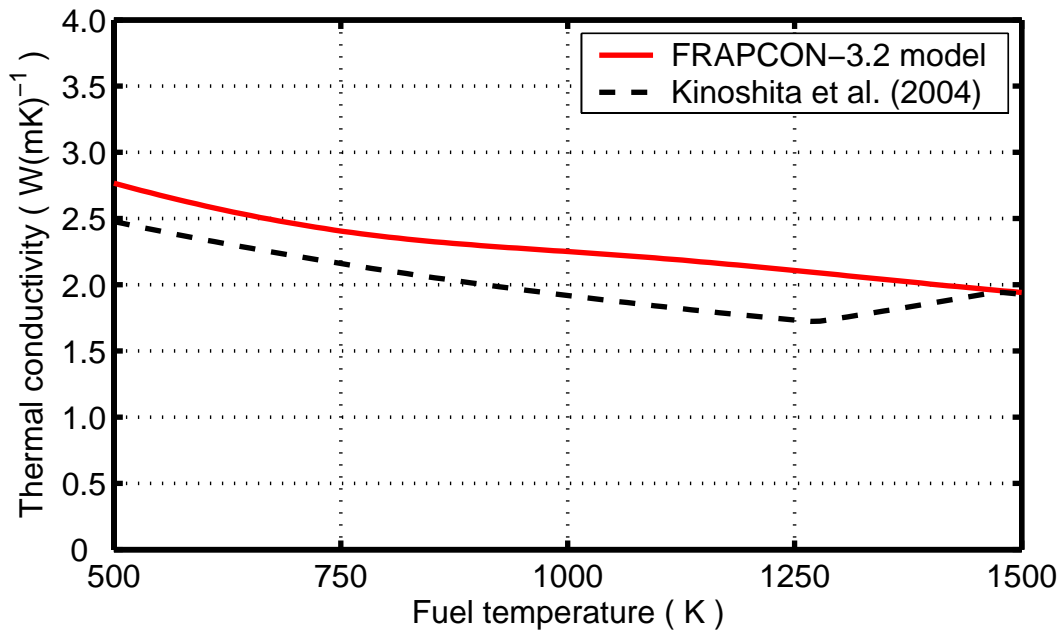


Figure 2.21: Comparison of the model for thermal conductivity in FRAPCON-3.2 with the correlation proposed by Kinoshita et al. (2004). The conductivity is calculated for a fixed fuel porosity of 5 vol% and a burnup of 50 MWd(kgU)⁻¹.

The degradation of thermal conductivity with burnup, as calculated with the model by Kinoshita et al. (2004), is assumed to be affected by fuel restructuring between 50 and 80 MWd(kgU)⁻¹. As shown in figure 2.20, the thermal conductivity at 1200 K is even predicted to *increase* with burnup in this interval. This effect is claimed to result from recovery of lattice damage and from transfer of nanometre-sized fission gas bubbles to micron-sized pores under fuel restructuring. It should be noticed that these beneficial effects are offset by increased porosity in the fuel, an effect that is not accounted for in figure 2.20. Hence, the predicted recovery of thermal conductivity in figure 2.20 pertains to the fuel matrix alone, and not to the bulk material.

Nevertheless, theoretical assessments by Jernkvist and Massih (2002) indicate that the thermal conductivity of the fuel matrix should actually *decrease* as a result of irradiation induced fuel restructuring, contrary to the results reported by Kinoshita and co-workers. We therefore question the correctness of their model, and do not recommend it for implementation in FRAPCON without further verification with respect to experimental data from other studies. As shown in figure 2.20 and 2.21, their model differs significantly from the current correlation for UO₂ thermal conductivity in FRAPCON-3.2, which has been calibrated to in-reactor fuel centreline temperature data from measurements made on fuel pellets with radial average burnups up to 77 MWd(kgU)⁻¹ (Lanning et al. 2000). Such data allow integral assessments of the combined effect of all heat transfer models in the computer code, since the fuel centreline temperature is not only governed by the fuel thermal conductivity, but also by the pellet-clad gap conductance and the radial distribution of power within the fuel pellet. Hence, the current correlation for UO₂ thermal conductivity in FRAPCON-3.2 has been calibrated to give best-estimate fuel temperature predictions, when applied in combination with a specific set of other heat transfer models in the code. The correlation is applicable to high burnup, since the calibration has been made with fuel centreline temperature measurements on fuel pellets with radial average burnups up to 77 MWd(kgU)⁻¹.

In conclusion, the only revision we propose to the current correlation for UO₂ thermal conductivity in FRAPCON-3.2 is to use the calculated rim zone porosity from equation (2.7), when applying the correlation to the re-structured part of the fuel material. At present, the correlation is applied without considering the build-up of micron-sized porosity in the re-structured part of the fuel pellet. By using the calculated porosity for the restructured part of the pellet, the calculated fuel temperature will increase in proportion to the width of the rim zone, and also in proportion to the porosity volume fraction within the rim.

3 Models for zirconium alloy clad tube behaviour

3.1 Clad corrosion behaviour

Waterside corrosion of the clad tube is a key issue for nuclear fuel performance at high burnup, and consequently, accurate models for clad corrosion are important in analyses of high-burnup fuel rods. The current models for clad oxide growth and hydrogen pickup in FRAPCON-3.2 are fairly simple (Berna et al. 1997) and (Lanning et al. 1997a). Clad oxide growth is calculated by distinct models for BWR and PWR conditions, but the models do not consider the influence of coolant chemistry, clad heat treatment or clad alloy composition on the corrosion rate. Clad hydrogen pickup is calculated through models that discriminate between BWR and PWR conditions, and between standard Zircaloy-2 and Zircaloy-4 clad materials. Models for Zr-Nb type clad materials are currently not available.

In the following, we first use recent PWR clad corrosion data from high burnup fuel rods to assess the current PWR clad corrosion models in FRAPCON-3.2. These models were formulated in the mid-eighties, which means that they were originally calibrated to corrosion data from fuel rods with significantly lower burnups than achieved today. Moreover, the clad materials used today in PWRs differ from those used in the seventies and eighties. Finally, we use recent corrosion data for the Zr-Nb clad alloys ZIRLO™ and M5™ from open literature to make the PWR clad corrosion models in FRAPCON-3.2 applicable to these materials.

3.1.1 Clad oxide growth

The models for clad oxide growth in FRAPCON-3.2 originate from the work by Garzarolli et al. (1982). The models are also used in the Electric Power Research Institute (EPRI) steady-state fuel analysis code ESCORE, Fiero et al. (1987). Under PWR conditions, the clad oxide layer thickness δ_{ox} [m] is assumed to grow according to

$$\frac{d\delta_{ox}}{dt} = \begin{cases} \frac{C_1}{\delta_{ox}^2} e^{-Q_1/RT_{co}} & \delta_{ox} < 2\mu\text{m} \\ (C_2 + C_3 (\phi/\phi_o)^{0.24}) e^{-Q_2/RT_{co}} & \delta_{ox} \geq 2\mu\text{m} \end{cases}, \quad (3.1)$$

where T_{co} [K] is the clad metal-to-oxide interface temperature, ϕ [$\text{m}^{-2}\text{s}^{-1}$] is the fast neutron flux ($E > 1\text{MeV}$), R is the universal gas constant and ϕ_o , C_1 , C_2 , C_3 , Q_1 and Q_2 are empirical and constant model parameters, as defined in table 3.1. When applying equation (3.1) in FRAPCON-3.2, the clad is assumed to be completely free of oxide ($\delta_{ox}=0$) at beginning of life. The reader is referred to Lanning et al. (1997a) for details on the numerical implementation of equation (3.1) in FRAPCON-3.2, and to Lanning et al. (1997b) for details on the performed assessment of the model.

Measured data on clad corrosion in open literature are usually presented as plots of the maximum oxide thickness measured for a certain rod, versus the rod average burnup. Such data are not very useful for assessing clad corrosion models, since the in-reactor clad corrosion is a function of time at temperature rather than rod average burnup. This is particularly true for PWR conditions, where the clad temperature depends strongly on axial elevation, coolant inlet temperature and coolant mass flux. However, since we lack background information on the exact operating conditions for the literature corrosion data, we have calibrated the FRAPCON PWR corrosion models with respect to clad maximum oxide thickness as a function of rod average burnup by studying a rod from a standard 17×17 fuel assembly design, subjected to nominal operating conditions for the Ringhals 3 PWR in Sweden. This nominal reference case is summarized in table 3.2, where also the most important results of the calculations with FRAPCON-3.2 are given.

Model parameter		Value
C_1	[m^3s^{-1}]	7.29×10^{-14}
C_2	[ms^{-1}]	9.31×10^{-4}
C_3	[ms^{-1}]	2.75×10^{-3}
ϕ_0	[neutrons $\text{m}^{-2}\text{s}^{-1}$]	5.24×10^{18}
R	[$\text{Jmole}^{-1}\text{K}^{-1}$]	8.3143
Q_1	[Jmole^{-1}]	135 188
Q_2	[Jmole^{-1}]	114 526

Table 3.1: Model parameters used in equations (3.1) and (3.2).

Fuel design and operating conditions		Value
Rod average linear heat generation rate	[kWm^{-1}]	18.3
Rod active length	[mm]	3658
Clad tube outer diameter	[mm]	9.55
Fuel rod pitch	[mm]	12.6
Coolant pressure	[MPa]	15.5
Coolant inlet temperature	[K]	557 ± 5
Coolant mass flux	[$\text{kgm}^{-2}\text{s}^{-1}$]	3760
Main results		
Max oxide-to-water interface temperature	[K]	603.5 ± 5
Clad fast neutron flux (>1MeV)*	[$\text{m}^{-2}\text{s}^{-1}$]	7.42×10^{17}
Clad surface heat flux*	[kWm^{-2}]	586

Table 3.2: Reference case used for assessment of the PWR clad corrosion models in FRAPCON-3.2.

In the calculations, we introduced a ± 5 K variation of the coolant inlet temperature from its nominal value of 557 K. The purpose of this variation was to study the impact of coolant temperature on the calculated clad oxide growth.

* Evaluated at the axial position of max oxide-to-water interface temperature.

The calculated maximum oxide-to-water interface temperature was obtained in the upper part of the fuel rod, approximately 30 cm below the upper plenum. It should be remarked that the oxide-to-water interface temperature in table 3.2 is unaffected by the clad oxide thickness. This is not so for the metal-to-oxide interface temperature T_{co} in equation (3.1), which, due to the poor thermal conductivity of ZrO_2 , increases as the oxide layer grows.

3.1.1.1 Zircaloy-4 oxide growth

The current model for clad oxide growth under PWR conditions in FRAPCON-3.2 is originally calibrated to corrosion data for standard Zircaloy-4 cladding (Zr-1.5Sn-0.2Fe-0.1Cr by wt%). The model, as defined by equation (3.1), is in figure 3.1 compared with in-reactor corrosion data presented by Shimomura et al. (2004). In addition to standard Zircaloy-4, data are also shown for low-tin Zircaloy-4 cladding (Zr-1.3Sn-0.2Fe-0.1Cr by wt%), a material that is commonly used in Japanese PWRs.

The calculations were done for the reference case defined in table 3.2. The thick full line corresponds to a clad oxide-to-water interface temperature of 603.5 K, whereas the thin dashed lines are the results of a ± 5 K variation of this temperature. The corrosion model in FRAPCON-3.2 does a fairly good job up to a rod average burnup of about 40 $MWd(kgU)^{-1}$, or alternatively, up to a clad maximum oxide thickness of about 30 μm . Beyond this point, the model clearly underestimates the clad corrosion rate.

The same conclusion was reached by Limbäck et al. (1994), who compared the FRAPCON/ESCORE model for clad oxide growth with another dataset for in-reactor corrosion of standard and low-tin Zircaloy-4 in PWRs.

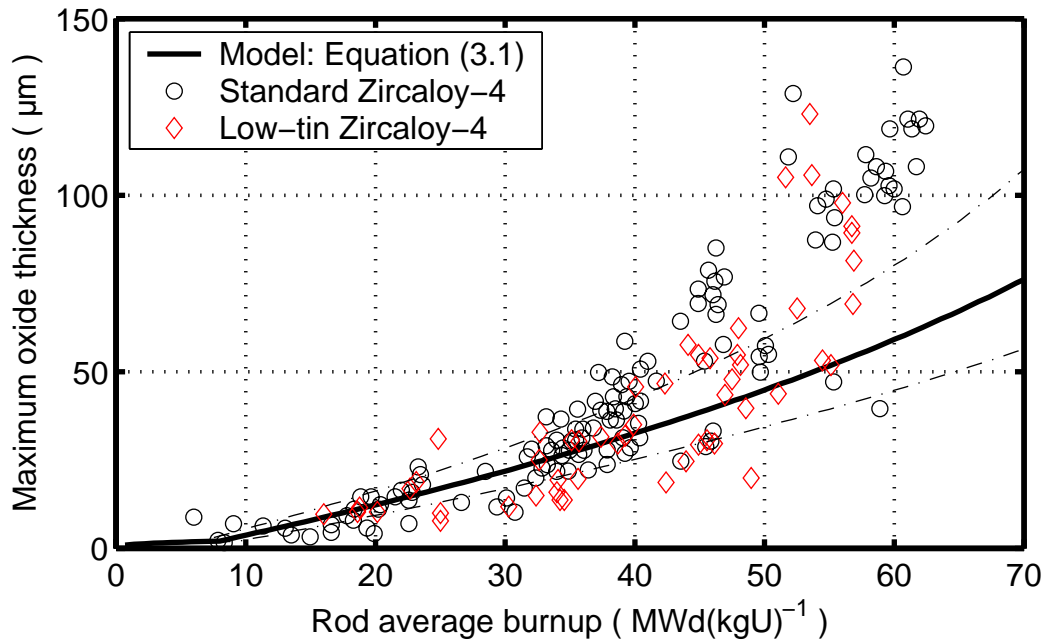


Figure 3.1: Clad oxide growth for Zircaloy-4, as calculated with the FRAPCON-3.2 standard PWR model, in comparison with data by Shimomura et al. (2004). The thick full line corresponds to a clad oxide-to-water interface temperature of 603.5 K, whereas the thin dashed lines are the results of a ± 5 K variation of this temperature.

They suggested that the enhanced corrosion rate following an oxide accumulation of 30-40 μm could be explained by hydride precipitation at the clad metal-to-oxide interface, which disrupts the material coherency at the interface. Moreover, Limbäck et al. (1994) introduced a second transition point in equation (3.1), which catered for the corrosion enhancement that they assumed to be associated with hydride precipitation. Based on a best fit to their dataset, they modified equation (3.1) to

$$\frac{d\delta_{ox}}{dt} = \begin{cases} \frac{C_1}{\delta_{ox}^2} e^{-Q_1/RT_{co}} & \delta_{ox} < 2\mu\text{m} \\ \left(C_2 + C_3 (\phi/\phi_o)^{0.24} \right) e^{-Q_2/RT_{co}} & 2 \leq \delta_{ox} \leq 35\mu\text{m} \\ 1.8 \left(C_2 + C_3 (\phi/\phi_o)^{0.24} \right) e^{-Q_2/RT_{co}} & 35 < \delta_{ox} \end{cases} \quad (3.2)$$

Hence, according to the observations of Limbäck and co-workers, the corrosion rate is enhanced by a factor 1.8 beyond a clad oxide thickness of 35 μm , as a result of hydride precipitation at the metal-to-oxide interface. Equation (3.2) was applied to the reference case in table 3.2, and the result is compared with the data by Shimomura et al (2004) in figure 3.2. Even though the high-burnup data are still underestimated, a comparison of figure 3.1 and 3.2 clearly reveals that equation (3.2) is superior to equation (3.1), and most data in figure 3.2 are within the ± 5 K temperature band. We therefore conclude that equation (3.1) should be replaced by equation (3.2) in FRAPCON-3.2, in order to improve the predictability of the PWR corrosion model for Zircaloy-4 cladding at high burnup. Finally, it should be mentioned that Limbäck (1996) has reviewed and compared a number of clad oxidation models for application to PWR conditions, among others those given by equations (3.1) and (3.2).

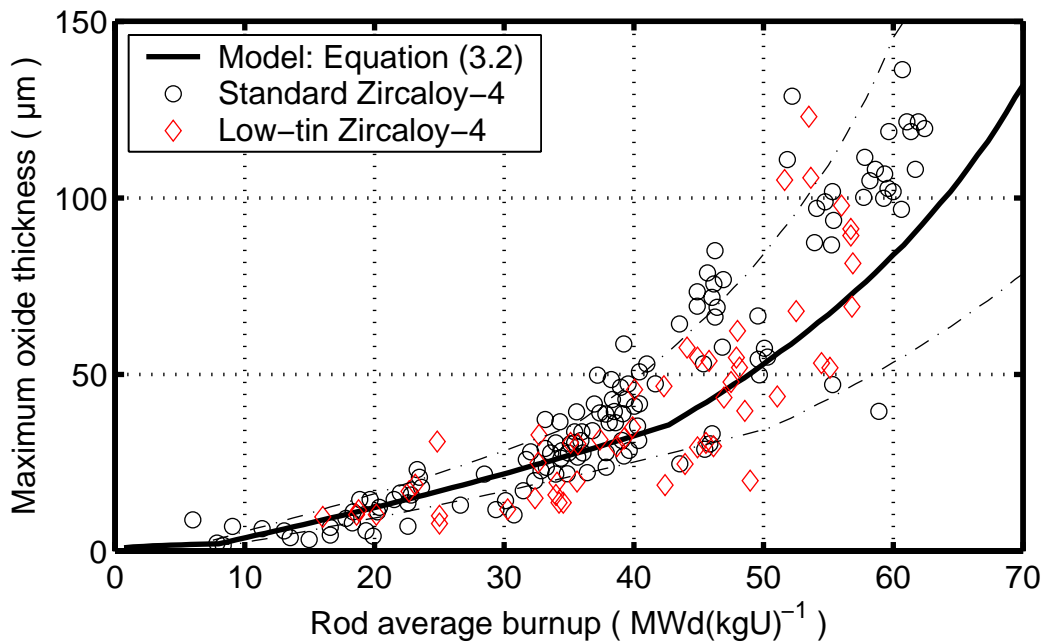


Figure 3.2: Clad oxide growth for Zircaloy-4 in comparison with data by Shimomura et al. (2004). The thick full line corresponds to a clad oxide-to-water interface temperature of 603.5 K, whereas the thin dashed lines are the results of a ± 5 K variation of this temperature.

3.1.1.2 ZIRLO oxide growth

ZIRLO is a trademark of Westinghouse Electric Company, which designates a Zr-Nb clad tube material for use in pressurized water reactors. The first fuel assemblies with ZIRLO cladding were loaded into PWRs in the early nineties, and based on operating experience gained over the years, the original ZIRLO has been gradually modified to improve the material. Consequently, there is a variation in both corrosion performance and other properties among ZIRLO-type materials. The original material, often referred to as standard ZIRLO, was composed of Zr-1.0Nb-1.0Sn-0.1Fe by wt% and heat treated by a final stress relief anneal. The current material, named optimized ZIRLO by Westinghouse, is partially recrystallized and has a lower tin content (0.67 wt%). Westinghouse has also produced other versions of ZIRLO, with intermediate concentrations of Sn.

Unfortunately, in-reactor corrosion data for ZIRLO cladding are often presented without proper discrimination of various versions of the material, which makes it difficult to evaluate the data. However, it is clear that in-reactor clad oxide growth is somewhat slower for ZIRLO type materials than for Zircaloy-4. This is illustrated in figure 3.3, which shows in-reactor corrosion data for ZIRLO, presented by Kaiser et al. (2000) and Shimomura et al. (2004). It is not clear from these references if the data pertain to standard or optimized ZIRLO, but since the corrosion rate seems fairly high, there is reason to believe that the material in question is standard ZIRLO.

A comparison of figure 3.3 with figure 3.2 reveals that oxide growth is slower for ZIRLO than for Zircaloy-4. More precisely, a best fit to the ZIRLO data in figure 3.3 was obtained by pre-multiplying the oxide growth rate in equation (3.2) by 0.78.

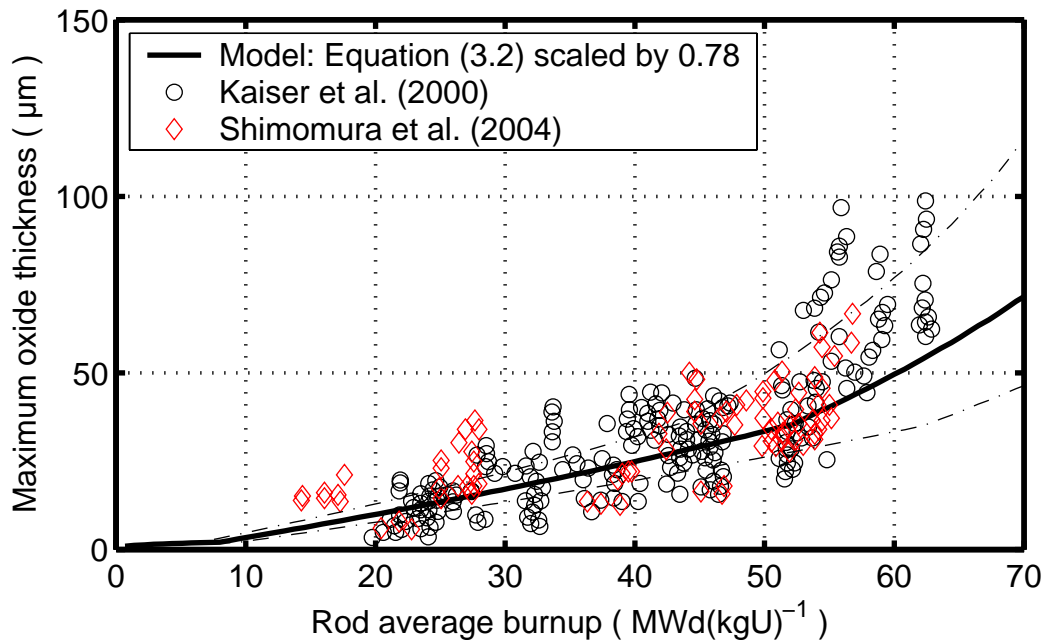


Figure 3.3: Calculated clad oxide growth for ZIRLO in comparison with data by Kaiser et al. (2000) and Shimomura et al. (2004). The thick full line corresponds to a clad oxide-to-water interface temperature of 603.5 K, whereas the thin dashed lines are the results of a ± 5 K variation of this temperature.

The result of this scaling is shown in figure 3.3, where the calculated oxide growth for the reference case in table 3.2 is plotted. The oxide growth is well captured by the model up to the second transition at $\delta_{ox}=35 \mu\text{m}$, but the enhanced oxidation rate beyond this point is underestimated by the model. However, since the high-burnup corrosion acceleration indicated by the data in figure 3.3 is more severe than what is expected from the current (optimized) versions of ZIRLO, we still believe that the correlation in equation (3.2) is applicable to ZIRLO. Therefore, the only modification we propose for applying equation (3.2) to ZIRLO is to scale the oxidation rate on the right-hand-side by 0.78. Hence, according to our evaluation of in-reactor corrosion data, the oxide growth rate is about 20 % lower for ZIRLO than for Zircaloy-4. This finding is in line with the results of a recent comparison of clad alloys, presented by Tsukuda et al. (2003).

3.1.1.3 M5 oxide growth

M5 is a trademark of Framatome ANP, which designates a ternary alloy used for clad tubes in pressurized water reactors (Mardon et al. 2000). The composition is Zr-1.0Nb-0.13O by wt%, and in contrast to most other PWR clad materials, M5 is fully recrystallized in the final step of the clad tube fabrication process. In comparison with Zircaloy-4 cladding, M5 has better corrosion performance and a higher resistance to creep deformation (Mardon et al. 1997).

In-reactor corrosion data for M5 cladding is shown in figure 3.4. The data are taken from a conference paper by Seibold and Mardon (2002), and they clearly show that the oxide growth is slower for M5 than for ZIRLO and Zircaloy-4 clad materials; confer figures 3.2 and 3.3. For comparison, the oxide growth for the reference case in table 3.2 was calculated through equation (3.2).

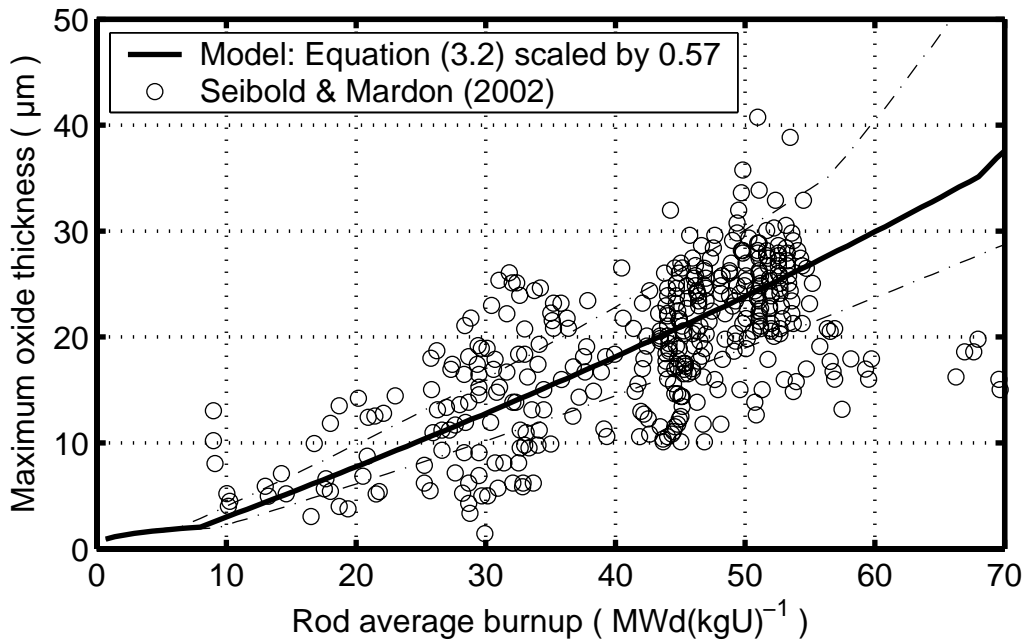
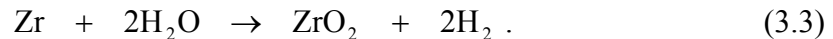


Figure 3.4: Calculated clad oxide growth for M5 in comparison with data by Seibold and Mardon (2002). The thick full line corresponds to a clad oxide-to-water interface temperature of 603.5 K, whereas the thin dashed lines are the results of a ± 5 K variation of this temperature.

A best fit to the M5 data, as shown in figure 3.4, was obtained by scaling the oxide growth rate in equation (3.2) by 0.57. Hence, according to our evaluation of the data presented by Seibold and Mardon (2002), the in-reactor oxide growth rate of M5 is about 40 % lower than for Zircaloy-4. It is interesting to note that no trend for acceleration of the clad corrosion rate at high burnup can be found in the data of Seibold and Mardon in figure 3.4. The measured oxide thickness is generally below 35 μm , which is the second transition point to accelerated corrosion in equation (3.2). Here, we shall recall that Limbäck et al. (1994) proposed this threshold, based on the observation that hydride precipitation took place at the clad metal-to-oxide interface when the oxide layer thickness reached 30-40 μm . This observation pertains to Zircaloy-4, and may not apply to M5 cladding, which has a much lower hydrogen pickup; see section 3.1.2. In fact, if hydride precipitation is the root cause to accelerated oxide growth at high burnup, the acceleration should start at oxide thicknesses $\gg 35 \mu\text{m}$ for M5 cladding. At this moment, experimental data are unavailable to support or confute this assumption, and a threshold oxide thickness of 35 μm will therefore be used in equation (3.2) also for M5 cladding. In conclusion, the only modification we propose for applying equation (3.2) to M5 is to scale the oxidation rate on the right-hand-side by 0.57.

3.1.2 Clad hydrogen pickup

Waterside corrosion of the clad tube results in a gradual increase of the materials hydrogen content, since hydrogen is liberated in the corrosion process (IAEA, 1998). The process may in simplified terms be written



Most of the hydrogen that is produced in the corrosion process is dissolved into the coolant water, but a certain fraction is picked up by the clad material. This pickup fraction depends on the clad material properties, coolant conditions and also on the clad oxide layer thickness; the hydrogen pickup fraction generally decreases as the oxide layer thickens. The latter effect is neglected in the model for clad hydrogen pickup in FRAPCON-3.2, and a constant pickup fraction is used, which is set according to clad material (Zircaloy-2/4) and coolant conditions (BWR/PWR) as shown in table 3.3.

Clad material	BWR	PWR
Zircaloy-2	0.29	0.48
Zircaloy-4	0.12	0.15

Table 3.3: Clad hydrogen pickup fractions used in FRAPCON-3.2.

We have extended the current modelling approach for hydrogen pickup to ZIRLO and M5 cladding under PWR conditions, based on corrosion data reported in open literature. For ZIRLO, Sabol et al. (1997) reported that the hydrogen pickup fraction was comparable to that for low-tin Zircaloy-4. The same conclusion was reached by Tsukuda et al. (2003), who compared the hydrogen pickup fractions for ZIRLO and low-tin Zircaloy-4 cladding, irradiated to high exposures.

For clad tubes with oxide layers thicker than 30 μm , they measured hydrogen pickup fractions of 0.12-0.14 for ZIRLO and 0.12-0.17 for low-tin Zircaloy-4. We therefore conclude that a hydrogen pickup fraction of 0.15 can be used for ZIRLO as well as for Zircaloy-4. The advantage of ZIRLO over Zircaloy-4 with respect to hydrogen accumulation seems thus related to the lower corrosion rate, and not to the hydrogen pickup fraction.

The situation is different for M5 cladding, which is known to have very low hydrogen absorption in comparison with other PWR clad tube materials (Mardon et al. 1997). As shown in section 3.1.1.3, M5 has a lower oxidation rate than ZIRLO and Zircaloy-4, but the lower corrosion rate alone cannot explain the low hydrogen absorption for M5. Figure 3.5 shows the radial average hydrogen content in M5 and low-tin Zircaloy-4 cladding, measured in PWR fuel rods with various burnups (Mardon et al. 2000) and (Seibold & Mardon, 2002). For comparison, the calculated hydrogen pickup for the reference case in table 3.2 is also included for these two materials.* The calculations were done with FRAPCON-3.2, using the clad oxide growth models proposed in section 3.1.1 and assuming a constant hydrogen pickup fraction of 0.15 and 0.06 for low-tin Zircaloy-4 and M5, respectively. The latter pickup fraction was obtained by a best fit to the M5 data, as shown in figure 3.5. It is interesting to note that the calculated hydrogen content for low-tin Zircaloy-4 is in fair agreement with the measured data in figure 3.5. This indicates that the pickup fraction used for Zircaloy-4 in FRAPCON-3.2 is correct.

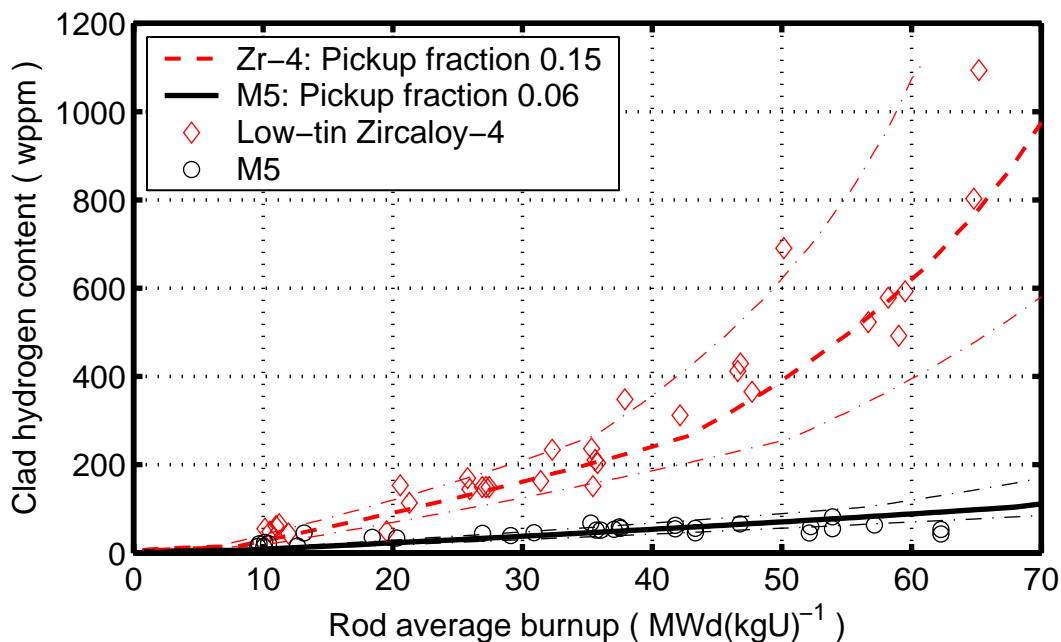


Figure 3.5: Calculated clad hydrogen pickup for low-tin Zircaloy-4 and M5, in comparison with data by Mardon et al. (2000) and Seibold and Mardon (2002). The thick lines correspond to a clad oxide-to-water interface temperature of 603.5 K, whereas the thin dashed lines are the results of a ± 5 K variation of this temperature.

* Note: The calculated curves are *hydrogen pickup*, whereas measured data are *total* hydrogen content, thus including the initial hydrogen content in the cladding. The initial hydrogen content is usually about 10 wppm.

To summarize, based on our evaluation of PWR clad corrosion data, we propose the following hydrogen pickup fractions to be used in FRAPCON-3.2:

- For standard Zircaloy-4, low-tin Zircaloy-4 and ZIRLO cladding, a pickup fraction of 0.15 is recommended.
- For M5 cladding, a hydrogen pickup fraction of 0.06 is suggested, based on the rather few data available in open literature.

These recommendations pertain to typical PWR operating conditions and to analyses of fuel rods at high burnup. For fresh fuel with un-oxidized cladding, the hydrogen pickup fractions are generally higher. The database, upon which the above recommendations are based, includes measurements performed on fuel rods that were operated up to average burnups of about $65 \text{ MWd}(\text{kgU})^{-1}$.

3.2 Clad mechanical properties

There is a progressive change in the clad tube mechanical properties during irradiation, which is caused by accumulation of irradiation damage in the material and by clad waterside corrosion. The irradiation damage saturates early in life, usually within the first years of fuel operation. Changes of the clad material properties by corrosion, on the other hand, progress continuously with increasing burnup. Effects of waterside corrosion are therefore generally more important than irradiation damage, when studying the clad mechanical properties of high-burnup fuel rods.

Although the external oxide layer in itself influences both the thermal and mechanical behaviour of high burnup fuel, the clad mechanical properties are primarily affected by the migration of dissolved hydrogen, produced by the metal-water reactions, into the material beneath the oxide layer. Hydrogen is known to have a detrimental effect on clad strength and ductility, since it precipitates as brittle zirconium hydrides at hydrogen concentration above the terminal solid solubility. Moreover, the hydride precipitation leads to swelling of the clad material, an effect that contributes to fuel rod axial growth at high burnup.

3.2.1 Yield stress

Precipitation of zirconium hydrides in the clad tube leads to embrittlement, which means that the materials ability to endure plastic deformation is reduced. Moreover, the hydrogen-induced embrittlement also leads to a loss of clad strength and to a reduced yield limit for the material. In order to evaluate these effects, an international test program, PROMETRA, is being carried out on various clad tube materials from highly irradiated PWR fuel rods (Desquines, 2004). The program is focused on the mechanical behaviour of severely corroded cladding under reactivity initiated accidents (RIA), and mechanical property tests are made at high strain rates to simulate the loading conditions under such accidents.

The PROMETRA program provides valuable data, and we have used these data to verify the correlation for clad yield stress that is currently used in FRAPCON-3.2.

This correlation is based on a model from the MATPRO materials property package (Hagrman et al. 1981), which has been modified to account for the effects of hydride precipitation in severely corroded Zircaloy-2 and Zircaloy-4 cladding (Lanning et al. 1997a). The correlation is confined to a rather narrow range of application, as defined in table 3.4, and it has to our knowledge not been verified with respect to experimental data for Zr-Nb type clad materials, such as ZIRLO and M5.

We have compared the yield stress correlation in FRAPCON-3.2 with the results of 21 hoop tensile tests and 4 burst tests, carried out on standard Zircaloy-4, ZIRLO and M5 cladding from high-burnup PWR fuel rods within the PROMETRA program. The test samples were taken from commercial fuel rods, irradiated to 55-74 MWd(kgU)⁻¹ rod average burnup in French and Spanish PWRs. The test conditions are summarized in table 3.4. It should be remarked that all the tests were carried out at strain rates that were far outside the range covered by the yield stress correlation in FRAPCON-3.2. In addition, the hydrogen content and oxide layer thickness were in many samples beyond the range of application for the model.

	Clad temperature [K]	Clad strain rate [s ⁻¹]	Hydrogen content [wppm]	Oxide thickness [μm]
Range of application for FRAPCON correlation	560 - 700	10 ⁻⁵ - 10 ⁻⁴	0 - 650*	0 - 100
Test conditions for standard Zircaloy-4	553 - 673	10 ⁻²	140 - 1040	15 - 130
Test conditions for ZIRLO	553	3×10 ⁻³ - 10 ⁰	650 - 760	80 - 95
Test conditions for M5	553	3×10 ⁻³ - 10 ⁰	105 - 120	15 - 17

Table 3.4: Conditions of selected PROMETRA tests, in comparison with the range of application for the FRAPCON-3.2 clad yield stress correlation.

Figure 3.6 shows the calculated clad yield stress ($\sigma_{y,0.2}$) for each of the 25 tests, in comparison with measured data. The calculated yield stress is for most of the tests within a ± 100 MPa error band, indicated by the thin dashed lines in figure 3.6. Moreover, the data for ZIRLO and M5 cladding are accurately captured by the yield stress correlation in FRAPCON-3.2. We note that the yield stress of M5 is somewhat lower than for standard Zircaloy-4 and ZIRLO cladding. This is consistent with the fact that M5 is recrystallized, whereas the other materials are stress relieved annealed as a final heat treatment in the manufacturing process. The impact of final heat treatment on the yield stress is successfully accounted for in the FRAPCON model.

In conclusion, the results indicate that the correlation for clad yield stress in FRAPCON-3.2 is applicable to a wider range of strain rates and clad hydrogen concentrations than what is reported in the model description (Lanning et al. 1997a).

* This range pertains to the amount of *excess* hydrogen in the cladding, i.e. the hydrogen in excess of the solid solubility.

Moreover, the correlation seems to be applicable not only to Zircalloys, but also to ZIRLO and M5 cladding. Additional experimental data are, however, needed to fully confirm this conclusion.

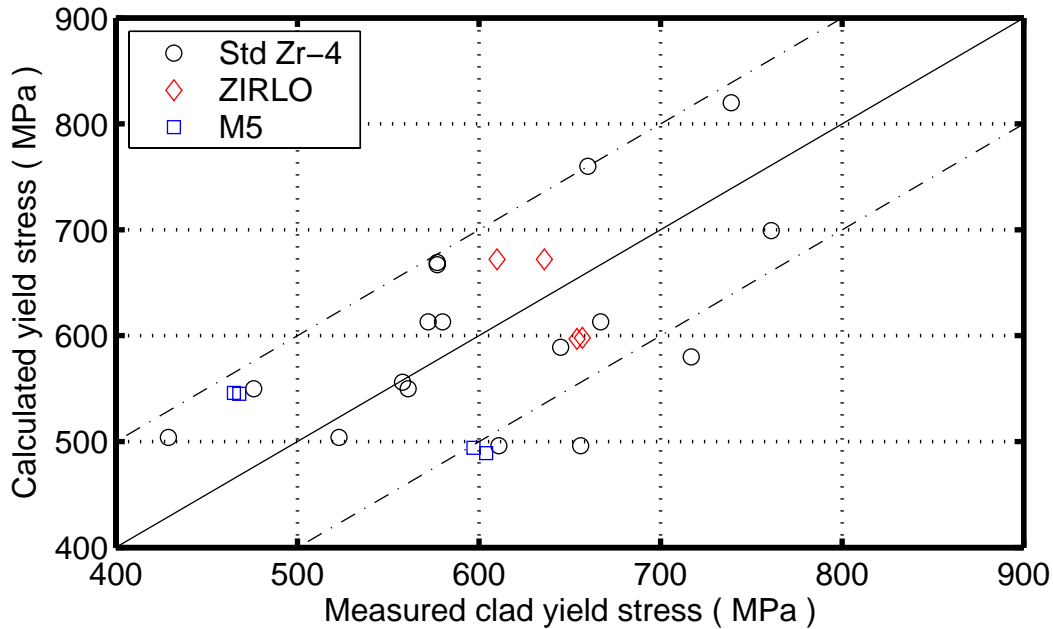


Figure 3.6: Calculated vs. measured clad yield stress for the PROMETRA tests in table 3.4.

3.2.2 Rod axial growth

Axial elongation of the cladding tube under in-reactor operation is a well-known phenomenon, which is somewhat carelessly termed ‘rod growth’. There are several deformation mechanisms that contribute to the axial growth:

- Irradiation-induced clad deformation, which accumulates with fast neutron fluence (Kubo, 1990). This deformation mechanism is anisotropic, and closely related to the material texture. Stress relieved annealed cladding grows about twice as fast in the axial direction as recrystallized cladding, as a result of differences in texture.
- Hydride-induced clad swelling. This deformation mechanism is caused by clad hydrogen pickup and subsequent formation of zirconium hydrides, which involves a volumetric expansion of 17 %. In severely hydrided cladding, with average hydrogen contents in excess of 500-700 wppm, axial growth from hydride-induced swelling usually dominates over irradiation-induced deformation.
- Clad creep and plastic deformation. Axial elongation of the clad tube by creep and plasticity requires axial tensile stresses in the clad tube. This is in contrast to the above deformation mechanisms, which take place also under stress-free conditions. Significant axial tensile stresses in the cladding tube may result from pellet-clad mechanical interaction at high burnup and high power.

Rod axial growth is in FRAPCON-3.2 modelled by use of a correlation between clad axial elongation and fast neutron fluence, which discriminates between recrystallized and stress relieved annealed Zircaloy materials (Lanning et al. 1997a).

Hence, the rod growth calculated by FRAPCON-3.2 is correlated to the fast neutron fluence, without explicitly accounting for the contribution from hydride-induced clad swelling. Instead, the effect of hydride-induced swelling is lumped together with the irradiation-induced growth in the aforementioned correlation to the fast neutron fluence. Consequently, we may suspect that this correlation will not work properly for a clad material that for some reason has an unusual relation between hydrogen content and fast fluence. The contributions from irradiation-induced clad deformation and hydride-induced swelling should therefore be separated, when formulating a model for rod axial growth.

Likewise, we may suspect that the correlation in FRAPCON-3.2 will overestimate the growth of a material like M5, whose hydrogen absorption is much less than that for Zircaloy-4 or ZIRLO. Figure 3.7 shows rod growth data for PWR fuel rods with M5 cladding, in comparison with the correlation for clad axial growth in FRAPCON-3.2. Obviously, the M5 data of Seibold and Mardon (2002) fall between the model predictions for axial growth of stress relieved annealed and recrystallized cladding. For fast neutron fluences ($>1\text{MeV}$) in excess of 10^{26} m^{-2} , the correlation for recrystallized material is closest to the experimental data. We therefore suggest that the model for recrystallized material should be used for M5 cladding, until sufficient data become available to formulate a particular growth correlation for this clad alloy.

Rod growth data for standard ZIRLO cladding (Zr-1.0Nb-1.0Sn-0.1Fe by wt%) have been reported by Sabol et al. (1994). These data thus pertain to the original version of ZIRLO, with a tin content and final heat treatment that are different from the current (optimized) ZIRLO material; see section 3.1.1.2. The rod growth measurements in the paper by Sabol et al. were made on fuel rods that had been irradiated in the BR-3 test reactor in Mol, Belgium, and in the North Anna Unit 1 reactor, which is a commercial PWR in Virginia, USA. The data are shown in figure 3.8, in comparison with the correlations for clad tube axial growth in FRAPCON-3.2.

Although the amount of data is limited, figure 3.8 suggests that the FRAPCON growth correlation for recrystallized cladding is applicable to standard ZIRLO. Additional data are needed for fast neutron fluences $> 7.5 \times 10^{25}$ to further corroborate this assumption. Moreover, rod growth data are warranted for the current (optimized) version of ZIRLO.

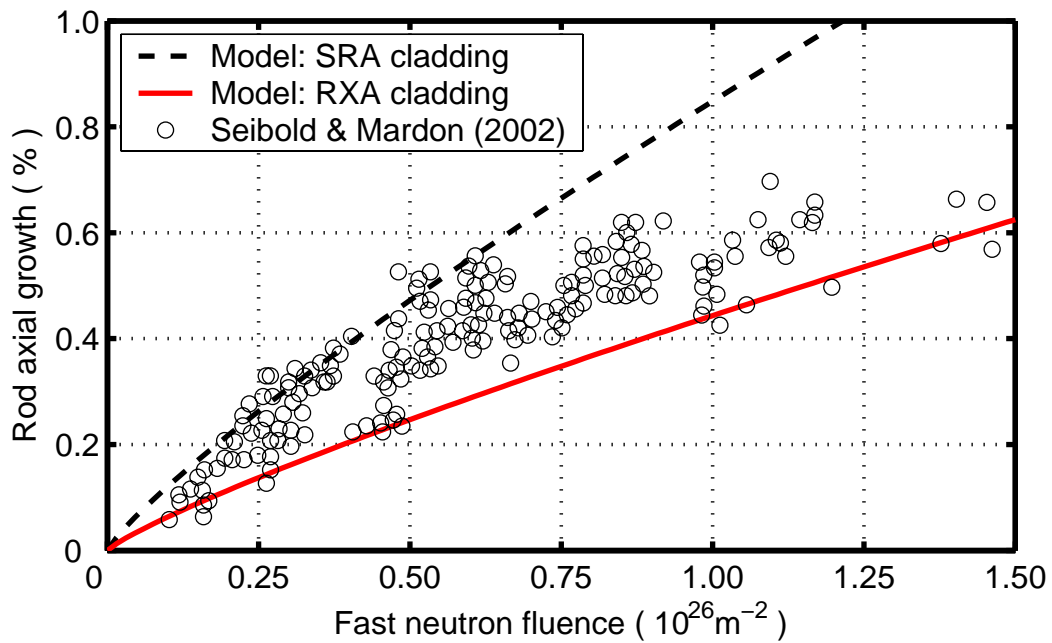


Figure 3.7: Axial growth data for PWR fuel rods with M5 cladding, in comparison with the FRAPCON-3.2 models for stress relieved annealed (SRA) and recrystallized (RXA) clad materials.

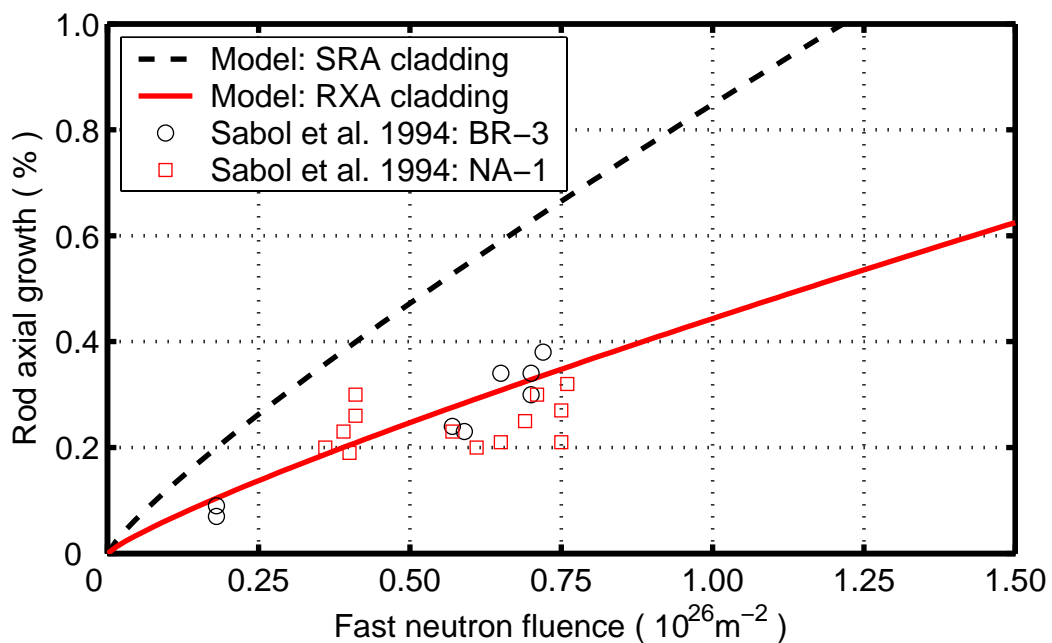


Figure 3.8: Axial growth data for PWR fuel rods with standard ZIRLO cladding, in comparison with the FRAPCON-3.2 models for stress relieved annealed (SRA) and recrystallized (RXA) clad materials. BR-3 and AN-1 allude to the reactors, in which the fuel rods were irradiated.

4 Summary and conclusions

Phenomena with particular relevance to the thermo-mechanical behaviour of LWR fuel rods at high burnup were studied in this report, and suitable models were proposed to cater for these phenomena in computer analyses of the fuel rod behaviour. The proposed models are intended for implementation in the FRAPCON-3.2 computer code, which is currently used by the Swedish Nuclear Power Inspectorate to analyse the thermo-mechanical performance of fuel rods under normal, steady-state reactor operation.

Among the phenomena studied in the report is the restructuring of UO₂ fuel at high burnup, the so called rim zone formation, and its effect on fuel porosity build-up, thermal conductivity and fission gas release. Theoretical as well as empirical models for irradiation-induced restructuring of UO₂ were evaluated, and a recent theoretical model by Rest (2004) was, after some modifications, found to successfully reproduce the experimentally observed formation of a high-burnup microstructure at the periphery of UO₂ fuel pellets. This restructuring is characterized by a simultaneous increase in micron-sized porosity and reduction in fuel grain size. A physically based model for build-up of rim zone porosity was formulated, and an empirical approach to handle enhanced athermal fission gas release from the restructured material was proposed. Moreover, the impact of UO₂ high-burnup restructuring on fuel thermal conductivity was discussed in light of recent experimental data from the High Burnup Rim Project.

Moreover, an integral thermal fission gas release model, which accounts for gas diffusion in UO₂ grain, gas capture by intragranular gas bubbles, irradiation-induced resolution, grain boundary gas saturation and grain boundary gas sweeping, was coded in a program module for implementation into FRAPCON-3.2. The module comprises new grain growth correlations, which were deduced using the data obtained from the ramp tests made on high burnup fuel in the Third Risø Fission Gas Release Project. Sample computations of fission gas release as a function of irradiation time at different isotherms at a high power density, carried out using this module, reveal the intimate connection between fission gas release and fuel grain growth due to the phenomenon of grain boundary sweeping. Following the implementation of this module in FRAPCON-3.2, the code should be benchmarked with a number of available ramp tests, such as the Third Risø Fission Gas Release Project, to qualify it for fission gas release analysis of fuel rods subjected to power ramps.

Models for the clad tube behaviour were also discussed, with special emphasis given to clad waterside corrosion in high-burnup fuel rods. Models for clad oxide growth and hydrogen pickup in PWRs, applicable to Zircaloy-4, ZIRLO or M5 cladding, were formulated, based on recent in-reactor corrosion data for high-burnup fuel rods. The experimental database behind these models comprises fuel rods with average exposures up to about 65 MWd(kgU)⁻¹. Our evaluation of this database indicates that the oxidation rate of ZIRLO-type clad materials is about 20 % lower than for standard Zircaloy-4 cladding under typical PWR conditions. Likewise, the oxidation rate of M5 seems to be about 40 % lower than for Zircaloy-4.

From the same database, we found that standard Zircaloy-4 and ZIRLO-type cladding have similar hydrogen pickup fractions (≈ 0.15) under typical PWR conditions, but that the pickup fraction is significantly lower for the M5 alloy (≈ 0.06). The new PWR clad corrosion models are intended for implementation in FRAPCON-3.2. With the new models, the code will be applicable to ZIRLO and M5 cladding, and its predictability of Zircaloy-4 clad corrosion at high fuel rod burnup will also be improved.

Finally, with the aim to extend the modelling capability to M5 and ZIRLO-type clad materials, the correlations for clad yield stress and axial growth in FRAPCON-3.2 were compared with measured data for these materials. By use of the PROMETRA database for mechanical properties of PWR clad materials at high exposures, the current clad yield stress correlation in FRAPCON-3.2 was found to be applicable to both M5 and ZIRLO without modification. Moreover, calculated rod axial elongations were in fair agreement with the in-reactor rod growth data at hand.

5 References

- Ainscough, J.B., Oldfield, B.W. and Ware, J.O., 1973.
Isothermal grain growth kinetics in sintered UO₂ pellets,
Journal of Nuclear Materials, 49, pp 117-128.
- Atkinson, H.V., 1988.
Theories of grain growth in pure single phase systems,
Acta Metallurgica, 36, pp 469-491.
- Bagger, C., Mogensen, M., and Walker, C.T., 1994.
Temperature measurements in high burnup UO₂ nuclear fuel: implications for thermal conductivity, grain growth and gas release,
Journal of Nuclear Materials, 211, pp 11-29.
- Barner, J.O., Cunningham, M.E., Freshley, M.D. and Lanning, D.D., 1993.
Evaluation of fission gas release in high-burnup light water reactor fuel rods,
Nuclear Technology 102, pp 210-231.
- Baron, D., Hermitte, B. and Piron, J.P., 1996.
An attempt to simulate the porosity buildup in the rim at high burnup,
Proc. IAEA Technical Committee Meeting on advances in pellet technology for improved performance at high burnup, Oct 28 - Nov 1, Tokyo, Japan, 1996.
- Berna, G.A., Beyer, C.E., Davies, K.L. and Lanning, D.D., 1997.
FRAPCON3: A computer code for the calculation of steady-state, thermal-mechanical behavior of oxide fuel rods for high burnup, U.S. Nuclear Regulatory Commission Report NUREG/CR-6534, Volume 2, December 1997.
- Bernard, L.C., Jacoud, J.L. and Vesco, P., 2002.
An efficient model for the analysis of fission gas release,
Journal of Nuclear Materials, 302, pp 125-134.
- Booth, A.H., 1957.
A method of calculating fission gas diffusion from UO₂ fuel and its application to the X-2-f test, AECL Report 496.
- Burke, J.E. and Turnbull, D., 1952.
Recrystallization and grain growth,
Progress in Metal Physics, 3, pp 220-292.
- Combette, P. and Zacharie, I., 1999.
Reply to comments by J. H. Evans about two papers,
Journal of Nuclear Materials, 275, pp 112-114.

- Desquines, J., 2004.
Release of the PROMETRA V2.1 material database (Zircaloy-4, Zirlo, M5),
CABRI Water Loop Note CWL 2004/64, IRSN, France.
- El-Saied, U.M. and Olander, D.R., 1993.
Fission gas release during grain growth in microstructure with a distribution of grain sizes, Journal of Nuclear Materials 207, pp 313-326.
- Feltham, P., 1957.
Grain growth in metals,
Acta Metallurgica, 5, pp 97-105.
- Fiero, I. B., Krammen, M.A. and Freeburn, H.R., 1987.
ESCORE - the steady-state core reload evaluator code: General description,
EPRI-NP-5100, Project 2061-6 -13 Final Report. Prepared for Electric Power Research Institute, Palo Alto, California, 1987.
- Forsberg, K. and Massih, A.R., 1985.
Fission gas release under time varying conditions,
Journal of Nuclear Materials, 127, pp. 141-145.
- Forsberg, K. and Massih, A.R., 1985.
Diffusion theory of fission gas migration in irradiated nuclear fuel UO₂,
Journal of Nuclear Materials, 135, pp. 140-148.
- Forsberg, K., Massih, A.R. and Andersson, K., 1986.
Calculation of fission gas migration in nuclear fuel with re-solution effect,
Proc. of the Enlarged Halden Programme Group Meeting on Fuel Performance Experiments and Analysis, Sanderstølen, Norway, March 1986.
- Forsberg, K., Lindström, F. and Massih, A.R., 1994.
Modelling of some high burnup phenomena in nuclear fuel,
Proc. of the IAEA Technical Meeting on Water Reactor Fuel Element Modelling at High Burnup and Experimental Support, Windermere, UK, September 1994.
- Forsberg, K. and Massih, A.R., 2001.
Theory of fission gas release during grain growth,
Transactions, SMiRT 16, Washington DC, August 2001.
- Forsberg, K. and Massih, A.R., 2005.
Kinetics of fission gas release under grain growth,
Under preparation.
- Garzarolli, F., Jung, W., Schoenfeld, H., Garde, A.M., Parry, G.W. and Smerd, P.G., 1982. *Waterside corrosion of Zircaloy fuel rods,*
EPRI Report NP-2789, Electric Power Research Institute, Palo Alto, California.

Grapengiesser, G., Massih, A.R., Nylund, O., Hyden, L., Andersson, S.O., Patrakka, E. and Rönnerberg, G., 1988.

High burnup evaluation activities in Sweden and Finland,
Proc. of the ANS International Topical Meeting on LWR Fuel Performance,
Williamsburg, April 1988.

Hagrman, D. L., Reymann, G.A. and Mason, G.E., 1981.

A handbook of materials properties for use in the analysis of light water reactor fuel rod behavior, MATPRO Version 11 (Revision 2), NUREG/CR-0479 (TREE-1280), prepared by EG&G Idaho, Inc., Idaho Falls, Idaho for the U.S. Nuclear Regulatory Commission, Washington, D.C., 1981.

Ham, F. S., 1958.

Theory of diffusion-limited precipitation,
Journal of Physics and Chemistry of Solids, 6, pp 335-351.

Hargreaves, R. and Collins, D.A., 1976.

A quantitative model for fission gas release and swelling in irradiated uranium dioxide,
Journal of British Nuclear Energy Society, 15, pp 311-318.

Hede, G., 1994.

Numerical solution of kinetic equations for fission gas release with grain growth,
M.Sc. Dissertation, Uppsala University, UPTEC 94 034E, Uppsala, Sweden, March 1994.

Hermansson, P. and Massih, A.R., 2002.

An effective method for calculation of diffusive flow in spherical grains,
Journal of Nuclear Materials, 304, pp 204-211.

Hillert, M., 1965.

On the theory of normal and abnormal grain growth,
Acta Metallurgica, 13, pp 227-238.

IAEA, 1998.

Waterside corrosion of zirconium alloys in nuclear power plants,
International Atomic Energy Agency, Report TECDOC-996, Vienna, Austria.

Jernkvist, L.O. and Massih, A.R., 2002.

Analysis of the effect of UO₂ high burnup microstructure on fission gas release,
Swedish Nuclear Power Inspectorate (SKI) research report 02:56, October 2002.

Kameyama, T., Matsumura, T. and Kinoshita, M., 1994.

Numerical analysis for microstructure change of a light water reactor fuel pellet at high burn-up, Nuclear Technology 106, pp 334-341.

Kaiser, R.S., Leech, W.J. and Casadei, A.L., 2000.

The fuel duty index (FDI) – A new measure of fuel rod cladding performance,
Proc. ANS Topical Meeting on Light Water Reactor Fuel Performance, Park City, Utah,
April 10-13, 2000

Khoruzhii, O.V., Kourtchatov, S.Y. and Likhanskii, V.V., 1999.
New model of equiaxed grain growth in irradiated UO₂,
Journal of Nuclear Materials, 265, pp 112-116.

Kinoshita, M., 1997.
Towards the mathematical modelling of rim structure formation,
Journal of Nuclear Materials, 248, pp 185-190.

Kinoshita, M., Sonoda, T., Kitajima, S., Sasahara, A., Kolstad, E., Matzke, H.,
Rondinella, V.V., Stalios, A.D., Walker, C.T., ray, I.L.F., Scheindlin, M., Halton, D.
and Ronchi, C., 2000. *High burnup rim project (II): Irradiation and examination to
investigate rim-structured fuel*, Proc. ANS Topical Meeting on Light Water Reactor
Fuel Performance, Park City, Utah, April 10-13, 2000.

Kinoshita, M., Sonoda, T., Kitajima, S., Sasahara, A., Kameyama, T., Matsumura, T.,
Kolstad, E., Rondinella, V.V., Ronchi, C., Hiernaut, J.P., Wiss, T., Kinnart, F., Ejton, J.,
Papaioannou, D. and Matzke, H., 2004.
High Burnup Rim Project (III): Properties of rim-structured fuel,
Proc. 2004 International Meeting on Light Water Reactor Fuel Performance, Orlando,
Florida, September 19-22, 2004.

Kogai, T., 1997.
Modelling of fission gas release and gaseous swelling of light water reactor fuels,
Journal of Nuclear Materials, 244, pp 131-140.

Kubo, T., 1990.
Irradiation growth in zirconium alloys under high fluences,
Res Mechanica, 29, pp 289-312.

Lanning, D. D., Beyer, C. E. and Painter, C. L., 1997a.
*FRAPCON-3: Modifications to fuel rod material properties and performance models
for high-burnup application*, NUREG/CR-6534, PNNL-11513, Vol. 1, prepared for the
U.S. Nuclear Regulatory Commission by Pacific Northwest Laboratory, Richland,
Washington, 1997.

Lanning, D. D., Beyer, C. E. and Berna, G. A., 1997b.
FRAPCON-3: Integral assessment,
NUREG/CR-6534, PNNL-11513, Vol. 3, prepared for the U.S. Nuclear Regulatory
Commission by Pacific Northwest Laboratory, Richland, Washington, 1997.

Lanning, D.D., Beyer, C.E. and Cunningham, M.E., 2000.
*FRAPCON-3 fuel rod temperature predictions with fuel conductivity degradation
caused by fission products and gadolinia additions*, Proc. ANS Topical Meeting on
Light Water Reactor Fuel Performance, Park City, Utah, April 10-13, 2000.

Lassmann, K., Walker, C.T., van de Laar, J. and Lindström, F., 1995.
Modelling the high burnup UO₂ structure in LWR fuel,
Journal of Nuclear Materials, 226, pp 1-8.

- Lassmann, K., 2000.
Numerical algorithms for intragranular diffusional release incorporated in the TRANSURANUS code,
International Seminar on Fission Gas Behavior in Water Reactor Fuels, Cadarache, France, 26-29 September, 2000.
- Lassmann, K. and Benk, H. 2000.
Numerical algorithms for intragranular fission gas release,
Journal of Nuclear Materials, 280, pp 127-135.
- Lassmann, K., Schubert, A., van de Laar, J. and Vennix, C.W.H.M., 2000.
Recent developments of the TRANSURANUS code with emphasis on high burnup phenomena, Proc. IAEA Technical Committee Meeting on nuclear fuel behaviour modeling at high burnup and its experimental support, June 19-23, Windermere, UK, 2000.
- Lee, B.H., Koo, Y.H. and Sohn, D.S., 2001.
Rim characteristics and their effects on the thermal conductivity in high burnup UO₂ fuel, Journal of Nuclear Science and Technology, 38(1), pp 45-52.
- Lewis, B.J., 1987.
Fission product release from nuclear fuel by recoil and knockout,
Journal of Nuclear Materials, 148, pp 28-42.
- Lifshitz, I.M. and Slyozov, V.V., 1961.
The kinetics of precipitation from supersaturated solid solutions,
Journal of Physics and Chemistry of Solids, 19, pp 35-50.
- Limbäck, M., Krammen, M.A., Rudling, P., Pati, S.R. and Garde, A.M., 1994.
Corrosion and hydriding performance of Zircaloy-2 and Zircaloy-4 cladding materials in PWRs, Proc. ANS Topical Meeting on Light Water Reactor Fuel Performance, West Palm Beach, Florida, April 17-21, 1994, pp 286-295.
- Limbäck, M., 1996.
Comparison of models for Zircaloy cladding corrosion in PWR's,
Halden Reactor Project Report HWR-468, Halden, Norway, March 1996.
- Lorenz, R.A., 1979.
ANS-5.4 fission gas release model III, low temperature release,
Proc. of the ANS Topical Meeting on LWR Fuel Performance, Portland, Oregon, April 1979.
- Manzel, R. and Walker, C.T., 2000.
High burnup fuel microstructure and its effect on fuel rod performance,
Proc. ANS Topical Meeting on Light Water Reactor Fuel Performance, Park City, Utah, April 10-13, 2000.
- Manzel, R. and Walker, C.T., 2002.
EPMA and SEM of fuel samples from PWR rods with an average burn-up of around 100 MWd/kgHM, Journal of Nuclear Materials, 301, pp 170-182.

- Mardon, J.P., Garner, G., Beslu, P., Charquet, D. and Senevat, J., 1997.
Update on the development of advanced zirconium alloys for PWR fuel rod claddings, Proc. ANS Topical Meeting on Light Water Reactor Fuel Performance, Portland, Oregon, March 2-6, 1997, pp 405-413.
- Mardon, J.P., Charquet, D. and Senevat, J., 2000.
Influence of composition and fabrication process on out-of-pile and in-pile properties of M5 alloy, Zirconium in the Nuclear Industry: 12th Int. Symp. ASTM STP 1354, Editors: G.P. Sabol and G.D. Moan, American Society for Testing and Materials, pp 505-524.
- Matthews, J.R. and Wood, M.H., 1980.
An efficient method for calculating diffusive flow to a spherical boundary, Nuclear Engineering & Design, 56, pp 439-443.
- Matzke, H.J., 1980.
Gas release mechanisms in UO₂- a critical review, Radiation Effects, 53, pp 219-242.
- Matzke, H.J., 1992.
On the rim effect in high burnup UO₂ LWR fuels, Journal of Nuclear Materials, 189, pp 141-148.
- Matzke, H.J., 1995.
The rim-effect in high burnup UO₂ nuclear fuel, In P. Vincenzini (ed), Ceramics: Charting the Future, Proc. World Ceramics Congress, Florence, Italy, June 28 - July 4, pp 2913-2920.
- Mogensen, M., Pearce, J.H. and Walker, C.T., 1999.
Behaviour of fission gas in the rim region of high burn-up UO₂ fuel pellets with particular reference to results from an XRF investigation, Journal of Nuclear Materials, 264, pp 99-112.
- Nogita, K. and Une, K., 1995.
Irradiation-induced recrystallization in high burnup UO₂ fuel, Journal of Nuclear Materials, 226, pp 302-310.
- Noirot, J., Noitot, L., Desgranges, L., Lamontagne, J., Blay, Th., Pasquet, B. and Muller, E., 2004. *Fission gas inventory in PWR high burnup fuel: Experimental characterization and modeling*, Proc. 2004 International Meeting on Light Water Reactor Fuel Performance, Orlando, Florida, September 19-22, 2004.
- Ohira, K. and Itagaki, N., 1997.
Thermal conductivity measurements of high burnup UO₂ pellet and a benchmark calculation of fuel centre temperature, Proc. ANS Topical Meeting on Light Water Reactor Fuel Performance, Portland, Oregon, March 2-6, 1997, pp 541-549.
- Olander, D.R., 1976.
Fundamental Aspects of Nuclear Reactor Fuel Elements, TID-26711-P1, National Technical Service, U. S. Department of Commerce, Springfield, Virginia, 1976.

- Olander, D.R. and Van Uffelen, P., 2001
On the role of grain boundary diffusion in fission gas release,
 Journal of Nuclear Materials, 288, pp 137-147.
- Paraschiv, M.C., Paraschiv, A. and Glodeanu, 1997.
On the fission gas release from oxide fuels during normal grain growth,
 Journal of Nuclear Materials, 246, pp 223-231.
- Paraschiv, M.C., Paraschiv, A. and Grecu, V.V., 1999.
A theoretical study of volatile fission products release from oxide fuels,
 Journal of Nuclear Materials, 275, pp 164-185.
- Phillips, R., 2001.
Crystals, Defects and Microstructure,
 Cambridge University Press, Cambridge, U.K., chap.10.
- Rest, J., 2004.
A model for the influence of microstructure, precipitate pinning and fission gas behavior on irradiation-induced recrystallization of nuclear fuels,
 Journal of Nuclear Materials, 326, pp 175-184.
- Rest, J. and Hofman, G.L., 1994.
Dynamics of irradiation-induced grain subdivision and swelling in U_3Si_2 and UO_2 fuels,
 Journal of Nuclear Materials, 210, pp 187-202.
- Rest, J. and Hofman, G.L., 1995.
Effect of recrystallization in high-burnup UO_2 on gas release during RIA-type transients, Journal of Nuclear Materials, 223, pp 192-195.
- Ronchi, C., Scheindlin, M., Staicu, D. and Kinoshita, M., 2004.
Effect of burn-up on the thermal conductivity of uranium dioxide up to 100.000 $MWd t^{-1}$,
 Journal of Nuclear Materials, pp 58-76.
- Sabol, G.P., Comstock, R.J., Weiner, R.A., Larouere, P. and Stanutz, R.N., 1994.
In-reactor corrosion performance of ZIRLO and Zircaloy-4,
 In: Zirconium in the Nuclear Industry: Tenth Int. Symposium, ASTM STP 1245,
 Eds: A.M. Garde and E.R. Bradley, American Society for Testing and Materials,
 Philadelphia, pp 724-744.
- Sabol, G.P., Comstock, R.J., Schoenberger, G., Kunishi, H. and Nuhfer, D.L., 1997.
In-reactor fuel cladding corrosion performance at higher burnups and higher coolant temperatures, Proc. ANS Topical Meeting on Light Water Reactor Fuel Performance,
 Portland, Oregon, March 2-6, 1997, pp 397-404.
- Schrire, D. and Lysell, G. 1991.
Fuel microstructure and fission product distribution in BWR fuel at different power levels, Proc. of the ANS-ENS International topical meeting on LWR fuel performance,
 Avignon, France, April 1991.

- Seibold, A. and Mardon, J.P., 2002.
M5 cladding experience in European PWRs,
 Jahrestagung Kerntechnik 2002, May 14-16, 2002, Stuttgart, Germany.
- Shimomura, T., Shimizu, J. and Kuwahara, H., 2004.
Design improvements of Mitsubishi fuel assemblies: Challenges for no fuel leak,
 Proc. 2004 International Meeting on Light Water Reactor Fuel Performance, Orlando,
 Florida, September 19-22, 2004.
- Sontheimer, F. and Landskron, H., 2000.
*Puzzling features of EPMA radial fission gas release profiles: The key to realistic
 modeling of fission gas release up to ultra high burnup of 100 MWd/kgM with CARO-E*,
 Proc. IAEA Technical Committee Meeting on nuclear fuel behaviour modeling at high
 burnup and its experimental support, June 19-23, Windermere, UK, 2000.
- Speight, M.V., 1969.
*Calculation on the migration of fission gas in material exhibiting precipitation and re-
 solution of gas atoms under irradiation*,
 Nuclear Science & Engineering, 37, pp 180-185.
- Spino, J., Vennix, K. and Coquerelle, M., 1996.
*Detailed characterization of the rim microstructure in PWR fuels in the burn-up range
 40-67 GWd/tM*, Journal of Nuclear Materials, 231, pp 179-190.
- Thomas, L.E., Beyer, C.E. and Charlot, L.A., 1992.
Microstructural analysis of LWR spent fuels at high burnup,
 Journal of Nuclear Materials, 188, pp 80-89.
- Tsukuda, Y., Kosaka, Y., Kido, T., Doi, S., Sendo, T., Gonzales, P. and Alonso, J.M.,
 2003. *Performance of advanced fuel materials for high burnup*,
 Proc. ENS TopFuel 2003/ANS LWR Fuel Performance Meeting, March 16-19, 2003,
 Wurzburg, Germany.
- Tucker, M.O. and Turnbull, J.A., 1975.
The morphology of interlinked porosity in nuclear fuels,
 Proceedings of Royal Society of London, 343, pp 299-314.
- Turnbull, J.A., 1974.
*The effect of grain size on the swelling and gas release properties of UO₂ during
 irradiation*, Journal of Nuclear Materials, 50, pp 62-68.
- Turnbull, J.A. and Tucker, M.O., 1974.
Swelling in UO₂ under conditions of gas release
 Philosophical Magazine, 30, pp 47-63.
- Turnbull, J.A., 1980.
A review of irradiation induced re-resolution in oxide fuels,
 Radiation Effects, 53, pp 243-250.

Turnbull, J.A., Friskney, C.A., Findlay, J.R., Johnson, F.A. and Walter, A.J., 1982.
The diffusion coefficient of gaseous and volatile species during the irradiation of uranium dioxide,
Journal of Nuclear Materials, 107, pp 168-184.

Turnbull, J.A., White, R.J. and Wise, C., 1988.
The diffusion coefficient for fission gas atoms in uranium dioxide,
Proc. of the IAEA Technical Committee Meeting on Water reactor Fuel Element Computer Modeling, Preston, UK, September 1988.

Turnbull, J.A., 2002.
The high burn-up restructuring of fuel, the so called rim effect: A consideration of its impact on steady-state and transient behaviour,
OECD Halden Reactor Project Report HWR-709, Halden, Norway.

Une, K., Nogita, K., Kashibe, S., Toyonaga, T. and Amaya, M., 1997.
Effect of irradiation-induced microstructural evolution on high burnup fuel behaviour,
Proc. ANS Topical Meeting on Light Water Reactor Fuel Performance, Portland, Oregon, March 2-6, 1997, pp 478-489.

Une, K., Nogita, K., Suzawa, Y., Hayashi, K., Ito, K. and Etoh, Y., 2000.
Effects of grain size and PCI restraint on the rim structure formation of UO₂ fuels,
Proc. ANS Topical Meeting on Light Water Reactor Fuel Performance, Park City, Utah, April 10-13, 2000.

Une, K., Nogita, K., Shiratori, T. and Hayashi, K., 2001.
Rim structure formation of isothermally irradiated UO₂ fuel discs,
Journal of Nuclear Materials, 288, pp 20-28.

Van Uffelen, P., 2000.
Modelling the variable precipitation of fission products at grain boundaries,
Journal of Nuclear Materials, 280, pp 275-284.

Van Uffelen, P., 2002.
Contribution to the Modelling of fission gas release in light water reactor,
Dissertation, Université de Liege, Belgium.

Walker, C.T., Knappik, P. and Mogensen, M., 1998.
Concerning the development of grain face bubbles and fission gas release in UO₂ fuel,
Journal of Nuclear Materials, 160, pp 10-23.

Walker, C.T., 1999.
Assessment of the radial extent and completion of recrystallization in high burn-up UO₂ nuclear fuel by EPMA, Journal of Nuclear Materials, 275, pp 56-62.

White, R.J. and Tucker, M.O., 1983.
A new fission-gas release model,
Journal of Nuclear Materials, 118, pp 1-38.

Appendix A: Assessment case for high-burnup fuel restructuring

The models for formation of a high-burnup fuel microstructure in section 2.1 are assessed by use of experimental data presented by Manzel and Walker (2000, 2002). They carried out post-irradiation examinations of commercial PWR fuel rods, which were operated to very high burnups in a Siemens-built power reactor. Our assessments are made by simulating the irradiation history for one of these fuel rods by use of FRAPCON-3.2, and comparing the calculated results with measured data.

The rod under consideration, 12C3, is of Siemens 15×15 standard design, as defined in table A.1. The rod was irradiated for nine cycles, or 2913 effective full power days, thereby reaching a rod average burnup of $97.8 \text{ MWd}(\text{kgU})^{-1}$. The irradiation history applied in our analyses of rod 12C3 is taken from the typical cycle average power values given by Manzel and Walker (2000), and the applied axial power distribution is taken from Manzel and Walker (2002). Figures A.1 and A.2 show the applied power history and axial power distribution, respectively.

At the end of the fourth irradiation cycle, when the fuel assembly had reached its nominal discharge burnup of about $60 \text{ MWd}(\text{kgU})^{-1}$, rod 12C3 was transferred to a new carrier assembly, containing partially burnt fuel, for further irradiation. After transfer to the new carrier assembly, the power rating decreased marginally from 17.5 kWm^{-1} in the fifth irradiation cycle to 14 kWm^{-1} in the ninth and final cycle. Hence, the end-of-life power level was fairly high, considering the extremely high burnup of the fuel rod. The reader is referred to the original papers by Manzel and Walker (2000, 2002) for further details on the irradiation conditions and the results of the post-irradiation examinations.

Fuel pellets			Cladding		
Material		UO ₂	Material		Zr-4
Density	%TD	95.3	Inner diameter	mm	9.47
Grain size	μm	10	Outer diameter	mm	10.75
Enrichment ²³⁵ U	%	3.5	Fill gas		
Pellet diameter	mm	9.30	Composition		He
Active rod length	mm	3660	Gas pressure	MPa	2.25

Table A.1: Design of standard PWR rod 12C3, considered in analyses.
%TD: Percent of theoretical density, Zr-4: Zircaloy-4.

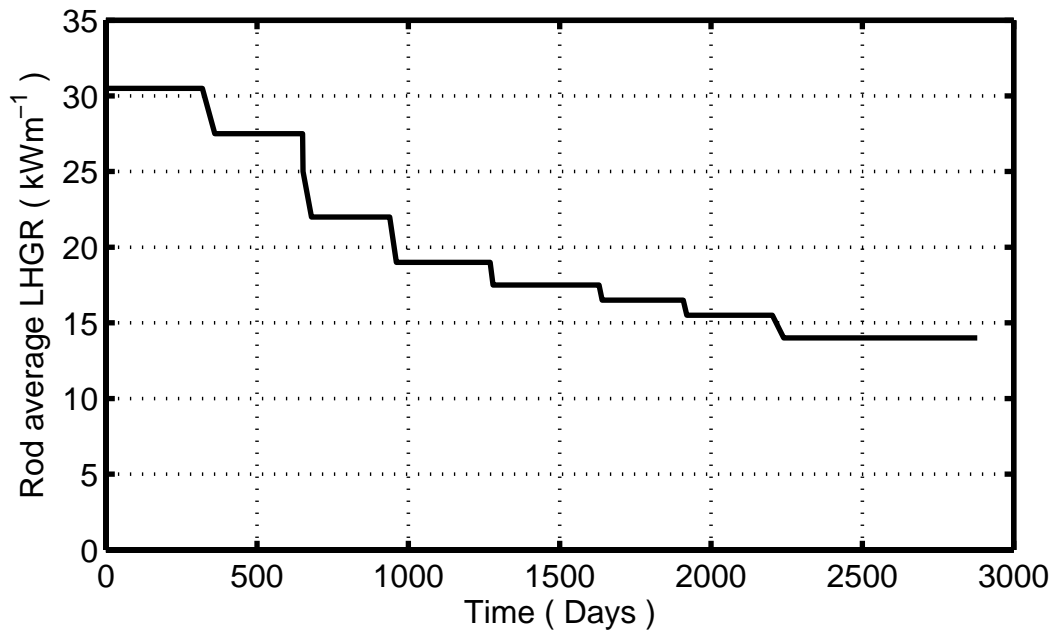


Figure A.1: Fuel rod power history, applied for simulating the irradiation history of rod 12C3.

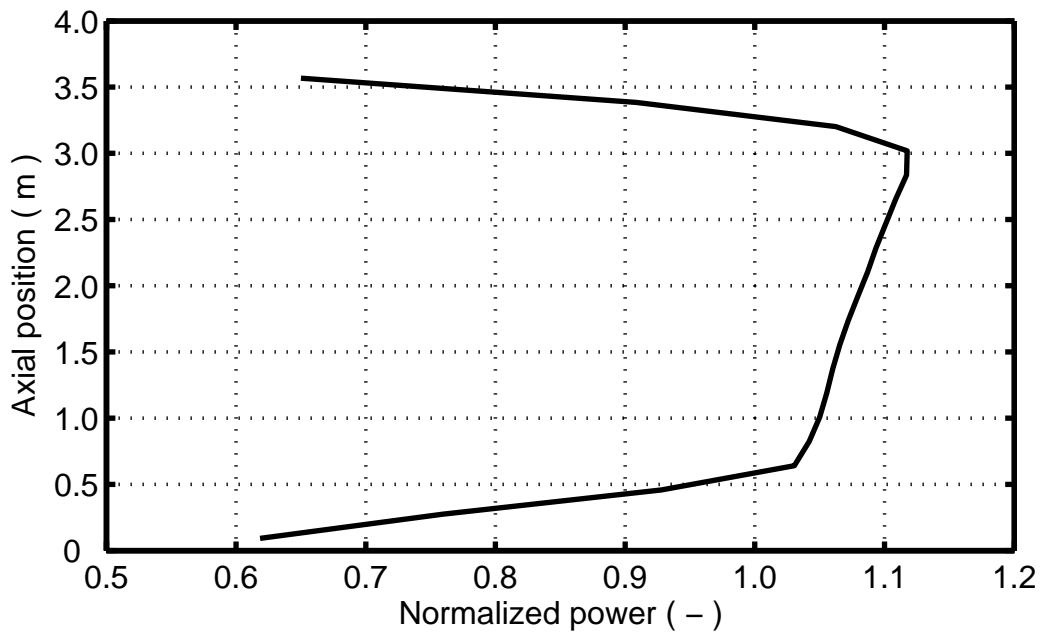


Figure A.2: Fuel rod power distribution, applied for simulating the irradiation history of rod 12C3. The power distribution was assumed not to change during irradiation.

Appendix B: Fission gas production rate

The production rate $\beta(t)$ of stable gas atoms (xenon and krypton) in nuclear fuel depends on the fission rate and the fission yield, see chapter of 13 in (Olander, 1976). In the calculations carried out here, we set $\beta(t) = 0.3\varphi$, where φ is the fission rate and 0.3 is the yield of gas atoms produced per fission. The relationship between φ and the volumetric power density q_v :

$$\varphi = 5.189 \times 10^{-14} q_v \text{ [mole m}^{-3}\text{s}^{-1}\text{]} \quad (\text{B.1})$$

is listed in table 2.3. Computation of the gas production

$$G_p = \int \beta(t) dt, \quad (\text{B.2})$$

for a constant power density $q_v = 707 \text{ MWm}^{-3}$ is plotted in figure B.1.

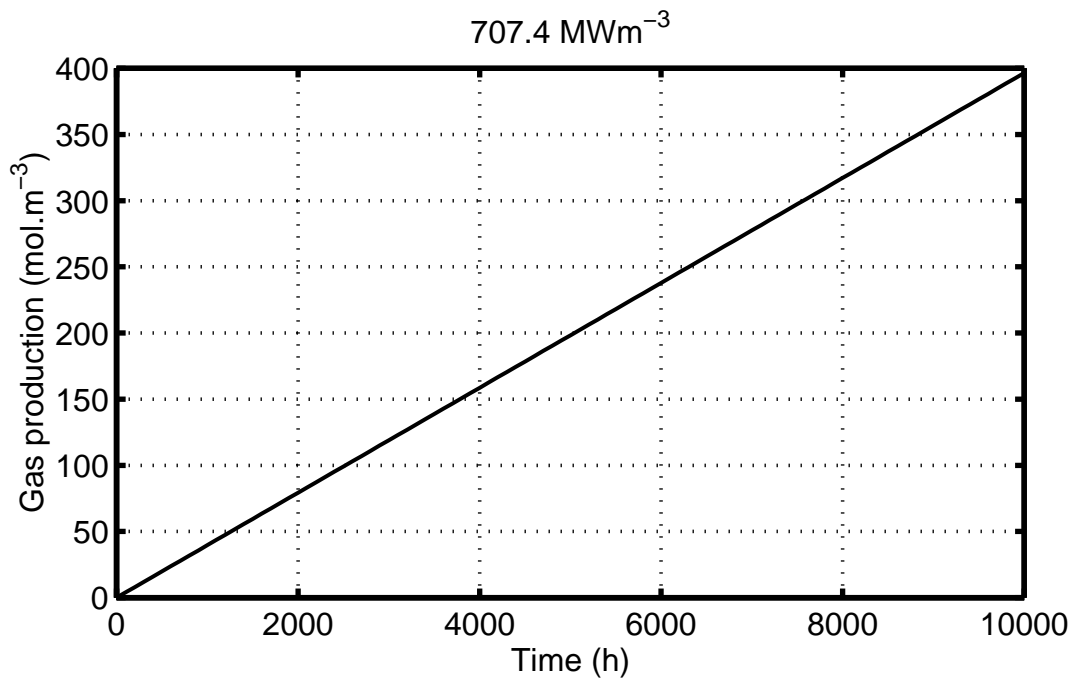


Figure B.1: Fission gas production for a constant power density $q_v = 707 \text{ MWm}^{-3}$.

Appendix C: Characteristic times of gas diffusion and grain growth

The characteristic time for gas diffusion is defined by $\tau_D \equiv R^2/2D$, whereas the corresponding quantity for grain growth is defined by $\tau_G \equiv R/2\dot{R}$, where R is the grain radius, D is the gas diffusivity in irradiated UO_2 and $\dot{R} \equiv dR/dt$ is the grain growth rate. We note that both R and D are temperature dependent, and R is also time dependent. Calculations of τ_D and τ_G as a function of temperature for variable R based on the model used here, described in subsection 2.2.3.2, are presented in figure 2.19. In this appendix, we present results of calculations of τ_D and τ_G for a hypothetical situation that the grain size is constant. We also calculate exactly the grain size dependence of τ_G .

Let us first calculate the temperature dependence of τ_D using the data listed in table 2.3 for a grain size $S = 12 \text{ }\mu\text{m}$, figure C.1. The results show the impact of intragranular gas bubbles (traps) on the time constant. The calculated characteristic times for the grain growth and the effective diffusion in UO_2 are displayed in figure C.2.

The grain size dependence of τ_G is obtained directly from equation (2.23) according to:

$$\tau_G = \frac{2R^2}{k(1 - R/R_m)}, \quad (\text{C.1})$$

where $R_m = S_m/2$ is calculated according to relation (2.28). The size dependence of τ_G is depicted in figure C.3, where $S_{\text{max}} = 2R_m$.

It is seen from figure C.2 that above a certain temperature, here 1750 K, the grain growth characteristic time becomes much shorter than the fission product gas diffusion time in UO_2 . This means that release at these temperatures are governed by grain growth and grain boundary sweeping rather than by diffusion, while at temperatures below this temperature, release is diffusion controlled process. Figure C.3 shows that as the grain size is increased, τ_G becomes longer and longer and eventually at $R = R_m$, it gets infinitely long, $\tau_G = \infty$, corresponding to the end of grain growth.

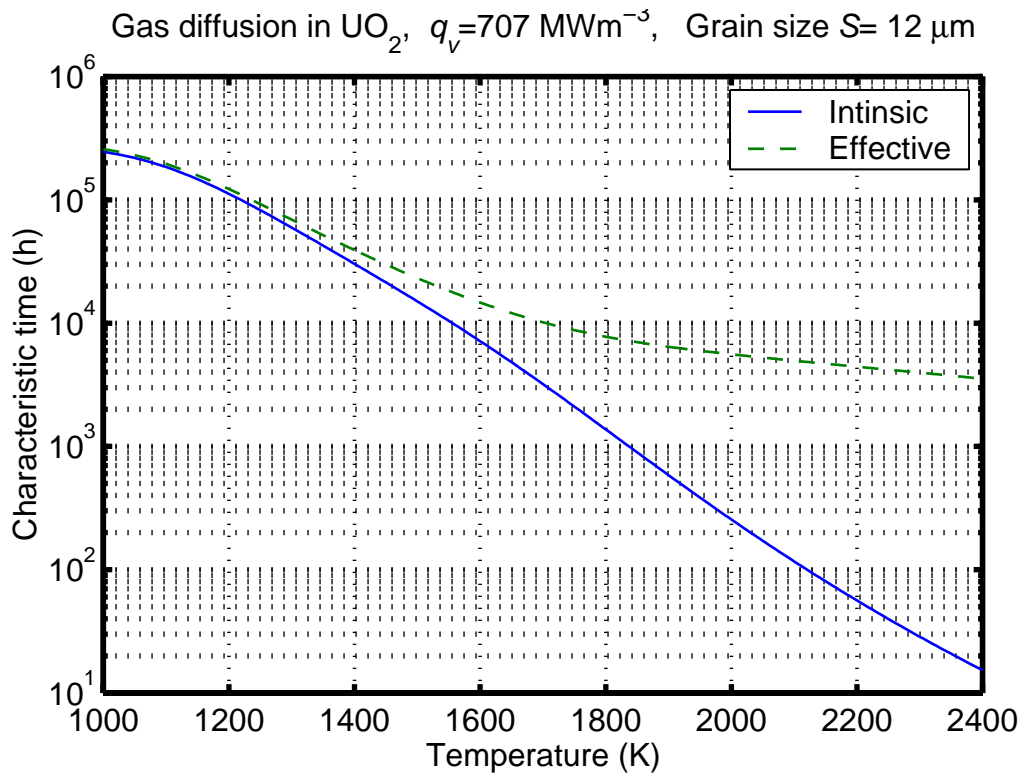


Figure C.1: Characteristic time for gas diffusion in UO_2 fuel. The gas diffusion coefficients used (intrinsic and effective) are presented in figure 2.14 and table 2.3.

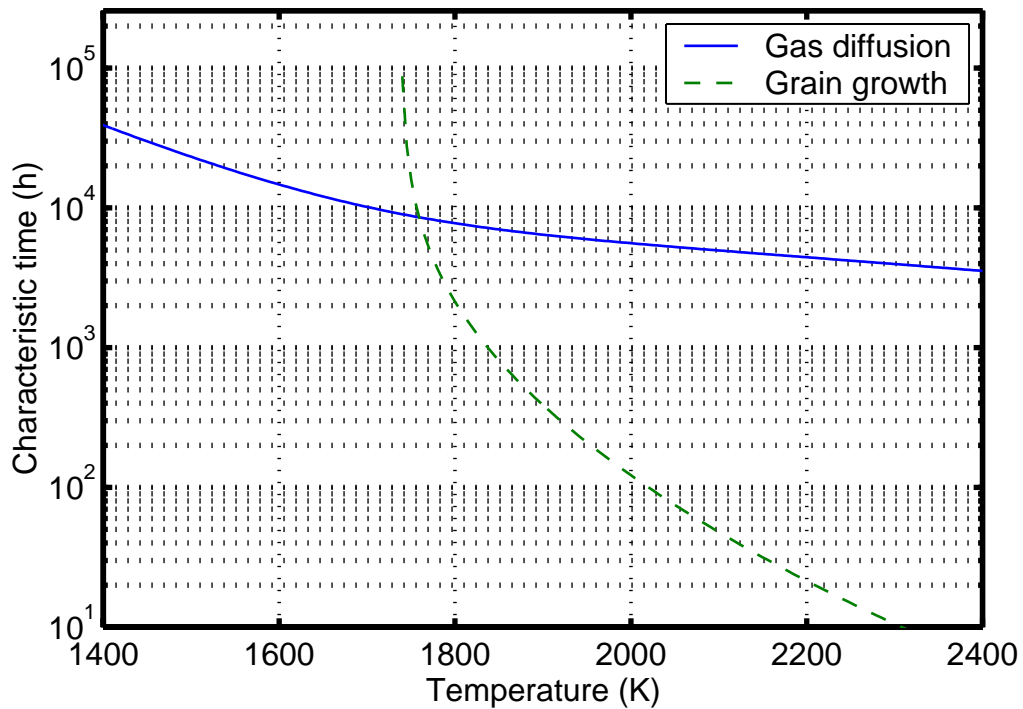


Figure C.2: Characteristic times for the effective gas diffusion in UO_2 fuel and for grain growth at a constant grain size.

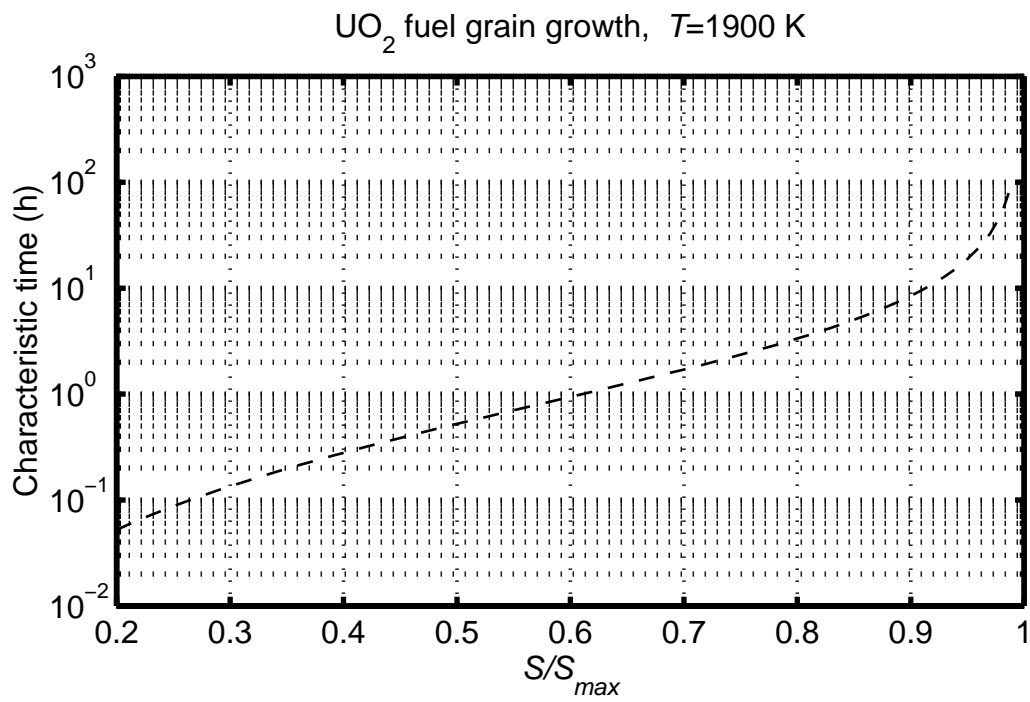


Figure C.3: Grain size dependence of the grain growth characteristic time at a constant temperature of 1900 K.

Appendix D: Fuel thermal conductivity correlation from HBRP

As part of the High Burnup Rim Project (HBRP), laser flash thermal diffusivity measurements were carried out on isothermally irradiated UO₂ fuel discs. The material, which had a ²³⁵U enrichment of 25.8% to attain a high burnup in short time, was irradiated to 33-96 MWd(kgU)⁻¹ in the Halden test reactor at constant temperature. The experimental technique and measured fuel thermal conductivities are documented in detail in a paper by Ronchi et al. (2004). A simple correlation for UO₂ thermal conductivity, based on these data, is due to (Kinoshita et al. 2004). The thermal conductivity of fully dense material, k_{100} [W(mK)⁻¹], is in this model correlated to temperature and burnup through

$$k_{100} = \frac{1000}{A(E) + B(E)T} + \frac{4.715 \cdot 10^9 e^{-16361/T}}{T^2}. \quad (D.1)$$

Here, T is the fuel temperature in Kelvin. A and B are burnup dependent functions, for which the following expressions are used, depending on fuel temperature:

For $T < 1273$ K:

$$A(E) = 40.0 + 4.12 E, \quad (D.2)$$

$$B(E) = \begin{cases} 2.2 \cdot 10^{-1} & E < 50 \\ 0.447 - 4.53 \cdot 10^{-3} E & 50 \leq E \leq 80 \\ 8.4 \cdot 10^{-2} & 80 < E \end{cases}. \quad (D.3)$$

For $1473 \text{ K} < T < T_{melt}$:

$$A(E) = 40.0 + 1.74 E, \quad (D.4)$$

$$B(E) = 2.2 \cdot 10^{-1} + 3.0 \cdot 10^{-4} E. \quad (D.5)$$

In equations (D.2) to (D.5), E is the local fuel burnup in MWd(kgU)⁻¹. The two temperature regions represent a low-temperature domain with damage accumulation in the fuel, and a high-temperature domain, in which damage recovery occurs. In the intermediate temperature region 1273-1473 K, the fuel thermal conductivity is set to linearly connect k_{100} in equation (D.1) between the two temperature regions.

For application of the above correlation to materials with porosity volume fractions, p , the following expression is used (Ronchi et al. 2004)

$$k(p) = k_{100} \left(1 - p(2.6 - 5 \cdot 10^{-4} T) \right). \quad (D.6)$$

Appendix E: Fuel thermal conductivity correlation in FRAPCON-3.2

The correlation for thermal conductivity of UO_2 fuel applied in FRAPCON-3.2 is a modified version of the model proposed by Ohira and Itagaki (1997). The modifications made to this model in FRAPCON-3.2 pertain to the low- and intermediate-burnup range, $E < 45 \text{ MWd}(\text{kgU})^{-1}$, where the original model by Ohira and Itagaki was found to underestimate the fuel thermal conductivity. The reader is referred to Lanning et al. (2000) for further details on the background to the modifications.

In the FRAPCON-3.2 model, the thermal conductivity of UO_2 fuel is correlated to fuel temperature and burnup through

$$k_{95} = \frac{1}{4.52 \cdot 10^{-2} + 2.46 \cdot 10^{-4} T + h} + \frac{3.5 \cdot 10^9 e^{-16361/T}}{T^2}, \quad (\text{E.1})$$

where $k_{95} [\text{W}(\text{mK})^{-1}]$ is the thermal conductivity of fuel with 5% porosity, $T [\text{K}]$ is the fuel temperature, and h is a burnup-dependent correction factor, which is given by

$$h(E, T) = 1.87 \cdot 10^{-3} E + \frac{3.8 \cdot 10^{-2} (1 - 0.9 e^{-0.04 E}) E^{0.28}}{1 + 396 e^{-6380/T}}. \quad (\text{E.2})$$

Here, E is the local fuel burnup in $\text{MWd}(\text{kgU})^{-1}$. A porosity correction factor according to Maxwell and Eucken is finally used for application of the above correlation to materials with porosity volume fractions, p , other than 0.05. Hence, the thermal conductivity of UO_2 with porosity p is calculated through

$$k(p) = 1.0789 k_{95} \frac{1 - p}{1 + 0.5 p}. \quad (\text{E.3})$$

www.ski.se

STATENS KÄRNKRAFTINSPEKTION
Swedish Nuclear Power Inspectorate

POST/POSTAL ADDRESS SE-106 58 Stockholm

BESÖK/OFFICE Klarabergsviadukten 90

TELEFON/TELEPHONE +46 (0)8 698 84 00

TELEFAX +46 (0)8 661 90 86

E-POST/E-MAIL ski@ski.se

WEBBPLATS/WEB SITE www.ski.se